
Electronic Thesis and Dissertation Repository

12-13-2013 12:00 AM

InterNAV3D: A Navigation Tool for Robot-Assisted Needle-Based Intervention for the Lung

Srikanth Bhattad
The University of Western Ontario

Supervisor
Dr. Rajni Patel
The University of Western Ontario

Graduate Program in Electrical and Computer Engineering
A thesis submitted in partial fulfillment of the requirements for the degree in Master of
Engineering Science
© Srikanth Bhattad 2013

Follow this and additional works at: <https://ir.lib.uwo.ca/etd>



Part of the [Biomedical Commons](#), and the [Other Electrical and Computer Engineering Commons](#)

Recommended Citation

Bhattad, Srikanth, "InterNAV3D: A Navigation Tool for Robot-Assisted Needle-Based Intervention for the Lung" (2013). *Electronic Thesis and Dissertation Repository*. 1760.
<https://ir.lib.uwo.ca/etd/1760>

This Dissertation/Thesis is brought to you for free and open access by Scholarship@Western. It has been accepted for inclusion in Electronic Thesis and Dissertation Repository by an authorized administrator of Scholarship@Western. For more information, please contact wlsadmin@uwo.ca.

InterNAV3D: A NAVIGATION TOOL FOR ROBOT-ASSISTED NEEDLE-BASED
INTERVENTION FOR THE LUNG

(Thesis format: Monograph)

by

Srikanth Omprakash Bhattad

Graduate Program in Department of Electrical and Computer Engineering

A thesis submitted in partial fulfillment
of the requirements for the degree of
Master of Engineering Science

The School of Graduate and Postdoctoral Studies
The University of Western Ontario
London, Ontario, Canada

© Srikanth Bhattad 2013

Abstract

Lung cancer is one of the leading causes of cancer deaths in North America. There are recent advances in cancer treatment techniques that can treat cancerous tumors, but require a real-time imaging modality to provide intraoperative assistive feedback. Ultrasound (US) imaging is one such modality. However, while its application to the lungs has been limited because of the deterioration of US image quality (due to the presence of air in the lungs); recent work has shown that appropriate lung deflation can help to improve the quality sufficiently to enable intraoperative, US-guided robotics-assisted techniques to be used. The work described in this thesis focuses on this approach.

The thesis describes a project undertaken at Canadian Surgical Technologies and Advanced Robotics (CSTAR) that utilizes the image processing techniques to further enhance US images and implements an advanced 3D virtual visualization software approach. The application considered is that for minimally invasive lung cancer treatment using procedures such as brachytherapy and microwave ablation while taking advantage of the accuracy and teleoperation capabilities of surgical robots, to gain higher dexterity and precise control over the therapy tools (needles and probes). A number of modules and widgets are developed and explained which improve the visibility of the physical features of interest in the treatment and help the clinician to have more reliable and accurate control of the treatment. Finally the developed tools are validated with extensive experimental evaluations and future developments are suggested to enhance the scope of the applications.

Keywords

Lung cancer, tumor, brachytherapy, microwave ablation, radiofrequency ablation, VTK, ITK, image processing, 3D visualization, virtual reality, needle maneuvering, needle bending, needle tip detection, needle retraction, image guided intervention, medical imaging, InterNAV.

Acknowledgments

I am very grateful to all the people that helped me achieve this goal. Firstly, I would like to thank my supervisor Dr. Rajni Patel for giving me an opportunity to work in CSTAR and for his constant guidance, encouragement and support during my thesis work. I would also like to thank Dr. Malthaner for all the talks he had with me and for helping me carry out experiments from time to time.

I would like to thank all my friends and colleagues at CSTAR, especially Abe, Chris and Ran for being such a wonderful team to work with and for their constant source of help and inspiration, their support and those lengthy discussions without which things would be little tougher.

I would also like to thank my family members for standing by me all these years, patiently supporting me in my endeavor to achieve success and happiness.

Lastly, I would like to thank Mathworks, the developers of the open source project: VTK and ITK, and all the people who contributed in getting so many wonderful tools in the hands of students; providing them the required momentum in developing the applications for carrying out the research work.

Table of Contents

Abstract	ii
Acknowledgments	iii
Table of Contents	iv
List of Tables	vii
List of Figures	viii
List of Appendices	xv
List of Abbreviations	xvi
Chapter 1	1
1 Introduction	1
1.1 Cancer overview	1
1.2 Lung cancer statistics	3
1.3 Types of lung cancer	4
1.4 Treatment	5
1.4.1 Conventional treatment approach	5
1.4.2 Minimally invasive intervention	6
1.4.3 Current scenario	12
1.5 Image-guided intervention	14
1.6 Robot-assisted minimally invasive surgery	15
1.7 InterNAV	16
1.8 Thesis contribution.....	19
1.9 Thesis outline	21
Chapter 2	22
2 System Architecture: Hardware and Software	22
2.1 System overview	22

2.2	System initialization and working	24
2.3	System components	28
2.3.1	Hardware components	28
2.3.2	Software components.....	43
Chapter 3	49
3	User Interface: Modules and Working	49
3.1	User interface	52
3.1.1	Right dock.....	52
3.1.2	Left dock	54
3.1.3	Top dock (toolbar menu)	67
3.1.4	Bottom dock (system log).....	67
3.2	Modules and working	68
3.2.1	Virtual needle and path projection.....	68
3.2.2	Current needle path visualization.....	71
3.2.3	Needle path prediction	72
3.2.4	Virtual US probe and the real-time 2D US image	74
3.2.5	US video output window, target selection and visualization.....	77
3.2.6	Volume rendering and opacity transfer.....	78
3.2.7	Surface rendering and sub-surface reconstruction.....	80
3.2.8	Region reconstruction	83
3.2.9	Motion simulation.....	84
3.2.10	Needle navigation	84
3.2.11	Camera movements and additional windows	85
3.3	Remarks	87
Chapter 4	88
4	Experimental Overview	88

4.1	Experimental test-bed	88
4.1.1	Motion induction.....	91
4.2	Calibration.....	97
4.2.1	Needle tool tip calibration.....	97
4.2.2	US image calibration.....	100
4.2.3	Robotic calibration.....	104
4.3	Experiments and validations	108
4.3.1	Needle bending	110
4.3.2	Needle maneuvering	113
4.3.3	Tumor detection and reconstruction	117
4.3.4	<i>Ex-vivo</i> experiments: target selection and hitting	119
4.3.5	Needle retraction.....	126
4.3.6	<i>In-vivo</i> experiments.....	127
4.4	Review	133
Chapter 5	134
5	Summary, Conclusion and Future Work.....	134
5.1	Summary	134
5.2	Conclusion	138
5.3	Drawbacks and future work	140
Bibliography	143
Appendix A: Manufactured parts	156
Curriculum Vitae	159

List of Tables

Table 1.1: Lung cancer statistics (Canada)	4
Table 2.1: 5-DOF sensor accuracy.....	35
Table 2.2: 6-DOF sensor accuracy.....	35
Table 4.1: US image calibration value.....	104
Table 4.2: Evaluating the calibration	108
Table 4.3: Error analysis (needle tip detection)	112
Table 4.4: Needle maneuvering experimental analysis	116
Table 4.5: Error analysis (3D volume reconstruction).....	119
Table 4.6: Error analysis for needle target hitting	125
Table 4.7: Number of insertion attempts to reach the target.....	125
Table 4.8: Needle retraction analysis.....	127

List of Figures

Figure 1.1: Cancer – a leading cause of death (Canada).....	1
Figure 1.2: Death by cancer type	2
Figure 1.3: Percentage distribution of estimated cancer deaths (2013)	3
Figure 1.4: Brachytherapy	7
Figure 1.5: Brachytherapy seeds.....	8
Figure 1.6: Brachytherapy needles and stylets of different gauge size.....	9
Figure 1.7: Radiofrequency ablation.....	10
Figure 1.8: Radiofrequency ablation probes	11
Figure 1.9: Microwave ablation probes	11
Figure 1.10: Image guided intervention platform	15
Figure 1.11: InterNAV setup for lung brachytherapy.....	17
Figure 1.12: InterNAV user interface	17
Figure 2.1: System overview and working	23
Figure 2.2: Flowchart for system initialization and working.....	25
Figure 2.3: Ultrasound's Sonixtouch US machine	28
Figure 2.4: Laparoscopic probe used	29
Figure 2.5: US probe bent from the flexible part.....	30
Figure 2.6: US probe enclosed in a sleeve	30
Figure 2.7: Working of electromagnetic tracking system.....	31

Figure 2.8: Aurora field generator	32
Figure 2.9: NDI's Aurora electromagnetic tracker system	32
Figure 2.10: Field generator and the Cartesian co-ordinate space.....	33
Figure 2.11: 5-DOF sensor	34
Figure 2.12: 6-DOF sensor	34
Figure 2.13: Roll, pitch and yaw.....	36
Figure 2.14: Bevel-tip needle with 5-DOF sensor enclosed	36
Figure 2.15: Sleeve for radiofrequency ablation probe with the channel for EM tracking sensor	37
Figure 2.16: radiofrequency ablation probe with sensor attached to sleeve	37
Figure 2.17: Microwave ablation tool with sleeve and sensor attached	37
Figure 2.18: US probe with electromagnetic sensor attached using shrink wrap	38
Figure 2.19: US probe with the attached sleeve	38
Figure 2.20: AESOP robot.....	39
Figure 2.21: Remote workstation for ZEUS robotic system.....	40
Figure 2.22: ZEUS robotic setup	40
Figure 2.23: AESOP/ZEUS kinematic model	41
Figure 2.24: Kinematic model superimposed	41
Figure 2.25: Matrox frame grabber.....	42
Figure 2.26: Software architecture.....	43
Figure 2.27: Overview of SAW	44

Figure 2.28: VTK flow of control.....	46
Figure 3.1: User interface	51
Figure 3.2: Dock areas for the GUI interface	52
Figure 3.3: VTK window (3D virtual world)-multiple volumes	53
Figure 3.4: Typical VTK window.....	54
Figure 3.5: US real-time video stream.....	54
Figure 3.6: Control panel	55
Figure 3.7: System control.....	56
Figure 3.8: Pop-up menu.....	56
Figure 3.9: Sweep control	57
Figure 3.10: Round sweep	57
Figure 3.11: Flat sweep (straight sweep) mode	58
Figure 3.12: Multiple ablation volumes at different time intervals	61
Figure 3.13: Volume subtraction	63
Figure 3.14: Status panel.....	63
Figure 3.15: Movement control panel.....	64
Figure 3.16: Visualization control	65
Figure 3.17: Surface control	65
Figure 3.18: Surface opacity control.....	66
Figure 3.19: Volume control.....	66

Figure 3.20: Toolbar options.....	67
Figure 3.21: System log	67
Figure 3.22: Needle path projection.....	68
Figure 3.23: Needle updated path projection.....	69
Figure 3.24: Needle STL superimposed on the US image.....	70
Figure 3.25: Current needle path	71
Figure 3.26: Needle path prediction.....	72
Figure 3.27: Needle path prediction with the current needle path	73
Figure 3.28: US probe and the 2D US image rendered in 3D space	74
Figure 3.29: US image superimposed on a volume	75
Figure 3.30: Image capture model	76
Figure 3.31: Target selection and visualization	77
Figure 3.32: Opacity transfer function.....	79
Figure 3.33: Surface reconstruction.....	80
Figure 3.34: Surface reconstruction superimposed over volume.....	81
Figure 3.35: Sub-surface reconstruction	82
Figure 3.36: Region reconstruction.....	83
Figure 3.37: Needle eye view	85
Figure 3.38: Three orthogonal views	86
Figure 3.39: Oblique re-slices.....	86

Figure 4.1: Ball and socket joint (semi-spheres)	88
Figure 4.2: Ball and socket joint (attached)	89
Figure 4.3: Linear stage	89
Figure 4.4: Entire test-bed.....	90
Figure 4.5: Air pump mechanism	91
Figure 4.6: Motion inducing system	92
Figure 4.7: Rotational sweep capture model.....	93
Figure 4.8 Scatter plot for 2D to 3D image conversion	97
Figure 4.9: Pivot tool-tip calibration.....	98
Figure 4.10: Needle tip calibration	99
Figure 4.11: Pivot calibration values	99
Figure 4.12: US image plane calibration	101
Figure 4.13: Calculating dataset transformation	102
Figure 4.14: Phantoms used to evaluate calibrations.....	106
Figure 4.15: Evaluating the calibration using a phantom	107
Figure 4.16: Phantom volume and surface reconstruction.....	107
Figure 4.17: Needle with two 5-DOF sensors attached	110
Figure 4.18: Experimental setup for evaluating needle bending	111
Figure 4.19: Needle bending visualization and tip detection in the 3D virtual world	112
Figure 4.20: Needle insertion with and without the assistance of the developed modules ..	113

Figure 4.21: Re-orientation during an insertion procedure without the assistance of the built-in modules (displayed within the boxes)	115
Figure 4.22: Re-orientation during an insertion procedure with the assistance of the built-in modules (displayed within the boxes).....	115
Figure 4.23: Agar sphere being imaged.....	117
Figure 4.24: Experimental setup for 3D volume reconstruction.....	118
Figure 4.25: 3D volume and surface reconstruction	118
Figure 4.26: <i>Ex-vivo</i> experiment.....	120
Figure 4.27: Phantom tumors.....	121
Figure 4.28: Tissue sutured after implanting tumors and being imaged by US	121
Figure 4.29: Seed missed the target using InterNAV	122
Figure 4.30: Electromagnetic tracker attached to the phantom tumor.....	123
Figure 4.31: Volume reconstruction of duck gizzard	124
Figure 4.32: Needle insertion and retraction path.....	127
Figure 4.33: Phantom tumor with the attached electromagnetic tracker placed within the lung and sutured	128
Figure 4.34: 3D reconstructed volume.....	129
Figure 4.35: <i>In-vivo</i> 2D US image of the deflated lung.....	129
Figure 4.36: <i>In-vivo</i> lung experiment (needle hitting the target)	130
Figure 4.37: <i>In-vivo</i> thermal ablation (power 30W, microwave energy)	131
Figure 4.38: Ablation volume	131
Figure 4.39: Lung (post ablation)	132

Figure 4.40: Ablation zone cut in half	132
Figure A.1: US probe holder.....	156
Figure A.2: Test-bed assembly	157
Figure A.3: Ball and socket design	157
Figure A.4: Microwave ablation probe holder.....	158
Figure A.5: Radiofrequency ablation probe holder	158
Figure A.6: Radiofrequency ablation probe holder designed in two parts	158

List of Appendices

Appendix A: Manufactured parts.....	156
-------------------------------------	-----

List of Abbreviations

2D	Two dimensional
3D	Three dimensional
AESOP	Automated Endoscopic System for Optimal Positioning
API	Application Programming Interface
CISST	Computer Integrated Surgical Systems and Technology
CPU	Central Processing Unit
CSTAR	Canadian Surgical Technologies & Advanced Robotics
CT	Computed Tomography
DDR3	Double Data Rate type three
DOF	Degrees of Freedom
FDA	Food and Drug Administration
GB	Giga Byte
GHz	Giga Hertz
GUI	Graphical User Interface
HDR	High Dose Rate
ID	Identification Data
IDE	Integrated Development Environment
InterNAV	Interventional Navigation
ITK	Insight Segmentation and Registration Toolkit

LDR	Low Dose Rate
MIL	Matrox Imaging Library
MRI	Magnetic Resonance Imaging
NDI	Northern Digital Incorporated
OpenIGTLink	Open Network Interface for Image-Guided Therapy
PCI	Peripheral Component Interconnect
RAM	Random Access Memory
RMS	Root Mean Square
ROS	Robot Operating System
SAW	Surgical Assistant Workstation
STL	Stereo Lithography
Tcl/Tk	Tool Command Language
TM	Trade Mark
URI	Ultrasound Research Interface
US	Ultrasound
VTK	Visualization Toolkit

Chapter 1

1 Introduction

This chapter provides the background and motivation for the project, a literature review of the recent technologies, their operation and a brief overview of the previous version of the system. At the end, it outlines the contribution of the thesis in the context of the research project.

1.1 Cancer overview

Cancer is a disease that is a result of uncontrolled growth of cells. Cancerous cells further divide to form lumps of tissue referred to as tumors. Cancer can grow in almost any tissue or organ of the body. It needs to be controlled or else it can migrate to other healthy parts of the body causing a greater risk to the life of the patient. Lung cancer is one of the most prominent forms of cancer diagnosed today. Proper medical treatment is advised as early as possible to control the growth of cancerous tumors and destroy or resect them.

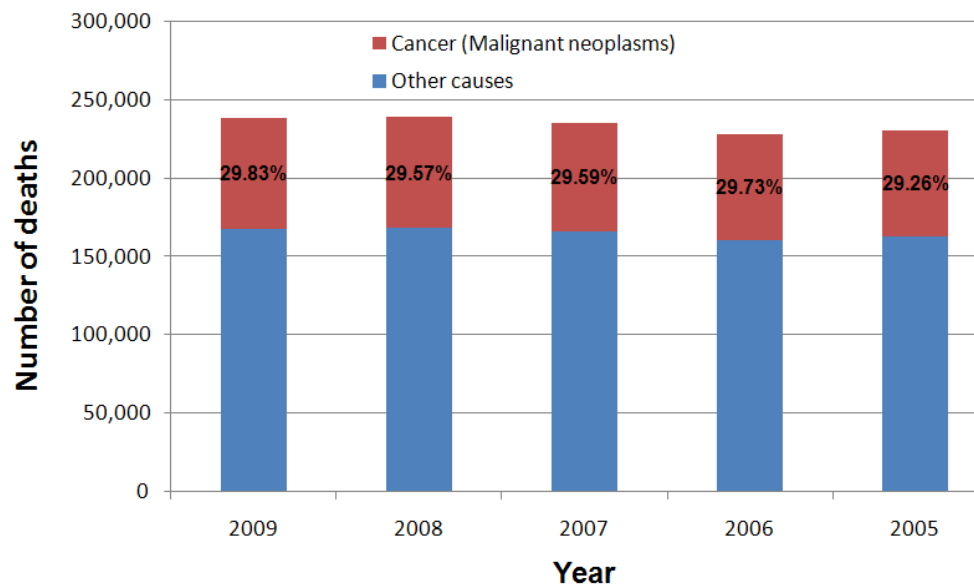


Figure 1.1: Cancer – a leading cause of death (Canada)

This section summarizes the data obtained from Canadian Cancer Statistics, 2013 [1]. It gives an overview of the cancer deaths in Canada. Most of the information and statistical data are projected estimations.

From Figure 1.1, the percentage of total deaths due to cancer for year 2009 was around 29.8 % in Canada. It is projected that in 2013, around 187,600 Canadians will be diagnosed with cancer and around 75,500 would die from it (approximately 27 % of total deaths in Canada). The following pie chart distinguishes between the cancer deaths estimated for the year 2013. An estimated 57% of total cancer deaths would occur due to lung (27%), colon (12%), breast (7%), pancreas (6%) and prostate (5%) cancer.

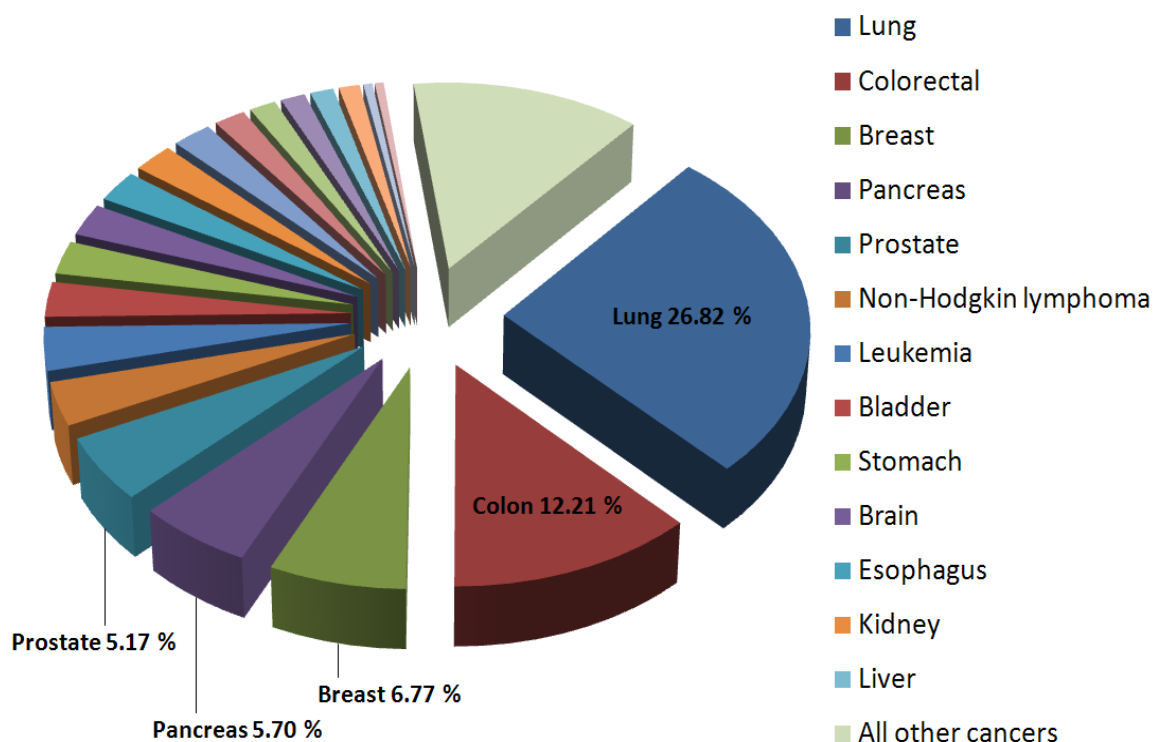


Figure 1.2: Death by cancer type

Figure 1.3 lists the percentage distribution of cancer deaths by sex estimated for year 2013. Lung cancer is the most prominent cancer, causing deaths in both males and females.

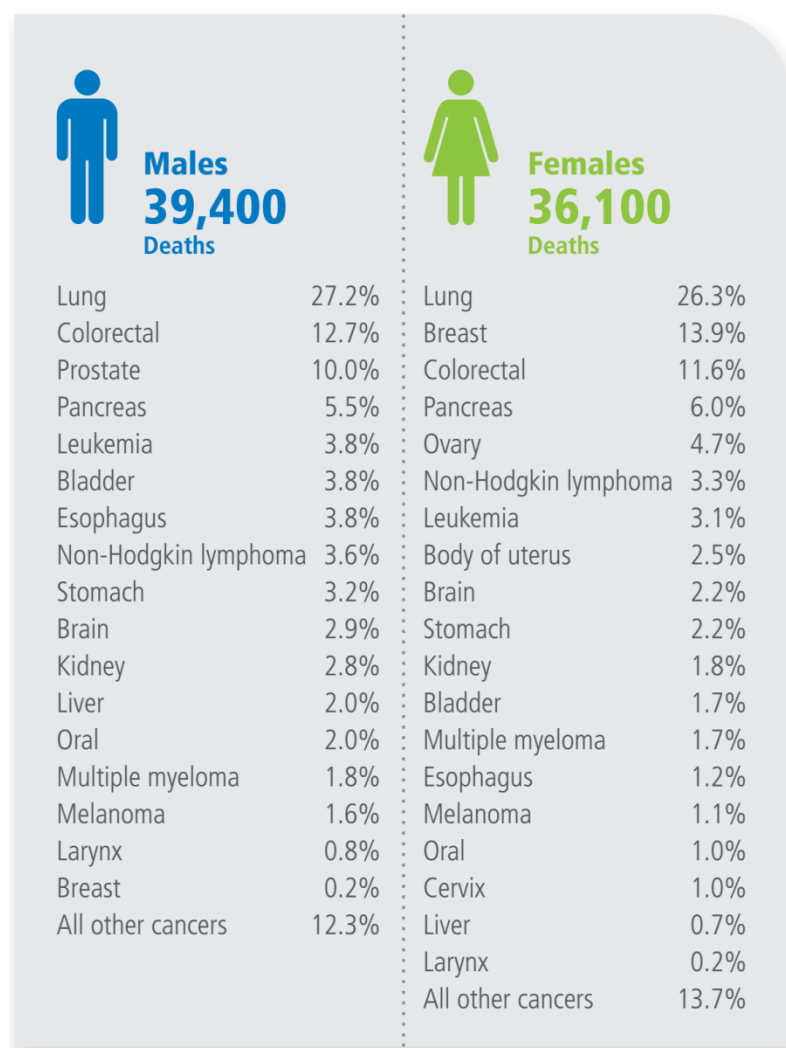


Figure 1.3: Percentage distribution of estimated cancer deaths (2013)

1.2 Lung cancer statistics

For 2013, around 25,500 Canadians would be diagnosed with lung cancer and around 20,200 would die of it. By the estimation provided, for every 1000 deaths (due to any reason), around 73 deaths would result from lung cancer.

Table 1.1: Lung cancer statistics (Canada)

Category	Males	Females
New Cases	13,300	12,200
Incidence rate (for every 100,000 people)	60	47
Deaths	10,700	9,500
Death rate (for every 100,000 people)	48	36
5-year relative survival (estimates for 2006-2008)	14%	20%

A major cause of lung cancer can be attributed to the cigarette smoking [1]. It is estimated that around 90% of lung cancers are caused by it, with factors such as intensity and duration of smoking playing a significant role in the incidence of the disease. The lifetime probability of dying from lung cancer is the highest among all forms of cancer. It is therefore of utmost importance to find suitable and viable techniques which could improve the current state of lung cancer treatment; and to make the whole process less traumatic for patients and easy to be performed by clinicians.

1.3 Types of lung cancer

Lung cancer is usually distinguished as either small cell lung cancer or non-small cell lung cancer depending on the size of the cancerous cells. Small cell lung cancer is highly attributed to smoking. This cancer grows rapidly in the course of the disease and has a tendency to spread quickly to other parts of the body. The non-small cell lung cancer on the other hand, spreads comparatively slowly. Depending on the type of the cancer diagnosed, appropriate treatment techniques are suggested to the patient. Needle biopsy, bronchoscopy, X-ray, CT scan, US etc. are some of the procedures most commonly used to diagnose lung cancer.

1.4 Treatment

This section mainly concentrates on conventional surgical and minimally invasive techniques for lung cancer treatment, their comparison in terms of advantages and drawbacks followed by current scenarios for treatment.

Surgical resection remains the primary treatment method for patients diagnosed with early-stage lung cancer. The cancerous part of the lung is completely removed by cutting out a small section (wedge resection), an entire lobe (lobectomy) or an entire lung (pneumonectomy) depending on the extent of the cancer. This type of surgery is more invasive because large incisions are made in the body so as to remove the tumor. It causes a lot of trauma to the patient. Some patients may not be considered fit to undergo such a procedure depending on their health and age. Considering this, a number of other treatment techniques such as chemotherapy, brachytherapy [2]–[5], external beam therapy [6], [7] thermal ablation therapy [8]–[10], cryotherapy [11], [12] etc. are suggested.

1.4.1 Conventional treatment approach

In this approach, usually surgical resection is applied to remove the tumor followed by chemotherapy and/or external beam radiation therapy. This is a very common approach for most of the malignant tumors formed in different organs such as lung, liver, prostate, breast, etc. Photodynamic therapy is also a new technique that can be used to treat cancer.

Wedge resection is a treatment where a small wedge shaped part of the lung is removed surgically which is infected by cancerous tissue. It is easy to recover and does not greatly affect the shape of lung. In lobectomy an entire lobe of the lung is resected. It is usually performed in early stage non-small cell lung cancer patients; whereas pneumonectomy consists of removal of a complete lung (patients are first diagnosed for their capacity to be able to breathe using just one lung). This kind of treatment is done very rarely and in only critical cases where a major portion of the lung is severely affected by cancer. The breathing capacity of the patient is reduced significantly post surgery.

Chemotherapy is the use of cytotoxic medication to kill cancerous cells as they are more prone to this kind of medication due to their tendency of dividing rapidly. It is a systematic treatment meaning that it can be used to kill the malignant cells in any part of the body as compared to radiation therapy which is a localized treatment method. Small cell lung cancer is usually treated with this therapy as this type of cancer has a tendency to spread faster. The therapy has side effects of hair loss, nausea and low blood cell counts.

External beam radiation therapy is a method of treatment where high energy radiation is used to kill cancerous tissue. An external machine is used to transfer the energy at the particular marked area of the body which overlies the tumor. There are other types of radiation therapies such as internal radiation therapy (brachytherapy) which will be discussed in a later section.

Cryotherapy is another way to treat cancer. It is mostly used as a localized cancer treatment where a probe (cryoprobe) is used to deliver extreme cold temperatures to the cancerous tissue so as to freeze and kill the underlying cancer cells. Image guidance is used to drive the probe to the target. Cryoprobe is inserted in a body through a bronchoscope or percutaneously (thus, it can also be considered as a minimally invasive intervention technique).

Photodynamic therapy [13], [14] consists of a patient being injected by special photosensitizing drug which gets absorbed by the body cells. The cancerous cells however retain them longer as compared to normal cells. The cancerous cells (now sensitive to light) are subjected to external light source which is passed through a bronchoscope. The light triggers the drug, destroying the cancerous cells.

1.4.2 Minimally invasive intervention

This is a relatively new type of interventional technique where small incisions about 1cm across are made in the body which act as access ports for laparoscopic instruments to enable them to reach the surgical site. Benefits of this technique are reduced trauma to the patient, faster recovery, and shorter hospital stay.

1.4.2.1 Brachytherapy

Brachytherapy consists of placing radioactive sources near or within the cancerous tumor so as to destroy it and prevent further spread of the cancer. This radiation therapy is a short distance concentrated radio therapy (“brachy” means “short” in Greek). It can be used in combination with other treatment methods for better results.

The two main brachytherapy types are Low Dose Rate (LDR) and High Dose Rate (HDR) brachytherapy. This treatment is widely used to treat prostate cancer [15]–[17] and recent advances show its viability to lung cancer treatment [6].

Endobronchial brachytherapy [18]–[20] which involve placing a radioactive source near the tumor through the use of a catheter and guide wires is a type of HDR brachytherapy [15]. As the name HDR suggests, it consists of a very highly radioactive source of energy placed at the target location for a fairly small amount of time. Once the procedure is completed, the source is retracted.

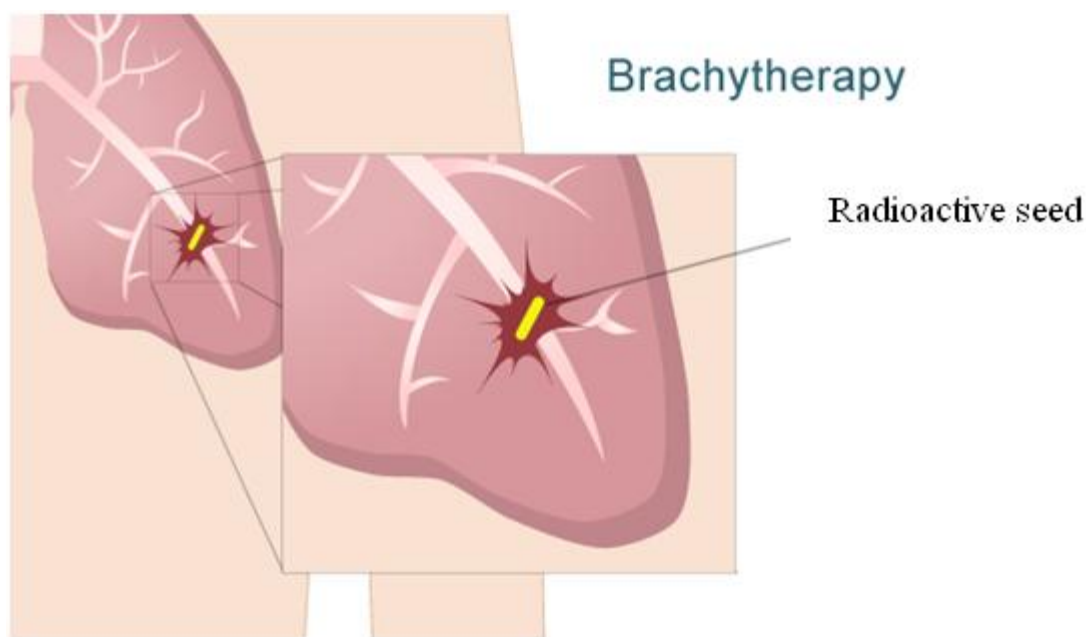


Figure 1.4: Brachytherapy

Interstitial Brachytherapy [17], [21]–[23] which involves direct implantation of low dose rate radioactive sources, typically Iodine-125 into the tumor to provide local

irradiation is a type of LDR brachytherapy [16]. In this case, the time for which the tumor is subjected to radiation is significant as compared to HDR, but the dose of radiation is fairly small. The sources are commonly referred to as “seeds” which are the size of rice grains.



Figure 1.5: Brachytherapy seeds

Usually multiple seeds are placed at different locations in the tumor based on a dosimetry plan, so as to provide sufficient dosage to destroy the cancer cells. A needle and a plunger design is used to deploy the seed at the given target location. Various types of brachytherapy needles based on different gauge sizes are available. Typical needle and plunger pairs of 2 different gauge sizes are shown below.

The dosimetry plan provides seed locations based on biopsy results and preoperative screening. The radiation decays to a safe level over a period of time. In [21], [24], it is shown that brachytherapy can be used in conjunction with wedge resection so as to address the possibility of recurrence of cancer due to possible remnants of cancer cells in the operated area of the lung. An important aspect of the treatment is the imaging feedback. Imaging [25]–[27] helps in determining the locations of tumors and in establishing target locations. It is also used to scan for the implanted seeds and to estimate the success of the entirety of the treatment.

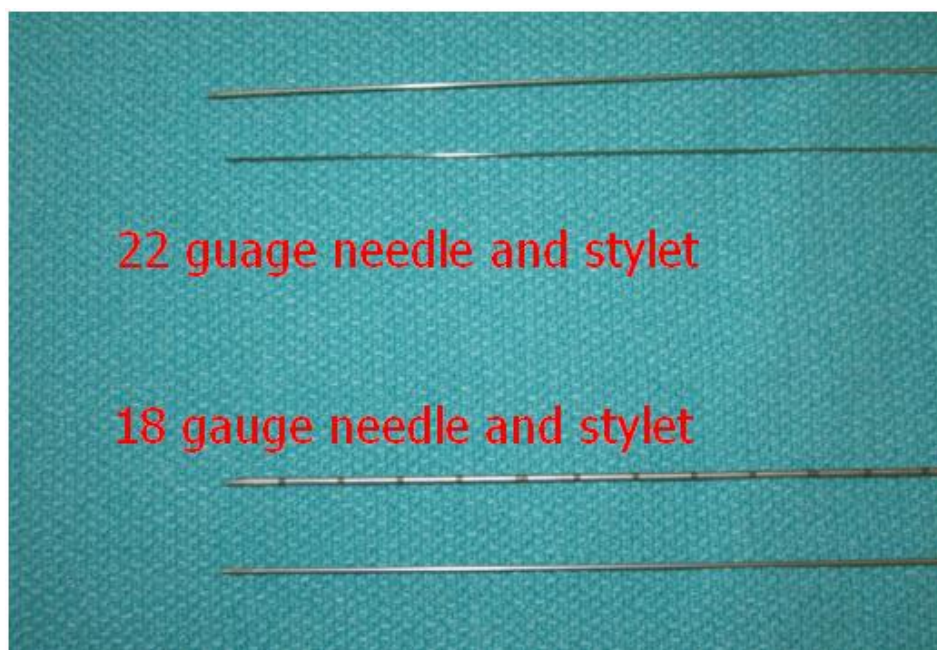


Figure 1.6: Brachytherapy needles and stylets of different gauge size

The advantages of brachytherapy can be summarized as being a local radiation therapy, a larger and more focused dose can be applied as compared to external beam therapy. It has a minimized risk of side effects and requires shorter treatment and recovery times compared with other treatment techniques.

There are some shortcomings to brachytherapy as mentioned in [28], [29] about the migration of seeds to other parts of body causing possible complications, and in some cases even causing development of new cancerous tissue. The way to prevent such undesirable effects currently is to follow-up on a regular basis to make sure that the seeds have not migrated. A recent research shows promising results to overcome the seed migration issue of brachytherapy [30]. It enhances the structure of the seed by adding a bio-absorbent polymer coating which allows the seed to affix itself at the target location. Another solution to the migration problem is to use seeds in the form of strands that can be woven into a mesh and secured to the tumor bed.

Some of the sources of error in this treatment technique are subjected to the errors caused in imaging (incorrect recognition of tumor, target, seed etc.). Hence, it is important to have an accurate and effective imaging and visualization solution to make the overall system robust [31]. Also the problems of needle flexing and tissue deformation need to be compensated for to comply with the required accuracy [32], [33]

1.4.2.2 Radiofrequency ablation

This is a minimally invasive thermal ablation technique in which a needle-like electrode is placed inside a tumor under image guidance. The electrode consists of an insulated metal shaft except for an exposed conductive tip that is in direct electrical contact with the cancerous tissue through which radiofrequency waves are passed with frequencies ranging from 450 to 500 KHz. This induces ionic agitation that destroys the cancer cells.

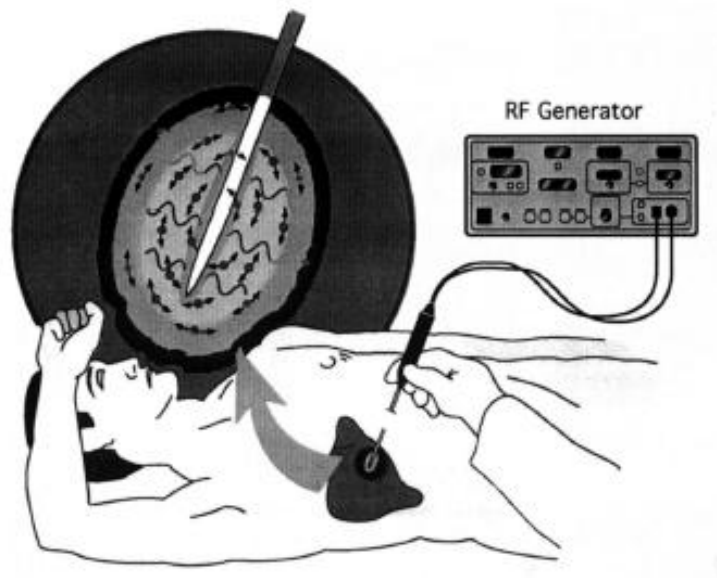


Figure 1.7: Radiofrequency ablation

The benefits of this technique include its ability to produce large volumes of coagulation necrosis adding to the advantage it has of a localized way of treating cancer [9]. Multiple radiofrequency electrodes can be used together to get larger necrosis volume [34]. The usual setup of radiofrequency ablation consists of single or multiple electrodes with a radiofrequency generator source, one or more grounding pads which act

as reference electrodes closing the electrical circuit and one or more image guidance modalities such as US, CT or MRI to help trace the needle towards the target. Figure 1.8 shows the radiofrequency ablation probe used to conduct experiments for this thesis.

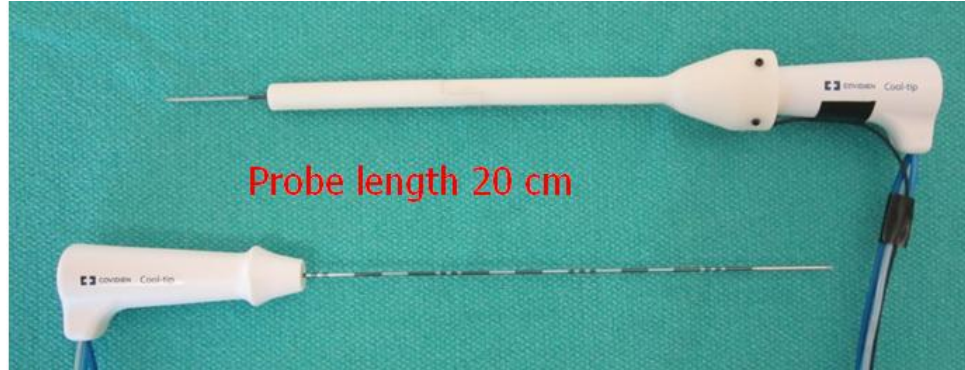


Figure 1.8: Radiofrequency ablation probes

It is essential to have image guidance to ensure proper placement of the electrode tip at target locations and to obtain feedback of the ablation process while the procedure is ongoing. Imaging is also used to evaluate the treatment after ablation is completed [35].

1.4.2.3 Microwave ablation

This is a similar concept to radiofrequency ablation except that microwave energy is used for ablation. Microwave ablation can be considered as a special case of dielectric heating, the tumor acting as a dielectric material in this case [36]. Microwaves lie in the frequency range between 900 to 2450 MHz.

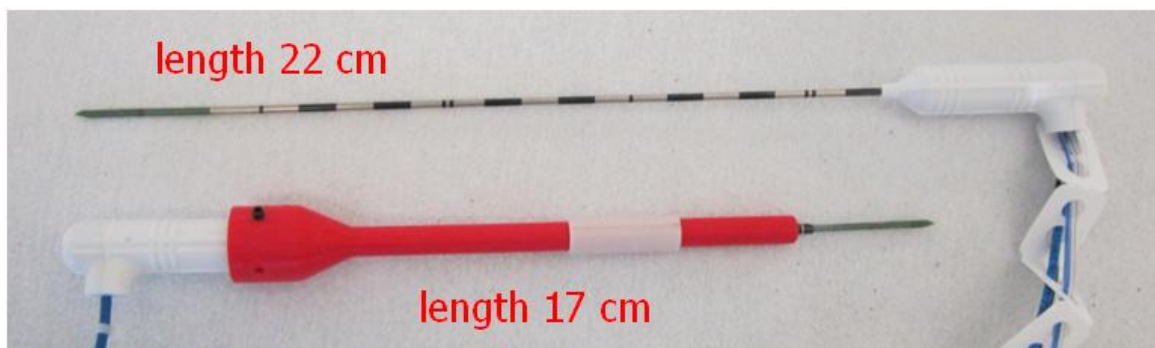


Figure 1.9: Microwave ablation probes

When applied to tissue, they induce an alternating electromagnetic field that forces water molecules to vibrate at a very high frequency. Due to this kinetic energy of water molecules, heat is generated thus causing thermal ablation. Microwave ablation is a relatively new technique that can be used in any type of procedure where radiofrequency ablation is currently used to ablate various forms of tumors. It offers almost all the benefits that radiofrequency ablation has to offer in addition to some advantages such as reduced procedure times, reduced heat-sink effects and lower intra-procedural pain and complication rates [37], [38]. The microwave ablation setup usually consists of a microwave ablation probe and a microwave energy generator. There is no need of grounding pads in microwave ablation which can be considered as another advantage over radiofrequency ablation resulting in a simpler procedural setup. Multiple microwave ablation probes can be used to achieve a bigger ablation volume. Image guidance helps to maneuver the needle to the target location.

1.4.3 Current scenario

For most of the tumors whether formed in the liver, breast, kidney, prostate etc., the basic treatment techniques of resection, chemotherapy, radiation therapy are preferred when the diagnosed cancer is at an early stage. Cancer recurrence rate is the lowest for these techniques. Combination of these techniques can be applied to minimize cancer recurrence [39]. Use of brachytherapy and other localized treatment techniques are usually performed when the patient is not deemed to be suitable for surgical resection due to age, health condition, the state of the cancer or other relevant reason. Minimally invasive surgery proves to be a good alternative as it significantly reduces trauma [40].

At present HDR brachytherapy and radiofrequency ablation techniques are being used for minimally invasive lung cancer treatment. CT, MRI imaging is used as a feedback modality to locate the targets and seed locations for cancer treatment due to the drawback of using US (produce bad images in presence of air). HDR brachytherapy is preferred over LDR brachytherapy as the issue of seed migration is averted in the former (since the radioactive sources used are retracted when the procedure is completed). Brachytherapy is a common treatment technique for prostate cancer where US can be

used effectively as an imaging modality (US imaging is much better in the prostate compared to the lung).

Among thermal ablation techniques, radiofrequency ablation is more commonly used since it is relatively older technique with sufficient clinical results demonstrating its effectiveness [41], [42]. Recent research described in [38] compares radiofrequency ablation and microwave ablation and shows that microwave ablation gives larger ablated necrosis region in relatively lower procedural time and can be alternative treatment option for lung cancer patients. The results are still from early stage research work and more tests need to be completed before microwave ablation can be completely accepted as a lung cancer treatment option. However, it has been proved that microwave ablation has all the benefits that radiofrequency ablation provides [43] while not being affected by the “heat sink” drawback for radiofrequency ablation [38].

For minimally invasive surgical techniques to work well, imaging is very important as it provides “real-time” feedback of the surgical site and helps to evaluate the entirety of the procedure [44]. Knowing the locations of the targets where brachytherapy seeds need to be injected, or the locations where the ablation probe antenna needs to be placed is vital. At certain times, situation arises where the needle gets deflected while it is being inserted in the tissue. It becomes critical to assess the situation, re-align and re-adjust the needle so that the tip can reach the specified target. Currently, the most feasible resource for imaging is US, which is cheap to use and gives live feedback of the surgical site, however, it is not possible to understand the complete scanned region by visualizing just a 2D image plane. US work well with liver and prostate brachytherapy. But with lungs due to the air artifacts present within the tissue, the image quality is much worse and makes it hard to understand the surgical site (drawback of US). With added motion due to heart beats and respiratory system, reaching the target becomes even more complex for the user.

A need to address the above-mentioned drawbacks provided the motivation for the work described in this thesis. A system would be designed that would overcome the drawbacks and integrate the various MIS techniques under a single architecture. This

would enable a clinician to perform cancer treatment more intuitively with a better cognition of the surgical site. The following sections describe the image-guided intervention approach and use of robots in the surgical field followed by a description of an older version of the system that was implemented at CSTAR (Canadian Surgical Technologies & Advanced Robotics, London ON, Canada). The final section lists the contributions made by this thesis and implementation of the InterNAV3D application system.

1.5 Image-guided intervention

Image-guided intervention is a relatively novel treatment approach which refers to the use of computerized imaging systems to provide feedback while treatment is being performed. The common medical imaging modalities include US, CT, MRI. With the help of this feedback, surgical tools are inserted into the body of the patient and maneuvered to the desired target location. Computers can also be used to process the images thus captured so as to segment out the physical attributes present in them. This helps in improved diagnostic capabilities, improved target selection and localization during the procedure. Integrating a virtual reality environment that depicts the surgical site and the movements of the tools and organs, could assist the user to gain better cognition for carrying out the treatment procedure. An image-guidance interventional system typically integrates image acquisition, image processing (registration, segmentation, etc.), virtual reality visualization and planning scheme techniques. Exploiting these, accurate interventions with minimal errors could be delivered. Image-guided intervention techniques are used in numerous types of surgical procedure [45]–[49]. Figure 1.10 shows a typical image-guided intervention platform. The advances in technology help to achieve improved patient outcome and safety, overall reduction in complications and patient morbidity.

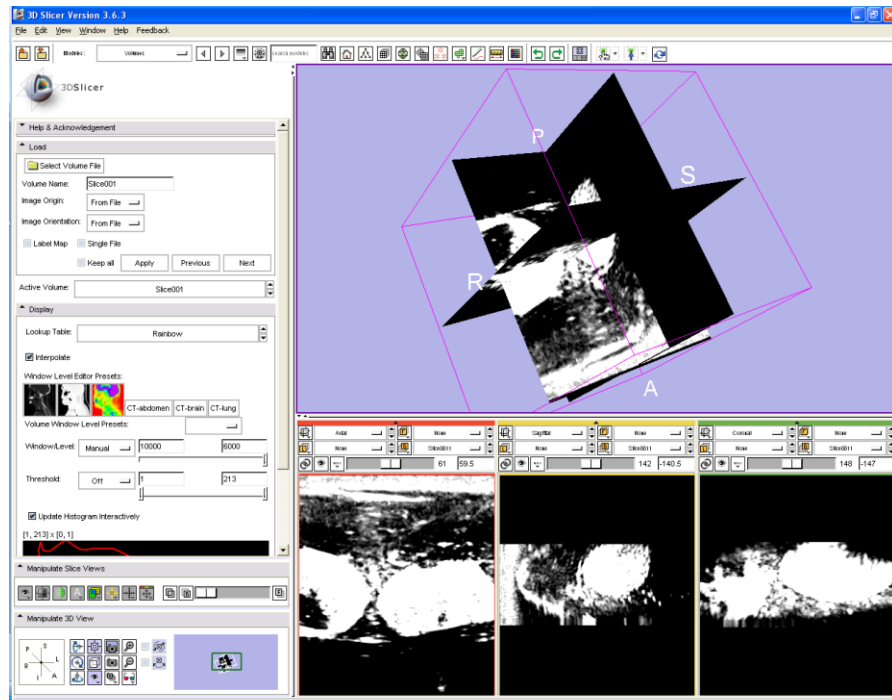


Figure 1.10: Image guided intervention platform

1.6 Robot-assisted minimally invasive surgery

Surgical robotics is a technology-driven area of medicine which has experienced a tremendous growth and improvement over the last 2 decades to improve upon the current scenario of surgical applications, mostly in MIS. It is driven by the motivation to achieve greater precision, less procedural time and faster recovery of patients (as a result of minimizing invasiveness) by overcoming the limitation of MIS so as to enhance the capabilities of the surgeon. Various research projects described in [2], [50]–[52] show the applications of robotics in MIS.

The primary drawback of hand-held tools for MIS is the limited dexterity offered by the surgical tools. These tools are not generally ergonomic and are in general challenging to learn to use efficiently. The surgeon has to hold tools the entire time and needs to be extra cautious not to make any aberrant movements. Additionally, hand tremors cause unwanted motions at the tool tip which can lead to inaccuracies and errors during surgery. Inclusion of a robot between the surgeon and the patient could help compensate for such errors by filtering out such tremors [53]. Filters can also be applied

to remove any sudden jerks or motion. The use of a master-slave robot combination (tele-operation) serves to improve the efficiency of the surgeon by providing more ergonomic conditions for the surgeon who sits at the master console during surgery. The most important aspect of robotic surgery is the improved accuracy of tool motion and placement. The new technique to include specialized tools with multiple degrees of freedom further enhances the surgeon's ability to perform complex procedures with ease [54]–[56]. The use of robots also reduces the time required to complete a surgical procedure [53], [57] compared to conventional MIS. Various operational modes such as auto aligning the tool, auto tool insertion etc. can be performed by the robot using the interface design provided. Several papers have been published in recent years that summarize the current state of surgical robotics [58], [59].

1.7 InterNAV

Due to high mortality of lung cancer, new projects are being implemented to improve its treatment system. Robotic technologies are being applied to make the system more robust, automated and easy to use. They reduce the errors generated due to hand tremors and fatigue [60], [61]. Integration of robotic technologies also provides the needed dexterity for certain surgical tasks. Image processing techniques improves the quality of the images and assists the user to perceive the artifacts present in the images clearly. The addition of a virtual reality environment provides an enhanced perspective of the surgical site. One such research project has been implemented at CSTAR and is a novel approach for interstitial brachytherapy. The system consists of master-slave operation, a seed placement device for injecting radioactive seeds and a laparoscopic ultrasound (US) probe for real-time imaging. These instruments are mounted on surgical robots (a ZEUS and an AESOP) made by Computer Motion Inc. These robots have been modified to bypass their controllers to obtain open architecture systems. This allows the implementation of custom designed controllers. Electromagnetic trackers were placed on the tools in order to track their real-time orientation and position [2]. Figure 1.11 shows the experimental setup. Detailed information will be presented in the upcoming chapters.

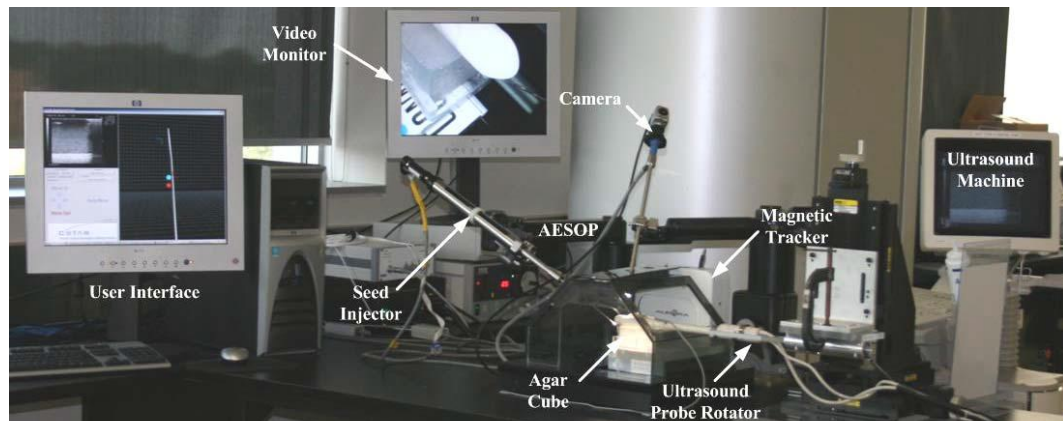


Figure 1.11: InterNAV setup for lung brachytherapy

As part of the system, a visualization and control software known as InterNAV was developed. It consists of a Graphical User Interface (GUI) which interacts with the robotic brachytherapy setup and the US machine, giving the ability to control the entire system. It is a virtual reality environment that displays a set of 2D US images in a 3D world. It enables the user to select target locations for brachytherapy seed injection.

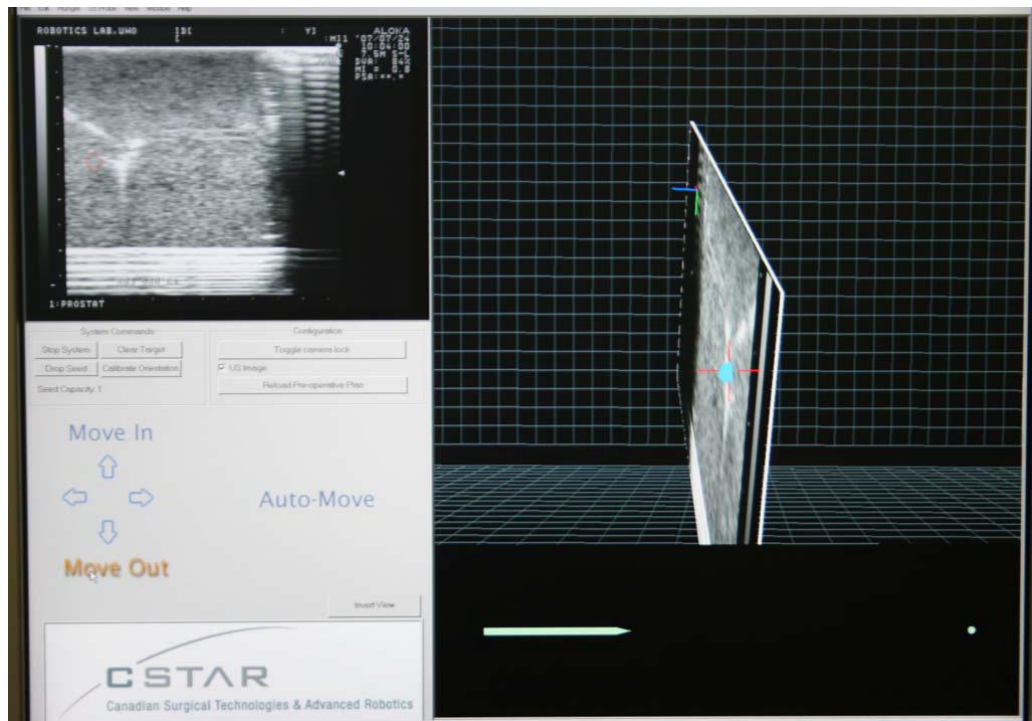


Figure 1.12: InterNAV user interface

An automated seed injection device mounted on a robotic arm is used to navigate and drop the seeds at those targets. A first person eye view of the system looking from the needle tip was implemented which helps in easy guidance of the needle. Figure 1.12 shows a snapshot of the InterNAV interface. Researchers have shown that the use of a robotic system and image guidance reduces tissue trauma and improves seed placement accuracy [4].

Though the system provides good results as compared to an open surgical procedure [2], [62] there are some drawbacks:

- The system provides a 3D virtual world view with a 2D image plane suspended in it at the specific location with respect to the electromagnetic tracker co-ordinate frame. Though it helped to visualize and understand the surgical site, it was very difficult to gain perspective of the size and structure of the tumor. Even with pre-operative imaging, judging the orientation of the tumor was very non-intuitive.
- The system lacked the capability to capture and visualize 3D images.
- At certain times, the needle bends and deflects while being inserted into tissue. The system lacked the features needed to provide information about the structure of the needle and its probable location after needle bending.
- Knowing the path history of the needle tip is very helpful in order to visualize the probable path the needle might take. This would help the clinician to retract the needle along the same path so as to keep tissue damage to a minimum. The system had no feature implemented for needle retraction.
- The use of US in the lung makes it prone for faulty recognition. Applying image processing techniques enhance the images and guide the user to determine various physical artifacts present in an image. InterNAV provided a real-time imaging feedback but lacked the feature to enhance the images for improved visualization.
- For lung cancer treatment, there is always a residual motion even after a lung is collapsed due to cardiac motion and/or due to respiratory motion of the

contralateral lung. The previous system had no features to account for motion compensation or visualization in the virtual world.

- InterNAV lacked the feature to implement other novel lung cancer treatment techniques such as radiofrequency ablation and microwave ablation.
- A feature to use the system as an offline processing and training tool by using pre-captured image data was not available in InterNAV.
- Re-evaluation and re-optimizing the dosimetry plan in real time is necessary as erroneous seed deployment may occur often. The process to re-evaluate the locations of the seeds and accordingly update the visualization system was also a missing feature.

All of the above drawbacks of InterNAV led to the development of a much more extensive, accurate and integrated system that has been termed InterNAV3D in this thesis.

1.8 Thesis contribution

This thesis mainly focuses on the development of InterNAV3D. It is a complete new system that was developed to incorporate all the missing features mentioned above and to overcome the drawbacks of the previous version of InterNAV. The various enhancements mentioned below are integrated in the new system which comprises the major part of the research contribution of this thesis.

A complete new and enhanced system, InterNAV3D, has been developed and evaluated. It uses the Visualization Tool Kit (VTK) and the Insight segmentation and registration Tool Kit (ITK) as the major developer interfaces for the design of the system. A new experimental test-bed has been developed along with the software interface which implements image processing techniques.

The new system includes a feature to grab a sequence of images in certain pre-defined capture modes which reconstructs and displays 3D image volume. A capability to

add multiple image volumes have been implemented which helps to form a complete 3D structure of the surgical site. It not only overcomes the problem of target selection in 2D view but also helps in optimizing dosimetry planning. Various modules such as surface reconstruction, cross-sectional slicer, etc. are included in the new system. These modules help to visualize the tumor in a more intuitive way. The surgical tools are modeled as Stereo Lithography (STL) objects and rendered in a real-time 3D visualization world, providing a more realistic view of the surgical site. Needle path projection, prediction and visualization history of needle tip location are integrated. It provides more generic real-time view of the needle structure and helps to understand the needle movement and its tracking behavior. An algorithm to visualize the needle tip and compensate the visualization for needle bending is integrated. Image processing techniques such as opacity control and visibility control to explore properties of the physical entities present in the 3D view have been implemented. Algorithms performing region growing segmentation, needle tip detection, etc. have been implemented. The full dexterity of robotic movements is utilized for capturing US images in various modes such as round (rotational) sweep, straight (flat) sweep, and ablation sweep.

An algorithm to construct 3D volumes using a series of captured images has been implemented. Various *ex-vivo* experiments were performed and the results are described in this thesis. Radiofrequency ablation and microwave ablation, along with a C-arm X-ray imaging modality have been incorporated in the newly designed system to improve the performance and reliability of tumor visualization and the lung cancer treatment procedure. A novel approach to estimate the entirety of the thermal ablation by evaluating the changes in the 3D volume is discussed. Recording and evaluating the target locations, compensating for any motion during visualization has been implemented. *Ex-vivo* and *in-vivo* experiments to evaluate the system were performed and the results are described. The versatility of the new system allows the implementation of the developed techniques for similar cancer treatment procedures in other organs such as liver, kidney and breast.

1.9 Thesis outline

Chapter 1 – Introduction: This chapter describes the current scenario for lung cancer treatment and gives a literature review followed by the motivation and research objectives of the thesis.

Chapter 2 – System Architecture: This chapter focuses on the hardware and software components of the system and also outlines the various algorithms developed and used in the system. It details the working of the system with an added focus on the integration of all the components

Chapter 3 –User Interface: This chapter presents an overview of the GUI, various modules developed and different modes of operation.

Chapter 4 –Experimentation and Results: This chapter gives a detailed overview of the various experiments performed and the results obtained. It also outlines several sources of errors, the calibrations performed and the logic behind the experiments conducted.

Chapter 5 –Conclusion and Future work: This chapter summarizes the overall design of the InterNAV3D system, its potential applications for cancer treatment in other areas, and some directions for the future work.

Chapter 2

2 System Architecture: Hardware and Software

As discussed in the previous chapter, there is a need to develop novel technologies to help treat cancerous tumors in the lung. InterNAV [3] was conceived as a research and development project to integrate the MIS technique of brachytherapy and robotics with virtual reality environment.

The contribution of this thesis was the development of InterNAV3D, which was created as an enhancement of InterNAV. It incorporates techniques of image processing, 3D visualization, motion simulation, and implements novel software modules for better needle maneuvering. Integration of all new techniques makes it a state-of-the-art package which improves on the time, speed, accuracy for the complete procedure with enhanced feature recognition techniques. The details of the implemented algorithms, new features and modifications will be provided in subsequent chapters. This chapter deals with the system architecture. Being a mechatronic system, it would be easy to understand its working by dividing the system into its hardware and software components and working down to the core developments.

Figure 2.1 illustrates the system and its organization. The following section details all of the individual components and their contribution to system co-ordination.

2.1 System overview

InterNAV3D has a software interface front end package installed on a computer which acts as a remote workstation. It is a graphical user interface that has a virtual reality 3D environment. It renders the physical entities present within the surgical site and mimics their motion in the virtual world. The 3D environment represents the Cartesian co-ordinate space of NDI's Aurora electromagnetic tracking system [63]. The field generator is placed below the test-bed such that the generated alternating magnetic field covers the surgical site. The virtual environment can visualize any 3D objects, volumes and similar data. The system also integrates various image processing and visualization modules to

help process the images received from the imaging modality. Currently, US is used as the primary real-time imaging feedback. The US machine used for this project is the Sonixtouch from Ultrasonix [64] and the US probe used is the laparoscopic probe LAP9-4/38. The output of the US machine is directed to a frame grabber, the Matrox Vio-Duo by Matrox imaging [65] which is installed on the PCI express slot of the computer motherboard. MIL is the software library that takes care of getting the US images from the frame grabber. The electromagnetic trackers attached to the needle tool and US probe feedbacks the current position and orientation information needed for virtual rendering.

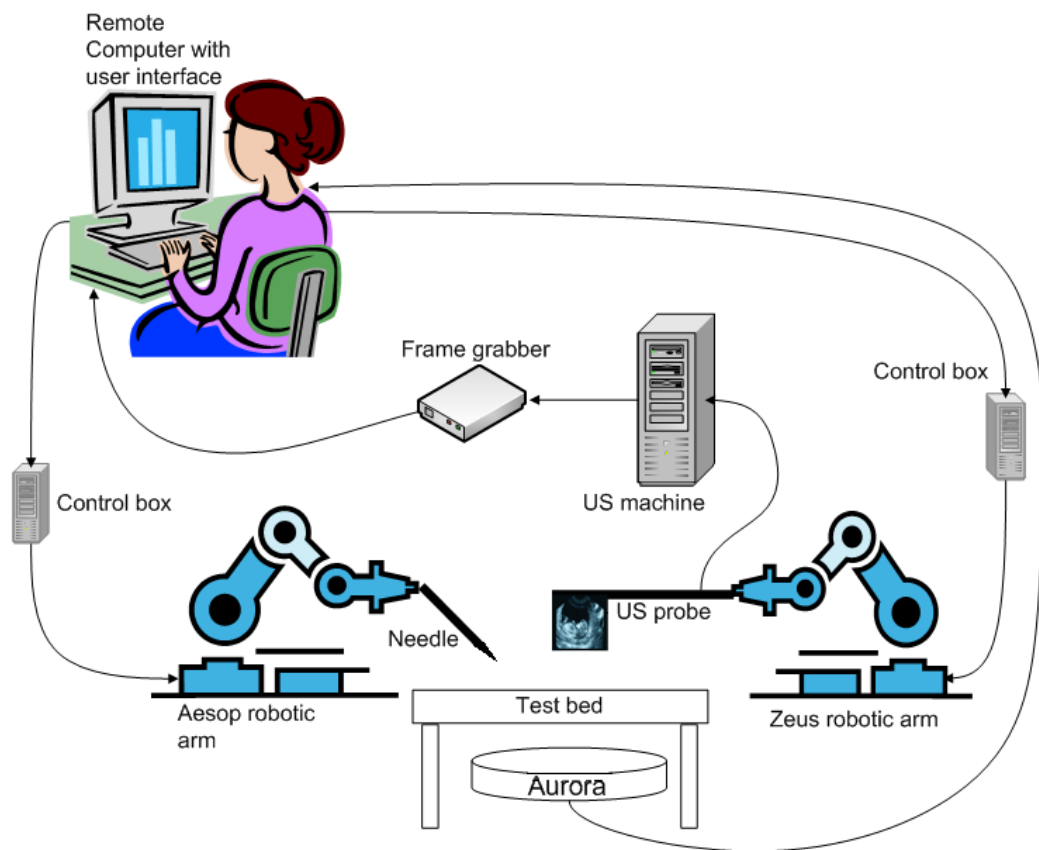


Figure 2.1: System overview and working

The field generator is installed under the physical setup/test-bed as shown in Figure 2.1. The feedback from Aurora is given to the computer. The InterNAV3D software then renders the captured images on the 3D world created by VTK by using the

tracking information from Aurora. VTK is a visualization library that was integrated with InterNAV3D for 3D mapping of the given information. It runs within InterNAV3D and gives visual representation of all the data. It takes care of all the mapping of the physical components in the virtual reality world. The inbuilt modules created in InterNAV3D run on VTK for visualization and rely on ITK for image processing. VTK and ITK go hand in hand in getting all the data to be processed and visualized as the system demands.

The needle tool and the US probe are mounted on the ZEUS and AESOP (Automated Endoscopic System for Optimal Positioning) robots which are attached to the computer through a controller device. The feedback from the magnetic tracker and the US machine helps in moving and orienting the robots so as to maneuver the needle tool and the US probe to be placed at the required location within the surgical site. There are two modes to maneuver the needle to the target: auto-mode and manual-mode. The auto mode inserts the needle automatically so that the needle tip hits the target whereas the manual mode lets the user control the needle maneuvering.

2.2 System initialization and working

The working of the system can be explained by studying the flowchart provided in Figure 2.2. We need to initialize the hardware and software components before the 3D environment is generated.

At system initialization, SAW (Surgical Assistant Workstation) commences its communication pipeline. It opens connections to hardware profiles (AESOP and ZEUS robots, Aurora magnetic tracker and electromagnetic sensors, Matrox frame grabber) so that they are ready to be used. Software libraries such as VTK and ITK are initialized. Required calibrations are performed and selective 3D components are displayed.

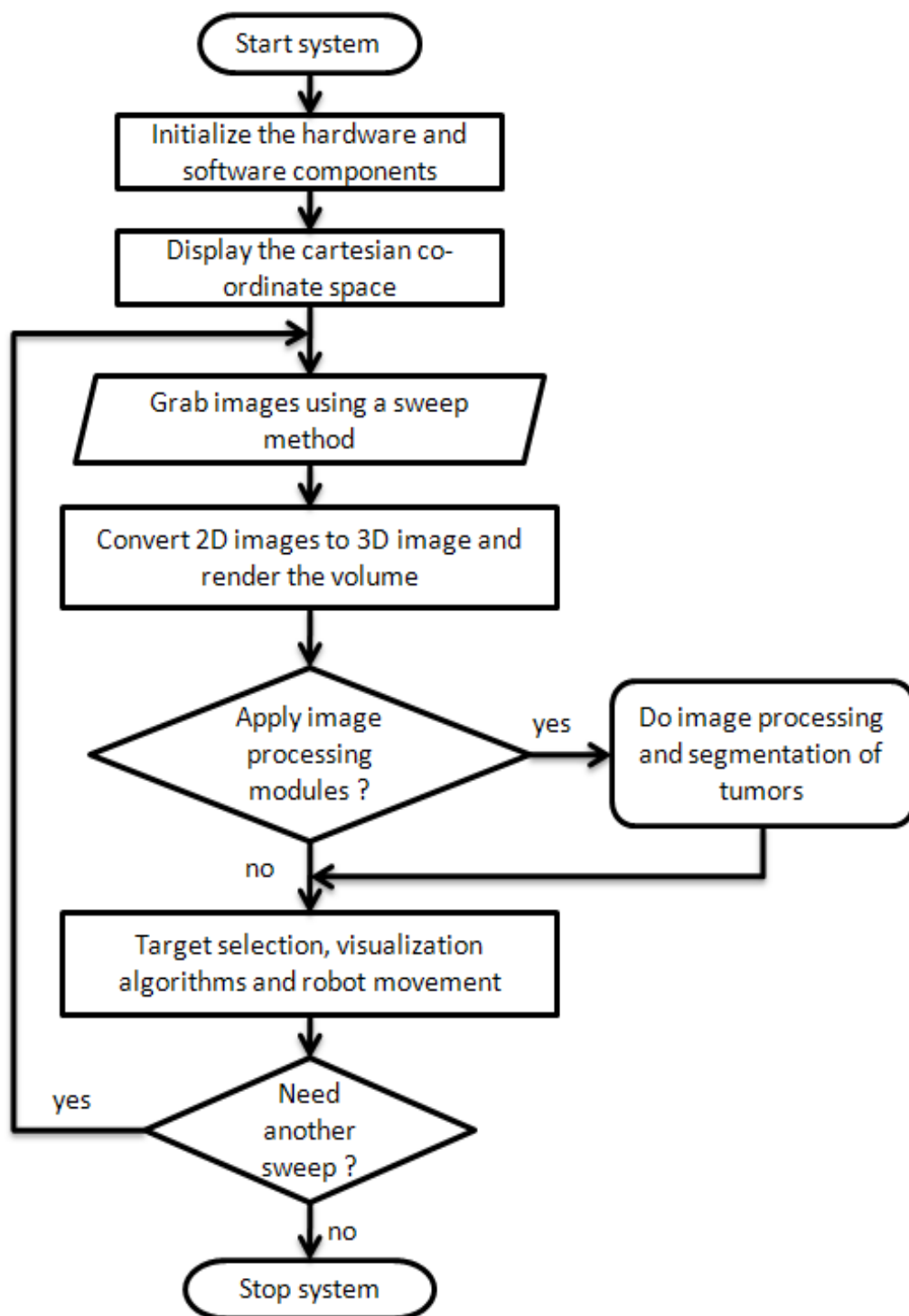


Figure 2.2: Flowchart for system initialization and working

The user needs to choose one of the sweep profiles (straight-flat sweep, round-rotation sweep, palpation sweep or ablation sweep) and provide the required parameters such as the number of images that need to be grabbed and the divergence (angle or time) between successive images. Accordingly, appropriate commands are passed to the US robotic arm which moves in the required fashion. The software then grabs images during the sweep motion. At the same time, the values from the electromagnetic tracker are recorded. Algorithm to convert the set of 2D images to a 3D image volume conforming to the shape of the sweep capture mode is initiated. As the 3D image is generated, it needs to be rendered at appropriate location in the virtual 3D space. For this, the electromagnetic sensor values recorded earlier are used and after applying appropriate calibration values from sensor to the US image location (discussed in Chapter 4); the volume is rendered in 3D space. Appropriate visualization parameters such as the opacity function and color-transfer function are applied. Simultaneously, surface reconstruction and region growing algorithms for locating the tumor are performed. The results are rendered on the 3D visualization window. If the user is satisfied, he/she can go to next step, else he/she can use the various built-in modules such as window thresholding, piece-wise opacity transfer function and many other to make the data more clearly presentable for understanding the nature of the surgical site, location of tumor, its structure and size. After this step, the user needs to select the target where he/she wants the needle tip to go. Once selected, the user can proceed manually or use the auto-move method built in the software to align and maneuver the needle to the selected target. There is another electromagnetic sensor present on the needle which helps to visualize the needle in the 3D visualization window. The tracker information is constantly queried and the visualization window is updated accordingly. It provides real-time feedback of the location and orientation of the tools connected to the robot and helps in determining appropriate commands that need to be sent to the robot to move it in a particular direction. The needle needs to be calibrated beforehand using the pivot calibration method (discussed in Chapter 4). The user can grab multiple volumes at several distinct locations during the procedure. These volumes are rendered and stitched together to form an enlarged 3D structure of the underlying tissue and provides better understanding of the surgical site. It helps in registering the tumors thus found with pre-operative imaging by

co-relating with the adjacent physical entities and other similar structures. The overall visualization of the surgical site is enhanced and helps user to understand the virtual world. It improves the visual perception of the user and helps him/her decide the next course of action.

Certain times needle gets deflected from its intended path within the tissue during an insertion procedure. It happens due to uneven tissue stiffness, the design of needle tip (such as bevel tip) or any similar reason. Grabbing multiple volumes during a needle insertion procedure provides with the useful information of the needle behavior within the tissue. It guides in determining the needle shape and location. Real-time US video feedback with enhanced image processing algorithms and visualization modules help to pin-point the location of the needle tip. Options for needle path prediction, needle path projection, etc. assist the user to predict and visualize the future path that the needle might take and in turn allow to update the needle orientation. The user determines the error with respect to the intended path and updates the needle maneuvering accordingly. The required course of action is revised and the needle is kept on the required track to the target. Once the user thinks he/she has reached the target, he/she performs a re-evaluation of the surgical site and applies the imaging and visualization modules needed to ensure that the target was reached successfully and accurately. Once the user is satisfied, appropriate treatment techniques such as deploying brachytherapy seed and/or thermally ablating the tumor are performed. If the user is not satisfied, he/she realigns the needle and repeats the complete maneuvering steps. After the method is performed, the needle is retracted using the same path as for insertion (using the needle path history visualization), to ensure that tissue damage is kept to a minimum and that the needle is retracted safely. Once the needle is out of the specified area, the user moves to the next target/tumor and performs the same steps or else stops the system if the procedure is deemed to be completed. This is essentially how the InterNAV3D system is expected to be used. More details about the hardware and software profiles are discussed in the next section.

2.3 System components

The system hardware and software components are described in detail below. Specific attention is given to the hardware that was used and the software that was integrated in the InterNAV3D system and the functions that they perform.

2.3.1 Hardware components

The following are the major hardware components.

2.3.1.1 US machine and imaging

As discussed in the previous chapter, US remains the most feasible source of real-time imaging due to the ease of use, cost-effectiveness and benefits over other imaging techniques (US being a non-ionizing radiation) [4].



Figure 2.3: Ultrasonix's Sonixtouch US machine

The US machine “Sonixtouch”, shown in Figure 2.3, from Ultrasonix was used for the experiments described in this thesis. The Sonixtouch machine is a diagnostic US system which comes with an US Research Interface (URI) installed. The URI is a term referring to the US machines which allows for various diverse operational modes that purely clinical system does not have. It gives a wider range of parameter modifications for generating US images. In addition to the URI, the US machine used also allows transducer prototyping and development of commercial US applications. It has an elastography mode that can be helpful for better image analysis (to be integrated in later versions of InterNAV3D). It is of significance to mention here that InterNAV3D is very customizable to accommodate any other US imaging system as well as any other medical imaging technology such as CT, MRI etc. A comprehensive outline of the principles behind the technology can be found in the literature, e.g., [66]–[72]. The US probe used for InterNAV3D is a flexible laparoscopic probe LAP9-4/38 as shown in Figure 2.4.



Figure 2.4: Laparoscopic probe used

The characteristic of this probe is its ability to move in 2 different degrees of freedom due to its flexible end. Figure 2.5 shows the transducer and its flexible end.



Figure 2.5: US probe bent from the flexible part

There are switches provided at the probe handle that help to maneuver the probe transducer. Currently this feature is not used in InterNAV3D since the robot used for the probe movement provides a higher dexterity and has better controlled movement and placement. For the experiments performed, the flexibility of the transducer end was restricted by attaching an external sleeve (manufactured in 3D printer) as shown in Figure 2.6.

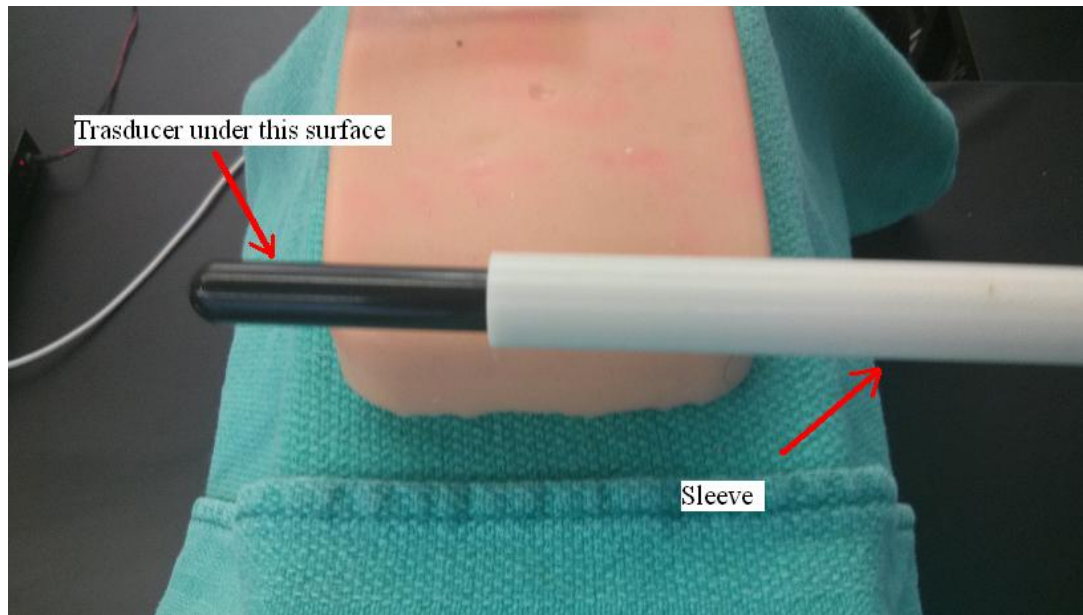


Figure 2.6: US probe enclosed in a sleeve

2.3.1.2 Electromagnetic tracker

InterNAV3D is designed for use in minimally invasive interventions. One way to track the tools during surgery when they are inside the patient's body is to use optical tracking (placing physical markers on the tools and using computer vision to deduce its position and orientation) by getting the video stream output from the endoscope. Though it is possible to get position and orientation in space using imaging techniques, it is difficult to determine these when the vision is blocked (for optical tracking to work, it is favorable to have a clear line of sight to the markers). For such cases, electromagnetic tracking can be helpful. The sensors can be installed on most of the surgical tools such as catheters, bronchoscopes, needles etc. [63], [73]–[77]. This tracking system determines the spatial parameters of embedded sensor coils when placed in an electromagnetic field. The concept behind the technology can be explained by looking at Figure 2.7.



Figure 2.7: Working of electromagnetic tracking system

A varying magnetic field is generated using the field generator device. When the sensor coil is placed inside this magnetic field, voltages are induced in them. Using these induced voltages, a measurement system determines the position and orientation of the sensor coil [78], [79]. A typical field generator is shown in Figure 2.8.



Figure 2.8: Aurora field generator

The magnetic field generated is of low field strength and can pass safely in human tissue, thus allowing the required measurements even when the line of sight constraint is not satisfied. For InterNAV3D, NDI's Aurora system was used as shown in Figure 2.9.

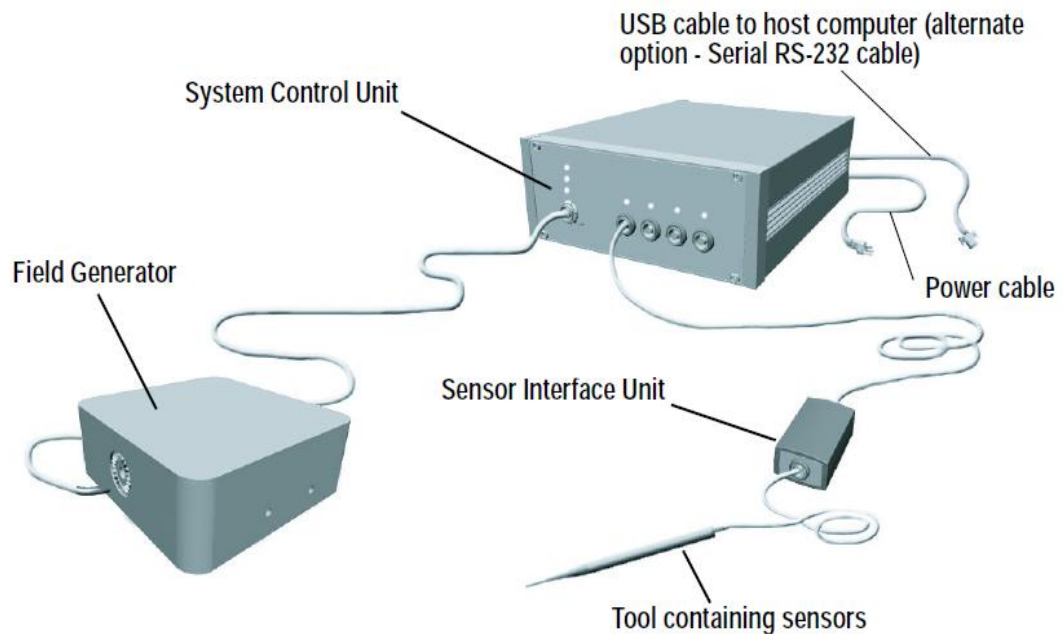


Figure 2.9: NDI's Aurora electromagnetic tracker system

This system is designed to be functional in environments with medical grade metals. Aurora comes with the Aurora Application Program Interface (API) which can be customized and used for research and development applications. This system is compliant with the medical equipment safety standards. A drawback however is still present. The measurement accuracy of the system is reduced if any ferromagnetic material comes in the vicinity of the magnetic field [80], [81]. Hence, proper placement of the field generator and use of compatible tools is advised, so as to minimize any such interference distortion. The origin of the co-ordinate system of Aurora lies at the center of the front surface of the field generator as shown in Figure 2.10.

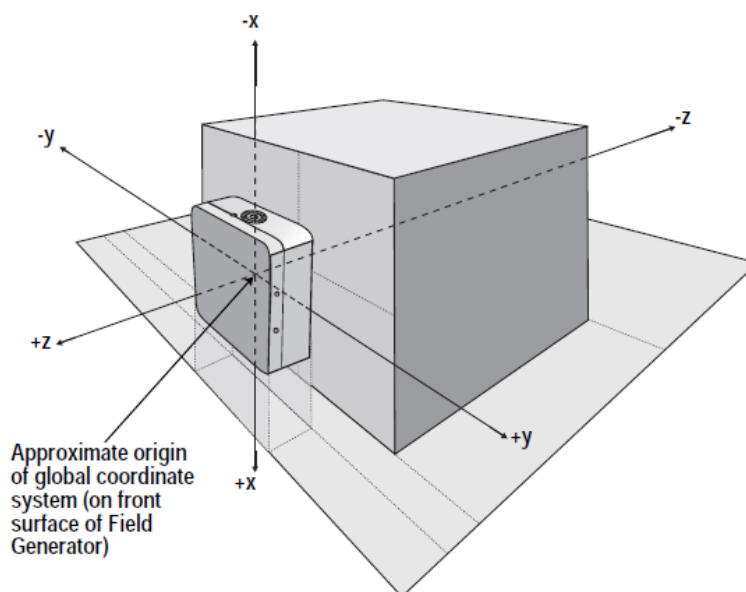


Figure 2.10: Field generator and the Cartesian co-ordinate space

Aurora supports two types of sensors based on the Degrees Of Freedom (DOF) needed for tracking: 5-DOF and 6-DOF.

They are manufactured in custom shapes (different lengths and radii) which make them more accessible for varied application requirements. A typical 5-DOF and 6-DOF sensor used for InterNAV3D are shown in Figure 2.11 and Figure 2.12 respectively.

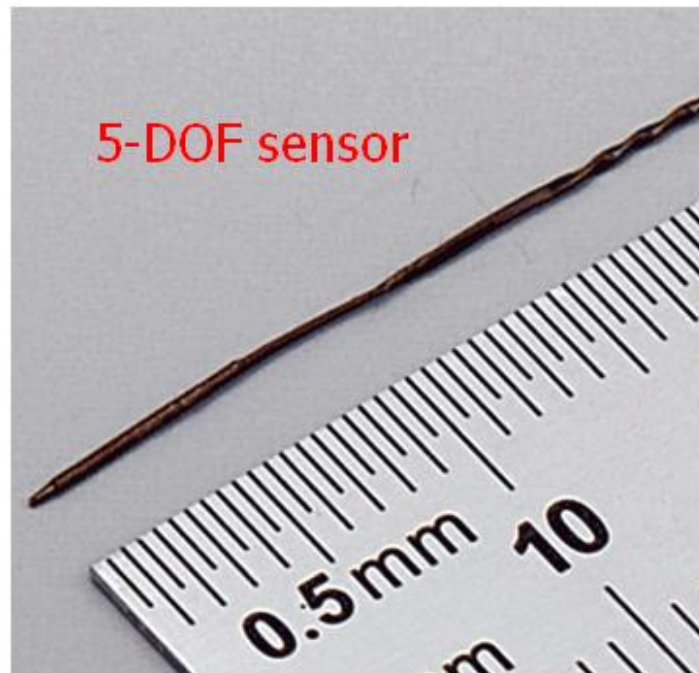


Figure 2.11: 5-DOF sensor

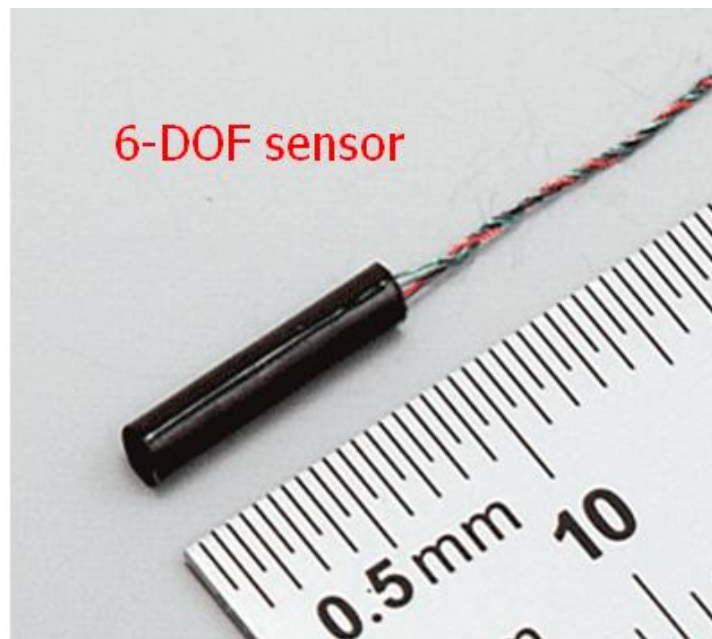


Figure 2.12: 6-DOF sensor

The diameter of the 5-DOF sensor is 0.5 mm and its length is 8 mm; whereas for the 6-DOF sensor the diameter is 1.8 mm and its length is 9 mm. Depending on the application and the physical position where the sensor needs to be installed, other sensors with different diameters and lengths can be used. The sensors are good for use in *in-vivo* applications.

The following table shows the accuracy of the tracking system as per NDI website.

Table 2.1: 5-DOF sensor accuracy

5-DOF sensor	RMS (Root Mean Square)	95% confidence interval
Position	0.7 mm	1.4 mm
Orientation	0.2 degrees	0.35 degrees

Table 2.2: 6-DOF sensor accuracy

6-DOF sensor	RMS (Root Mean Square)	95% confidence interval
Position	0.48 mm	0.88 mm
Orientation	0.3 degrees	0.48 degrees

The 5-DOF sensor gives the location of the sensor coil in Cartesian co-ordinate space (x, y, and z) with pitch and yaw as the orientation parameters. It lacks the ability to determine roll which is possible in 6-DOF sensor. Pitch, roll and yaw are the rotation angles made by the object around the 3 orthogonal axes passing through its origin. Figure 2.13 shows the pitch, roll and yaw for a typical 6-DOF sensor.

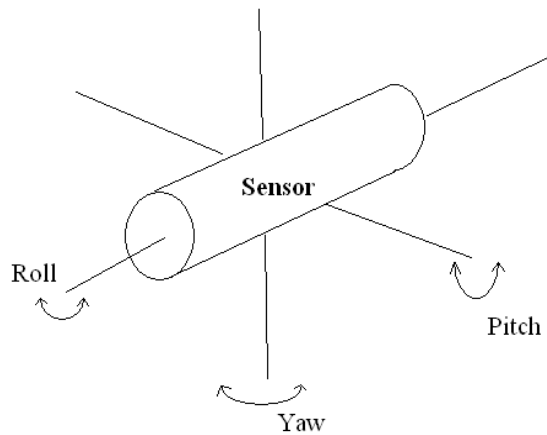


Figure 2.13: Roll, pitch and yaw

Depending on the tool, an appropriate sensor was selected. For experiments with a brachytherapy needle, the sensor can be aligned to the axis of the needle which makes the roll information vestigial. Hence a 5-DOF sensor was used. The sensor was placed aligned to the axis of the needle as shown in Figure 2.14.

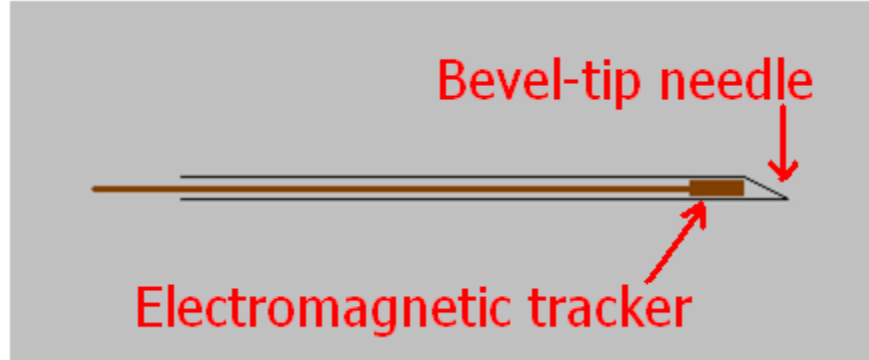


Figure 2.14: Bevel-tip needle with 5-DOF sensor enclosed

For thermal ablation needles, 6-DOF sensors were used since the information of roll was necessary to determine the location of the needle tip (by using the pivot calibration method). Specialized sleeves were manufactured for placing the sensor on the ablation needle and for attaching it to the robot. Figure 2.15 shows one such sleeve manufactured using a 3D printer.



Figure 2.15: Sleeve for radiofrequency ablation probe with the channel for EM tracking sensor

Figures 2.16 and 2.17 shows the ablation tools with the sleeve placed over them and the sensor attached within the sleeve.

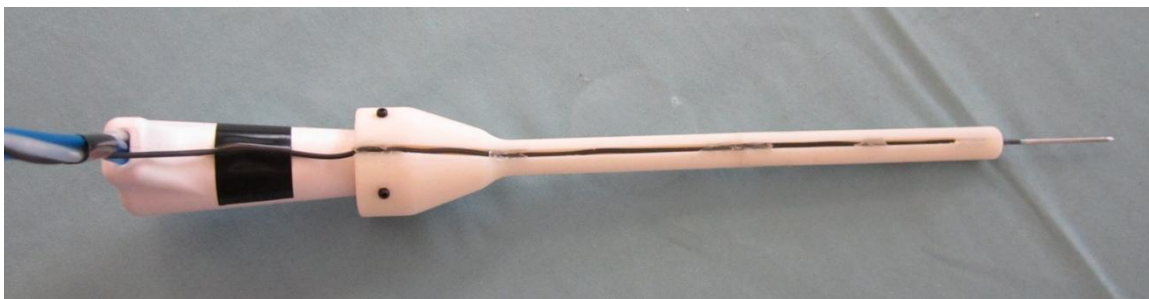


Figure 2.16: radiofrequency ablation probe with sensor attached to sleeve



Figure 2.17: Microwave ablation tool with sleeve and sensor attached

For the US probe, it was necessary to have the roll information so as to construct 3D volumes. Therefore, a 6-DOF sensor was placed on the surface of the probe as shown in Figure 2.18.

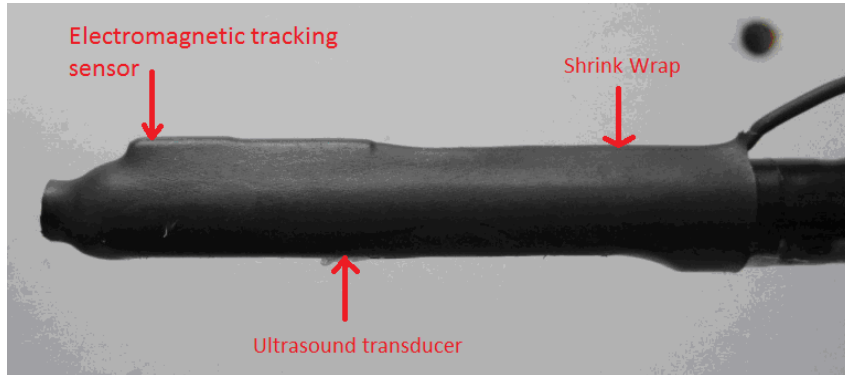


Figure 2.18: US probe with electromagnetic sensor attached using shrink wrap

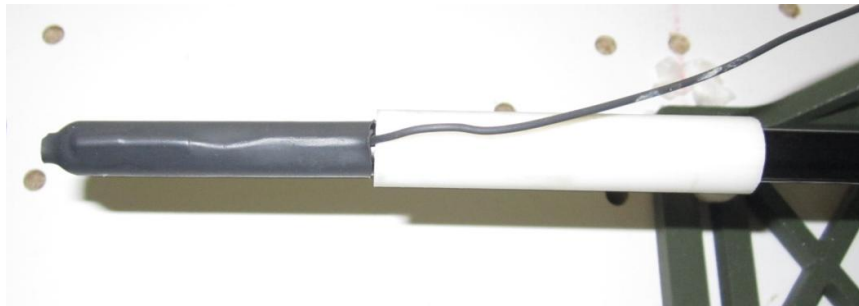


Figure 2.19: US probe with the attached sleeve

It is always important to ensure that the physical placement of the sensor does not change with respect to the surface it is placed on. For the calibration to work, the relative motion needs to be zero. For US probe, a shrink wrap was used to affix the sensor to its surface such that there is no relative motion between them. Figures 2.18 and 2.19 show the US probe with an attached sensor. Precaution was taken that the shrink wrap doesn't hamper the imaging by cutting out the part of shrink wrap which covers the transducer. After the installation of the sensor, a calibration was done to find the local transformation of the image with respect to the sensor location. The calibration method used is described in Chapter 4.

2.3.1.3 AESOP/ZEUS robot

The robotic setup used for the application in this project was the ZEUS robotic system. The conventional ZEUS robotic system consists of two ZEUS robotic arms, which are used to manipulate the surgical tools using a console workstation, and an AESOP robotic arm which is used to manipulate the laparoscopic camera with voice control. This robotic system was manufactured by Computer Motion Inc. These robots are no longer available commercially since Computer Motion merged with another company; Intuitive Surgical Inc. Figure 2.20 shows the AESOP robot.



Figure 2.20: AESOP robot

The ZEUS robotic surgical system was developed for minimally invasive surgery. The surgical tools were mounted on the two ZEUS robotic arms. This system was based on a master-slave theme where the surgeon sits at a remote console workstation, from where he/she can operate the robotic arms as shown in Figure 2.21. This console enabled the surgeon to operate on the patient with joystick-like devices converting the surgeon's hand movements into precise micro-movements of the tool inside the patient's body [82].



Figure 2.21: Remote workstation for ZEUS robotic system

The hand tremors could also thus be compensated by using the robots. AESOP was designed as a robotic device for holding and manipulating an endoscope. There is not much difference in the hardware architecture of the ZEUS and the AESOP. The AESOP was designed to react to voice commands from the surgeon. Proper placement and configuration of robot arms is necessary [83]. Figure 2.22 shows the ZEUS robotic setup for surgery.



Figure 2.22: ZEUS robotic setup

Figure 2.23 and 2.24 show the kinematics of the robot. These robots are able to move in 4-DOF, rendered by controlled movements of 4 motors (highlighted in blue in Figure 2.24). It also has 2 passive degrees of freedom (highlighted as purple in Figure 2.24) which helps in providing appropriate orientation of the tool based on the pivot point location.

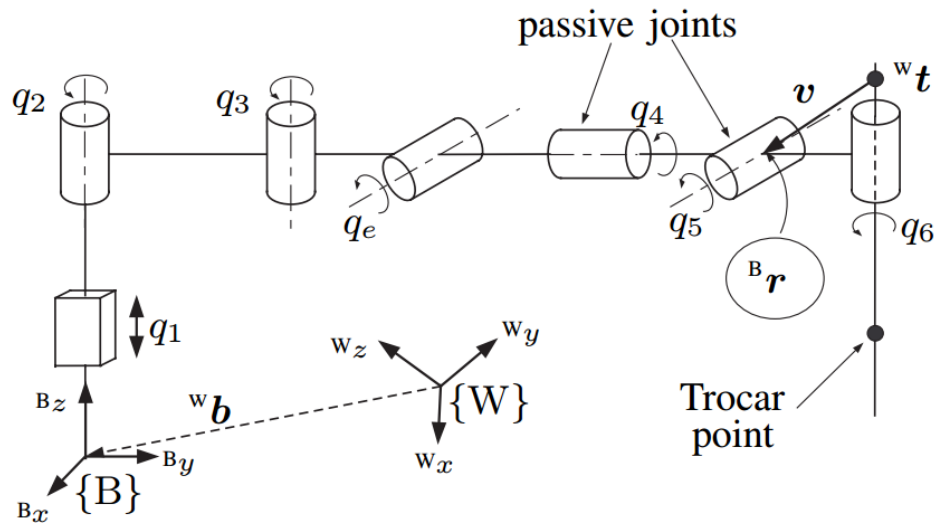


Figure 2.23: AESOP/ZEUS kinematic model

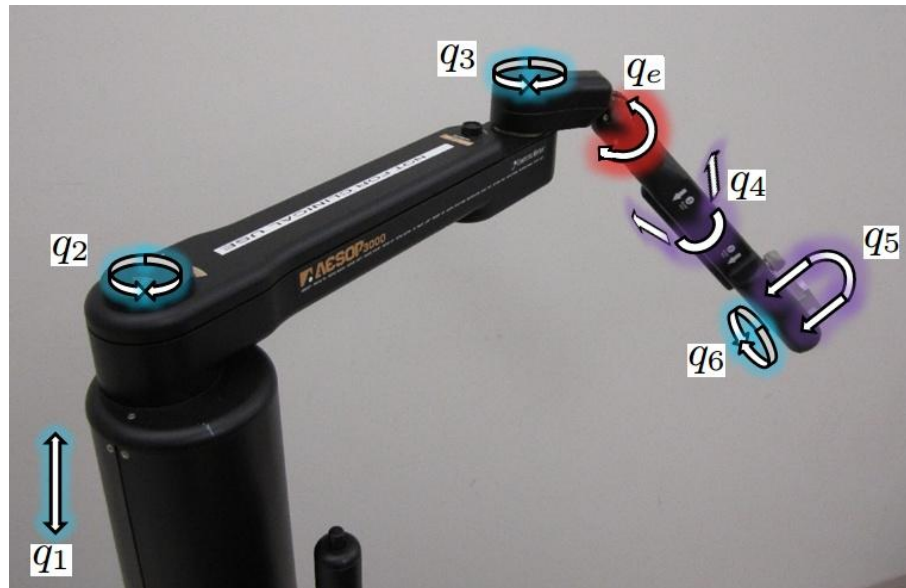


Figure 2.24: Kinematic model superimposed

During a surgery, the orientation of the tool depends on the trocar (pivot point), thus the orientation of the end effector to move in a specific direction can be set [84], [85]. It also has one manual joint which is fixed before the procedure (highlighted in red in Figure 2.24). “B” is the robot co-ordinate frame and “W” is the tracker (observer) co-ordinate frame. These robots were cleared by FDA for use in human surgery. InterNAV3D uses these robots for holding, positioning and maneuvering the tools. A custom control box (USB 2.0 compliant) was designed in CSTAR which helps to control the robot movements using the commands sent from interface designed for it. The software package that was developed in CSTAR has been customized with SAW so that these robots can be used as plug and play devices on any project based on SAW.

2.3.1.4 Frame grabber

The frame grabber is a hardware device that is used to capture still frames from analog or digital video stream. The frame grabbers can be external or internal (installed on the mother board). The frame grabber used for this system was an internal frame grabber MatroxVio-Duo which is compatible with PCI express and works on both 32/64 bit Windows and Linux operating systems [86] as shown in Figure 2.25.

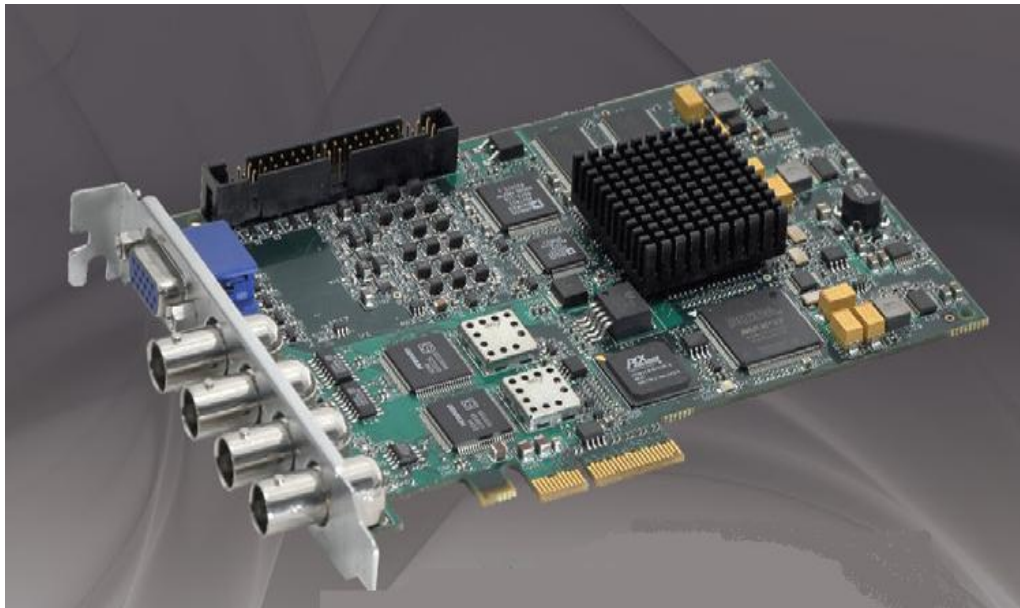


Figure 2.25: Matrox frame grabber

The US analog output is passed on to the frame grabber using an RF cable. Matrox provides an API for this card known as MIL (Matrox Imaging Library), which can be customized and accommodated with other interfaces to get images from this frame grabber.

2.3.1.5 Computer system

The following are the specifications of the computer system used:

Processor: Intel(R) Core(TM) i7 CPU 930 @ 2.80GHz

Motherboard: DX58SO

RAM: 3GB DDR3

Graphics card: NVIDIA GeForce GTX 560 1GB

2.3.2 Software components

The software system was built on Windows XP 32 bit in the QT environment. The various major components for the software package and their functions are described below.

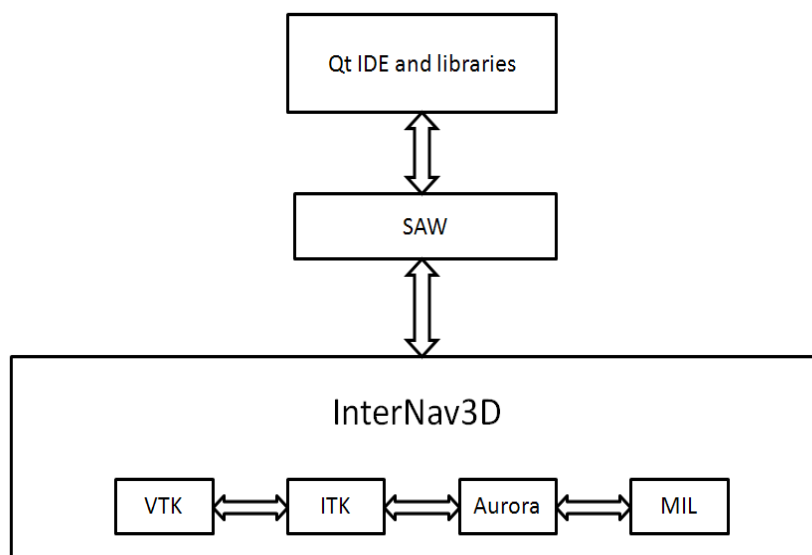


Figure 2.26: Software architecture

The block diagram in Figure 2.26 shows how the system is built in the software dimension.

2.3.2.1 SAW-CISST libraries

The Surgical Assistant Workstation (SAW) is a software framework that was developed by the research group CISST (Computer Integrated Surgical Systems and Technology) at John Hopkins University [87]. It is designed to integrate various hardware and software components used in the medical robotics field such as haptic interfaces, tracking systems, robots, open source libraries, imaging systems etc. under a single software umbrella where it is easy to connect and setup a data flow communication pipeline between them. Figure 2.27 shows a block diagram view of the working of SAW.

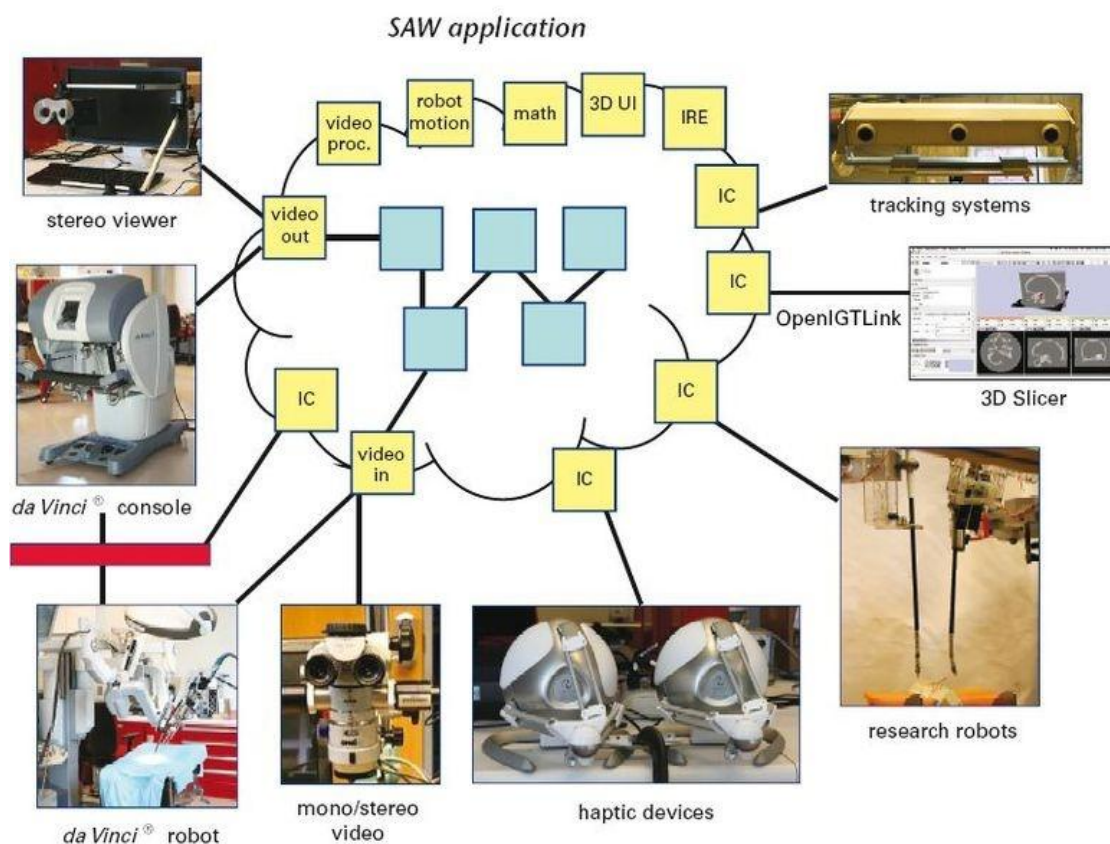


Figure 2.27: Overview of SAW

Here each and every block that is connected can be considered as an individual modular component. This package has a collection of interface modules to communicate with libraries (which represents different hardware profiles such as MIL, Aurora API, etc.) and common software interfaces (such as OpenIGTLink), which are used quite often in surgical workstations and development projects [88]. The implemented libraries thus created can be shared, reused and redeveloped under the open-source licensing agreement. After adding the SAW module, every device or software package that is integrated can behave as a plug and play interface.

The major benefit of SAW is that individual commonly used component libraries do not need to be re-coded for different projects; they can be reutilized every time a component needs to be connected in any other project where SAW is used. This saves the time and effort of re-coding the same interface code by different groups who need to use the same hardware and software profiles for their surgical system. SAW also helps in project collaboration when different research groups are working on similar setups at different locations [89]. Once the components are initialized the information flow occurs in the pipeline architecture of SAW.

2.3.2.2 Visualization tool kit

VTK is an open-source project library that helps to process the imaging data for 3D computer graphics, image processing and visualization. It is a C++ class library [90], [91] with interface layers for other languages such as Java, Python Tcl/Tk. It consists of an extensive source of tools that helps to deliver all the required 3D mapping functionalities such as advanced modeling techniques, texture visualization, surface reconstruction, scalar/vector data visualization, etc. It also provides a huge set of 3D data interaction widgets and integrates with the GUI implementation tools such as Qt and Tk. This cross-platform library works on Linux, Windows, Mac and other platforms. The data flow of VTK can be explained by the flowchart shown in Figure 2.28. The inputs to VTK are known as *vtksources*. It usually comprises of images, STL objects, 3D points, etc. It could also be the data that was passed from other libraries like ITK. These *vtksources* can then be forwarded to filters if needed, which could deliver various data manipulation

techniques such as interpolation, conversion, scaling etc. The output of the filter is passed to a mapper, which converts it to data objects.

VTK Visualization Pipeline

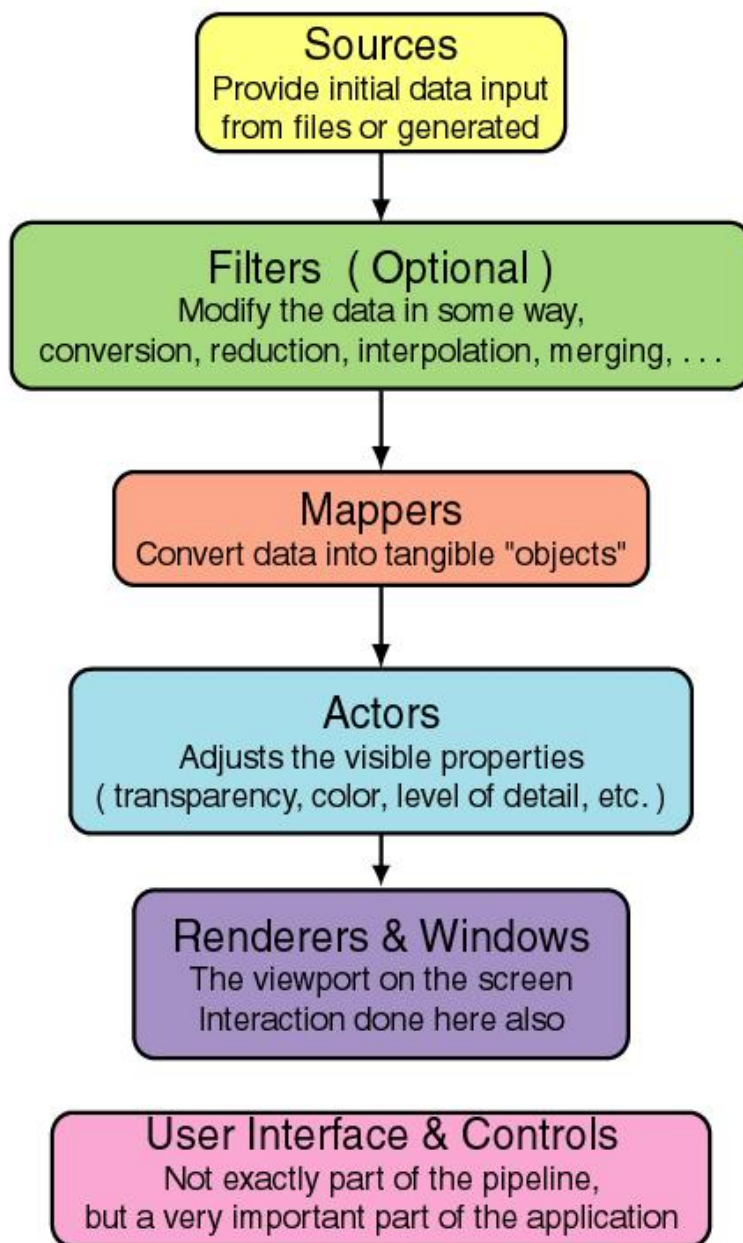


Figure 2.28: VTK flow of control

These data objects are raw physical entities that need to be placed in a 3D world. The mapper plays an important role to terminate the data processing pipeline and acts as a bridge to the rendering system. The outputs of mapper, as in “the objects”, are then transformed into *vtkactors* which represents the visual information. Properties such as color, transparency, texture, etc. can be modified for the *vtkactors*. For *vtkactors* to be rendered we need a renderer and a render window (multiple render windows can be initiated). This render window acts as a viewport which is visualized on the screen (3D world space). Here the actors are passed on for rendering and can be interacted with interface tools such as mouse, keyboard, phantom devices, etc. The interaction can be customized as per user requirements. In between the pipeline, there are multiple optional controls and directives such as *vtktransform*, *vtkcamera*, etc. that can be used for customizing the visualization.

2.3.2.3 Insight tool kit

ITK is the Insight segmentation and registration Tool Kit. It is a huge C++ library developed for performing image analysis on the most common image formats especially for medical imaging and multi-dimensional imaging data [92]–[94]. The library contains an implementation of a huge number of image processing algorithms. It is an open-source project initiated to fulfill the constant need for a package that can help analyze the images of the *visible human project* (described in the Appendix). Although it was developed on C++, it has wrappers for Python and Java and it is highly efficient for coding and software development. It works well with VTK for visualizing medical data and can be integrated with GUI development tools such as Qt and Tk.

2.3.2.4 MIL library

MIL is the library developed to integrate Matrox frame grabbers on a computer system. It helps to capture “image stills” from the frame grabber hardware in various compatible modes, and integrates a comprehensive collection of tools which help to implement computer vision techniques and software development.

In InterNAV3D, the MIL library is used to capture US images from the US machine video stream. MIL's SAW module was developed in CSTAR to help integrate the hardware profile with the CISST library package under InterNAV3D.

2.3.2.5 Aurora library

This library helps to integrate the Aurora magnetic tracking system to any software package. This API is highly customizable and allows for easy application specific software development. The SAW module for Aurora was developed to integrate it with the CISST package under InterNAV3D.

Chapter 3

3 User Interface: Modules and Working

InterNAV3D has a front-end GUI interface to help control the process of robot-assisted minimally invasive lung cancer treatment. It implements the methods of brachytherapy, thermal ablation, tissue biopsy under 3D visualization with added functionalities of image processing. It has an online and offline system mode for performing tumor detection analysis based on virtual visualization and image processing techniques.

The motivation for development of such a system was to fulfill the constant need of a stand-alone system that implements currently available minimally invasive surgical techniques and their integration, as well as to assist the surgeon on gaining a better understanding of the surgical site while searching for and detecting the tumors by improving on the visualization and image processing. One of the major hardships faced by surgeons during a minimally invasive surgical task is the limited visibility of the surgical site. The conventional method of using a laparoscopic camera with 2D US image feedback could assist; but it is hard to determine if the needle has hit the specified target. Determining the needle location is easy when US image plane and the needle axis co-align (such that complete needle is visible in the US image), but this is not always the case. For instance, in a brachytherapy procedure targets are selected all over the tumor by a dosimetry plan (determined by an optimized target planning algorithm to adequately cover the complete tumor) [95]–[98]. In such cases, it is seldom possible for the US image plane to follow the needle axis or vice versa. This makes it very hard to hit the specified target as the needle gets visualized as a bright spot in the US image plane (the angular cross-section of the needle). In other words, the use of 2D US image is very unintuitive. It is hard to visualize the complete structure, the position and the orientation of the surgical tools present in the surgical site. In such cases having 3D image enhances the visualization of the surgical site. The user can perceive the objects in the surgical site more clearly. Hence, 3D visualization is very important.

Imaging lung under US is very tricky. The US modality has a major drawback that it cannot image the underlying tissue perfectly if any air artifacts are present within. The lung is an organ that contains many air pockets. Therefore, for surgical procedures involving use of US with lung, the lung needs to be collapsed before the surgery (while other lung is used for respiration). A well collapsed lung is the one with least possible air stuck within. Added motion (lung respiration and heart beat movements) increases the complexity of the procedure. To image the lung, the US transducer needs to be in a constant contact with the lung surface. The surface being imaged might not be completely flat and touching the US transducer. Thus, the air artifacts, the motion (respiratory and heart movements), and the uneven surface generates unclear US images and makes it hard to determine and select correct target locations. For this reason, image processing techniques needs to be implemented to enhance the images and to figure out as much information as possible in determining the tumor, the target locations, the tools used and corresponding artifacts.

InterNAV3D implements various treatment techniques and integrates 3D virtual visualization with image processing tools. It has the ability to compensate for the tissue motion programmatically and enables its simulation and visualization. It also provides motion compensation for the selected target. It implements novel methods to predict the path that the needle is going to take along with a visualization history of the needle tip locations (during a needle insertion procedure). A needle retraction module that enables safe retraction of a needle along the path of a needle insertion is implemented. The GUI interface of the software is shown in Figure 3.1 and descriptions of all the integrated panels follow in subsequent sections.

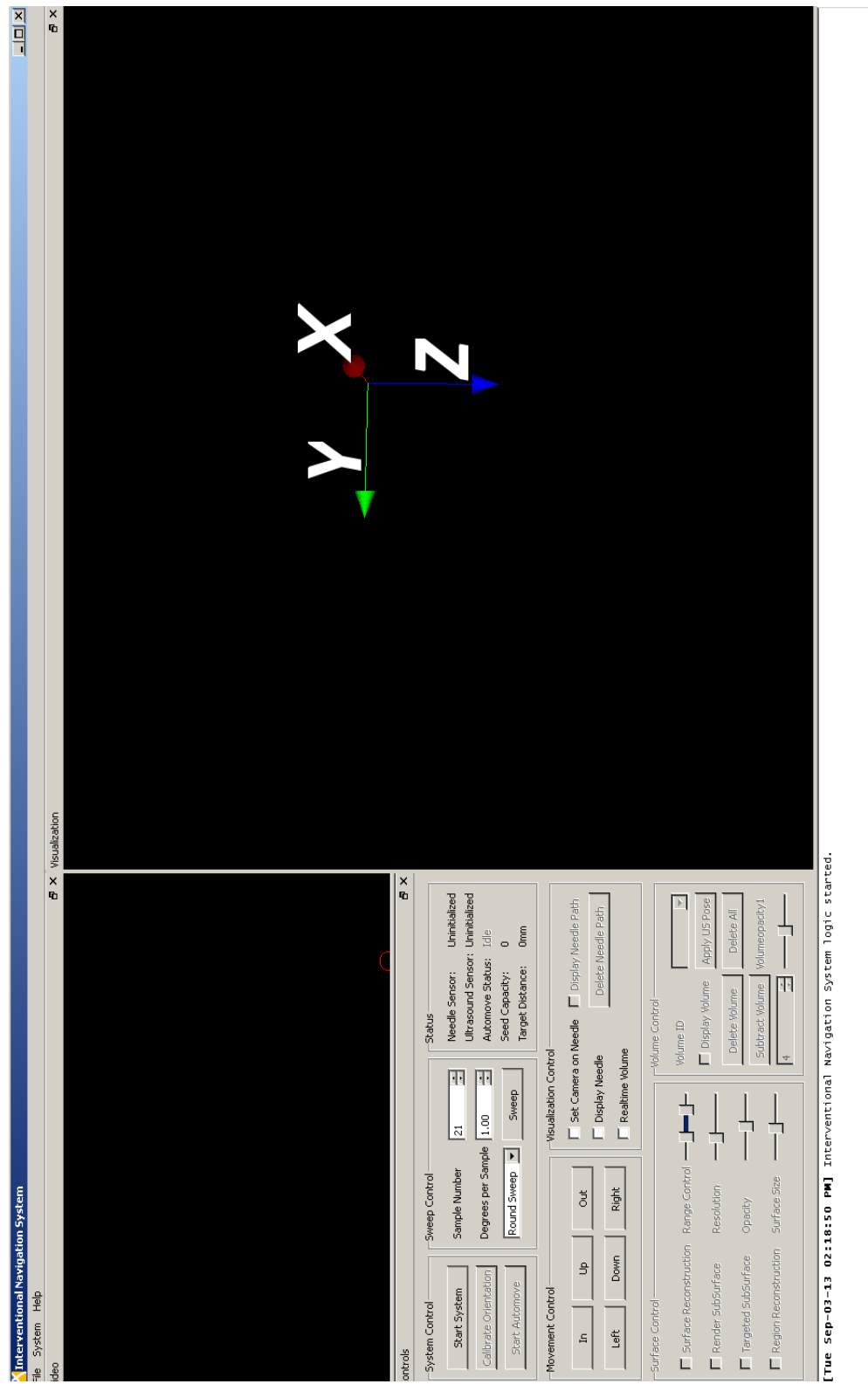


Figure 3.1: User interface

3.1 User interface

The user interface can be divided into different dock areas as shown in the Figure 3.2 below with nomenclature. The right dock area consists of the 3D virtual visualization window and the left dock area consists of the real-time US image window with the control panel. The bottom dock consists of the software output for important messages and information. The top dock consist a toolbar with various options and settings.

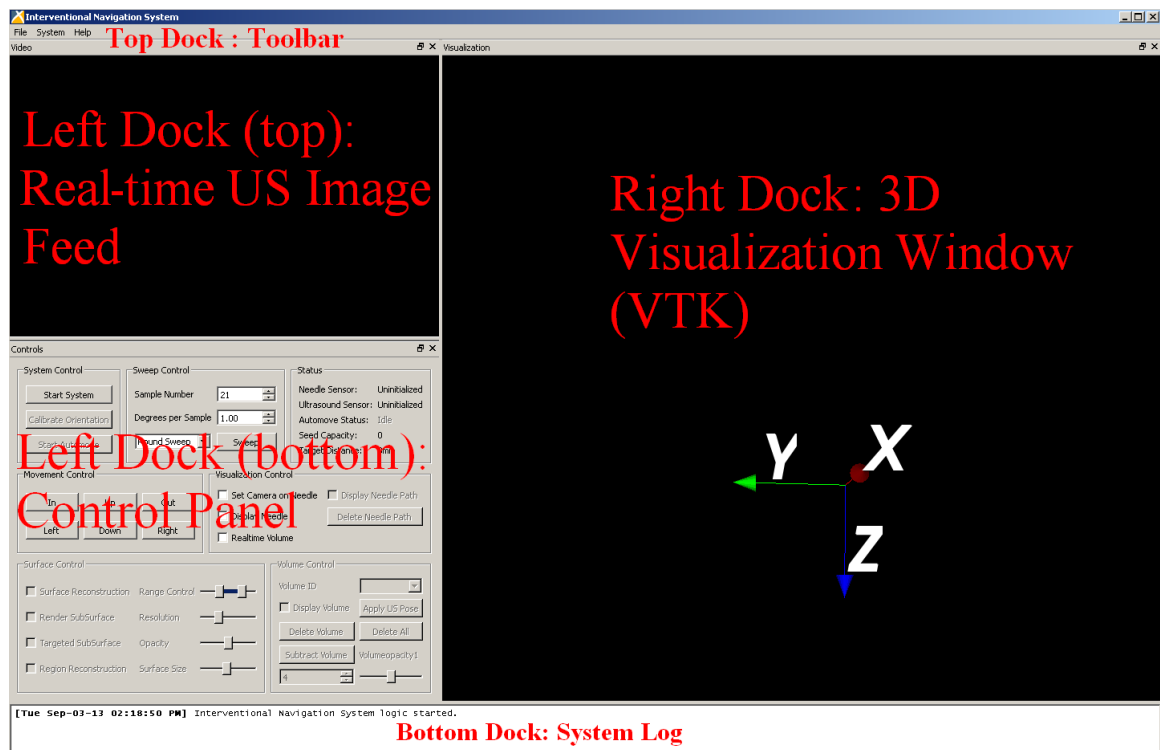


Figure 3.2: Dock areas for the GUI interface

3.1.1 Right dock

The right dock area consists of the VTK visualization window (3D virtual world). It renders real-time 2D image feed of the US image plane in a 3D Cartesian space with a virtual 3D US probe and the needle. These virtual objects represent the position and orientation of the surgical tools in the 3D space with the feedback provided by the Aurora tracker. Using the control panel, the images are captured in pre-defined fashion (different sweep methods) and processed to be displayed as 3D volumes in this 3D virtual world. It

can visualize multiple volumes simultaneously by accessing their respective positions (using Aurora tracker) in space as shown in the Figure 3.3.

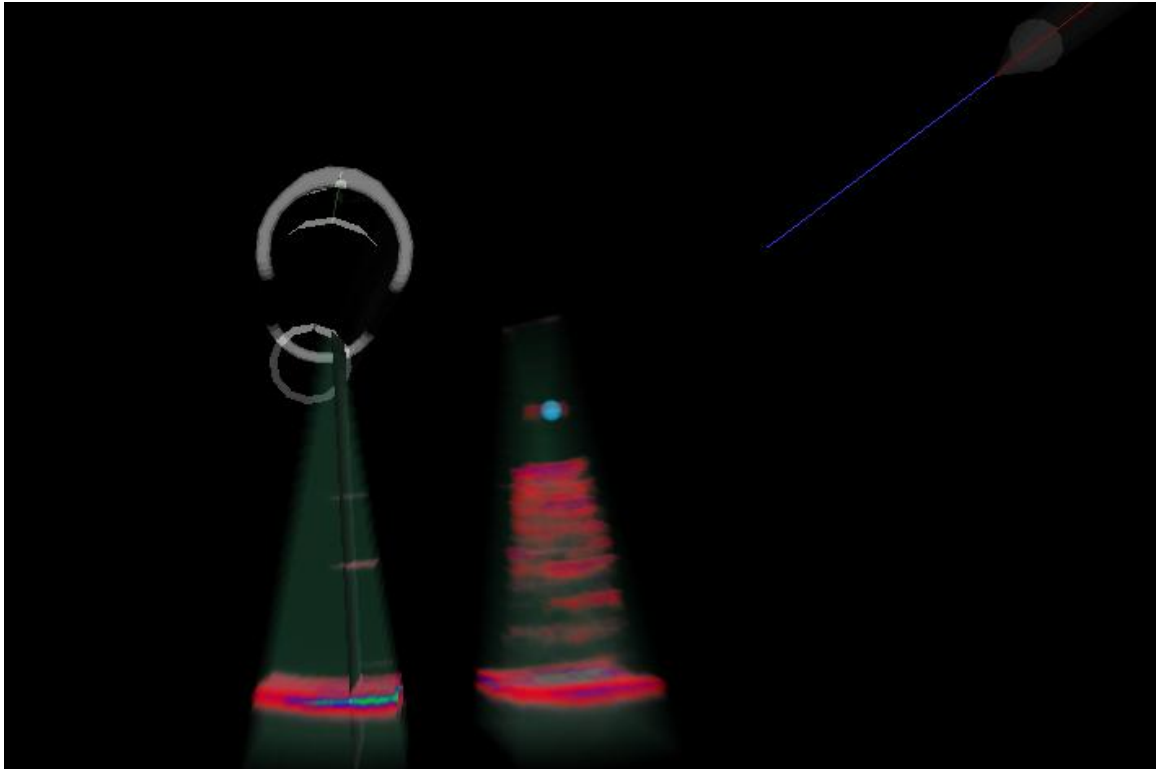


Figure 3.3: VTK window (3D virtual world)-multiple volumes

It also performs the surface reconstruction of the artifacts present in the volume and renders it in real-time. The volumes can be manipulated by using the image processing modules and the volume control panel for better visualization.

Interaction with the 3D virtual world can be performed using the mouse controls such as zooming in and out, moving at different angles and orientations, etc. As the tool and the probe move in real world, the same is visualized and moved in the virtual world. During a volume grab procedure, a series of images is captured by moving the US probe in a specific fashion. The virtual US image plane and the US probe can be seen moving synchronously with the real world probe. This enables user to understand the changes occurring in the surgical site. The 3D virtual world renders the orientation of every element present in the real world exactly the same as in the virtual world. The motion simulation module captures the movements of the real world surgical tools using the

Aurora sensor and simulates in the virtual world. Figure 3.4 shows a typical VTK window with a volume, a surface reconstruction object, a needle and a US probe.

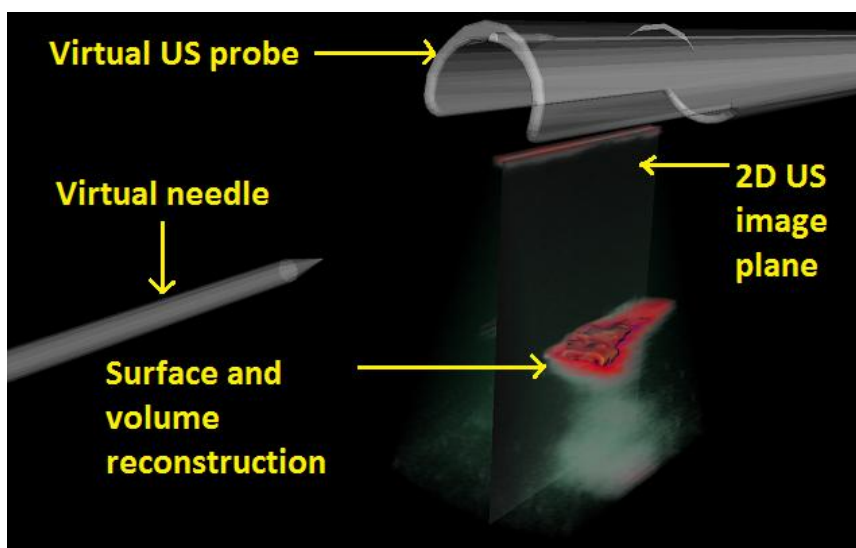


Figure 3.4: Typical VTK window

3.1.2 Left dock

The left dock area consists of 2 parts. The top part has real-time video feedback from the US machine, rendered in the video window as shown in Figure 3.5.



Figure 3.5: US real-time video stream

This window is an interactive tool that provides the conventional 2D US image view with additional interactive functionalities such as selecting target locations, selecting any specific regions for implementing the desired modular analysis and for assisting in calibration. Below the video window lies the control window in the bottom left dock area as shown in Figure 3.6. It consists of many panels and modules that are specific to the functionalities they deliver.

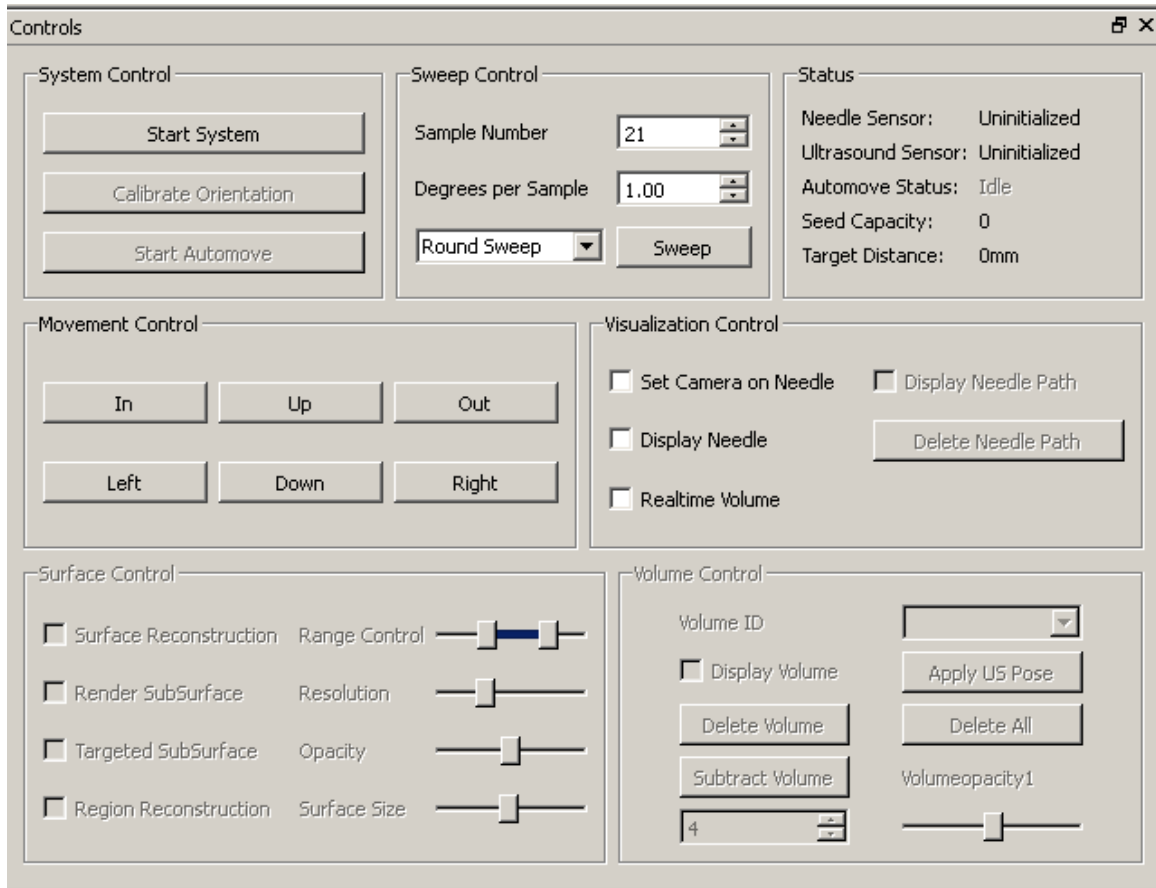


Figure 3.6: Control panel

3.1.2.1 System control

This consists of 3 push buttons as shown in the Figure 3.7 to initialize the system and control it during certain aspects of the procedure. The first button is Start/Stop system button that toggles the current state of the system from passive to active and vice versa (hardware, software profiles gets activated or deactivated). The second button is to calibrate the system for calculating the view vector at system initialization for the

visualization. It calculates the up vector that is required to place and orient the camera of the visualization window and performs other needed calibrations. The third button is used to start/stop the “automove” mechanism of the system that enables the tool to orient and align with the target.

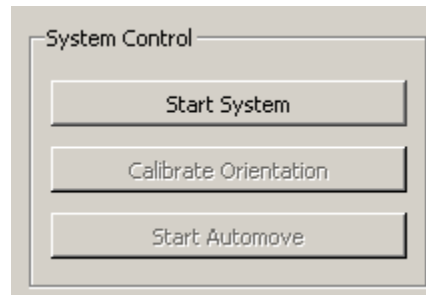


Figure 3.7: System control

Automove helps in faster and more efficient way for the tool to be aligned with ease using automatic manipulation from the software. As soon as the needle is aligned, a pop-up message appears, asking if the needle needs to be driven to the specified target as shown in the Figure 3.8

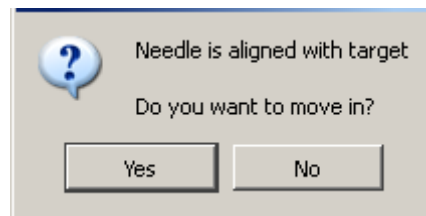


Figure 3.8: Pop-up menu

3.1.2.2 Sweep control

This control panel houses different methods of image capturing sweeps for the construction of 3D volume (using the set or series of images obtained with a certain fixed relation depending on the sweep method). Figure 3.9 shows the panel view. In the first box, the user inputs the number of samples (images per volume) that need to be grabbed. In the second box, the user inputs the time/distance gap or the angle between successive images. The third option is a drop-down menu to select the mode of operation for the image capture.

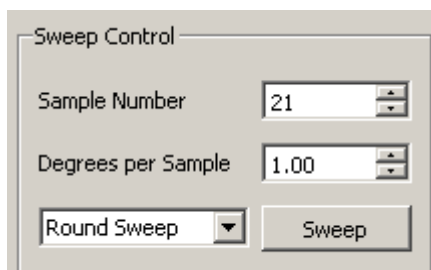


Figure 3.9: Sweep control

InterNAV3D has 4 modes:

1. **Round sweep (rotational sweep):** In this mode the images are grabbed by rotating the US probe about its longitudinal axis. Figure 3.10 shows a sample volume grabbed using this mode.

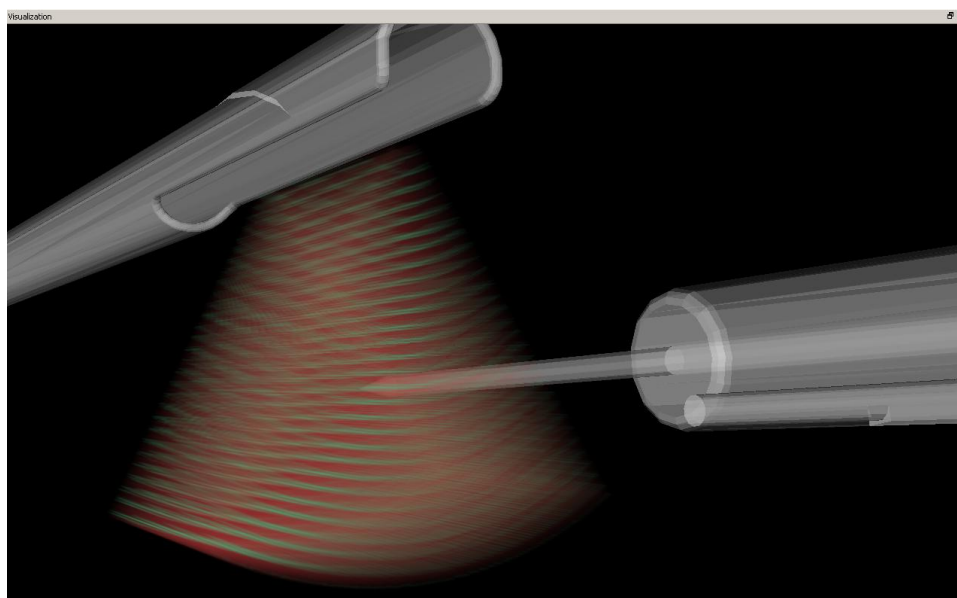


Figure 3.10: Round sweep

Due to the way the images are grabbed, it is not always possible to capture the complete specified region of the surgical site in a single sweep (depending on the location and size of the tumor). Multiple volumes might need to be captured and stitched together for a complete clean visualization of the surgical site.

2. **Flat sweep (straight sweep):** In this mode the images are captured while the US probe is moved around the fixed point (trocar/pivot point) along the surface of the tissue. The axis of motion thus passes through the pivot point and remains perpendicular to the surface of interaction between the US transducer and the underlying tissue. Figure 3.11 shows a typical volume grabbed using flat sweep.

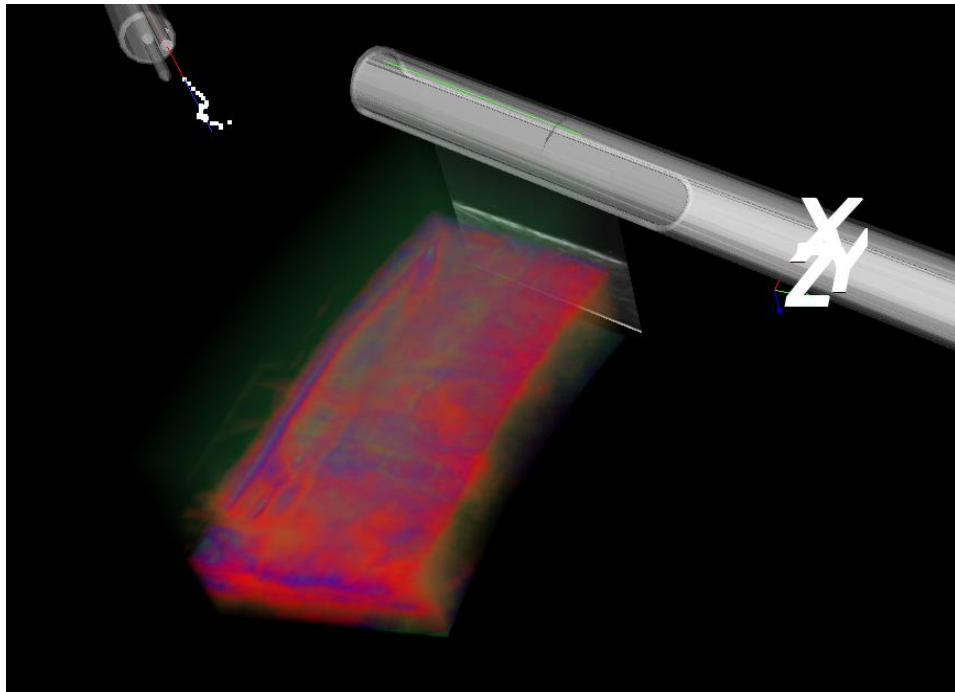


Figure 3.11: Flat sweep (straight sweep) mode

In this case since, it is very hard to predetermine the distance of the pivot point (needed for 3D image reconstruction) from the transducer which might change for every new sweep (henceforth termed as “pivot distance”). Also, continually checking the change in angle to grab a new image makes the sweep time-consuming. Considering this situation, a different approach was used. Here, a user inputs the time duration of the sweep and the number of frames that needs to be captured (resolution). The standard range for the time-distance values is provided. As soon as the sweep starts, the transducer moves along the surface of the tissue. The frame grabber captures the images at equal interval of time (total sweep duration divided by number of images). This method calculates the pivot distance and the total angle of the ablation volume in run-time by using the

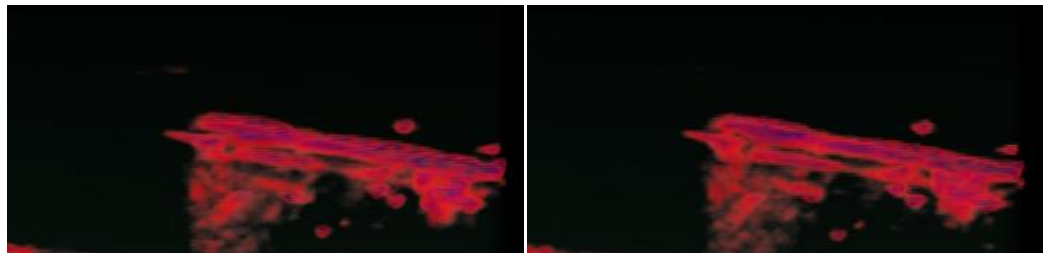
Aurora values and performing vector manipulation. This information is forwarded to a volume reconstruction algorithm that uses the sweep model information and constructs the 3D volume.

3. **Palpation sweep:** The third method is the palpation method. The US probe is palpated throughout the required surface along a single direction. The mathematical model of volume reconstruction of palpation is similar to flat sweep method. However, this method is comparatively slower as more robotic movement is needed (multiple degrees of freedom of the robot are used) to grab the images. The probe is lifted from the tissue surface and moved to the next location for every new image grab. The probe needs to be moved gradually while it is inside the patient's body so that the tissue damage can be kept to a minimum. The palpation method devised here has a fixed pivot point around which the US probe is moved with a fixed pivot distance.

This method is implemented as a future prospect for implementing additional techniques to enhance the imaging and visualization, for instance use of elastography and/or force sensing for improved tumor localization. The virtual volume model of the palpation sweep is similar to the volume structure of the flat sweep (assuming that tissue deformation is compensated). The pivot point and pivot distance calculation resemble the flat sweep method calculations.

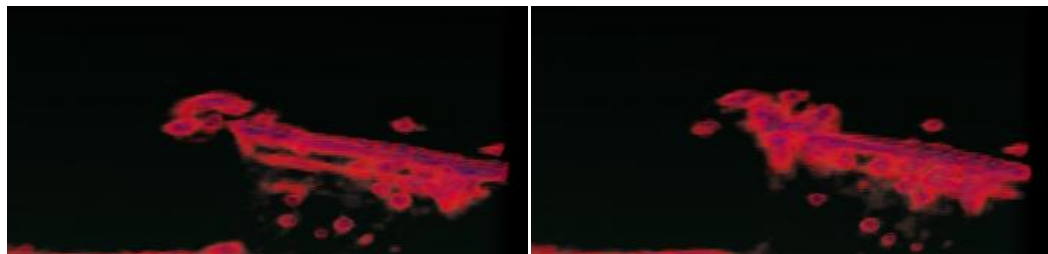
4. **Ablation sweep:** Ablation sweep is the final method that is included. The concept behind the design of this method is to detect the instantaneous changes that occur in the tumor while thermal ablation is being performed. A certain times, the ablation needle moves or gets misaligned causing healthy tissue to ablate while a part of tissue with tumors is left untreated. Determining the changes that occur in the tissue help formulate the new target location for placing the ablation needle tip so that the entire tumor is enclosed under the ablation zone. It also assists in determining the entirety of the ablation process. For such an application, a sweep method that is faster and repeatable was needed. It should be able to capture and process as many volumes as possible concurrently while they are being grabbed,

without affecting or changing the tissue physically. The round sweep method is the fastest and easiest way to get images (a single degree of freedom of robot movement is used) and also it does not change or relatively deform tissue for concurrent volumes. Hence, the continuous round sweep method with a fixed angle, fixed number of images and a fixed time period between successive volumes for concurrent sweeps is used for this method. The new image sweeps that are grabbed after a fixed interval of time are processed to form multiple volumes that are overlapped on top of each other in a virtual reality environment. This provides the ability to determine what region of tumor is getting ablated and if a change in the position of the needle and/or ablation parameters such as power, current or duration is needed (to make sure that the entire tumor is under the specified ablation region). A comparison of the changes that occur during the complete procedure can be visualized. This helps to predict the entirety of the ablation whilst it is being performed. Figure 3.12 below shows some of the sample volumes grabbed over time during an ablation procedure.



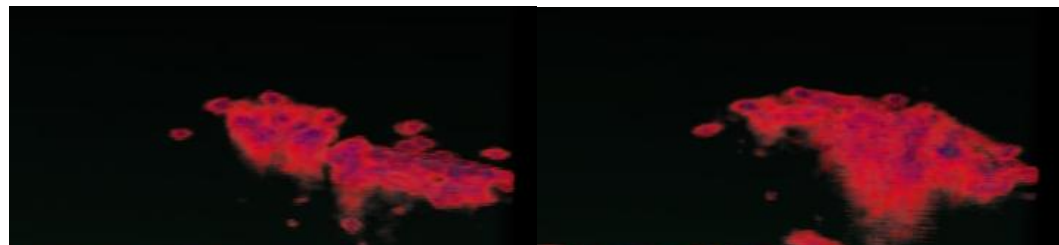
(a) Time: 0 seconds

(b) Time: 30 seconds



(c) Time: 60 seconds

(d) Time: 90 seconds



(e) Time: 120 seconds

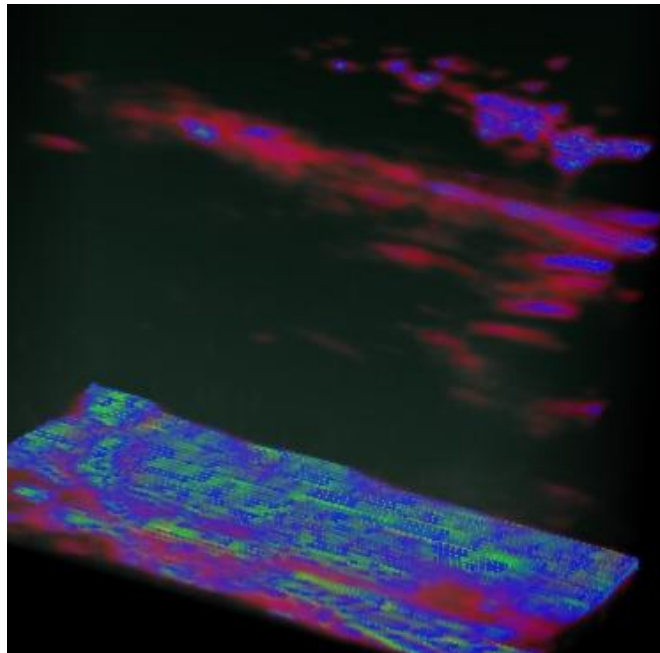
(f) Time: 150 seconds



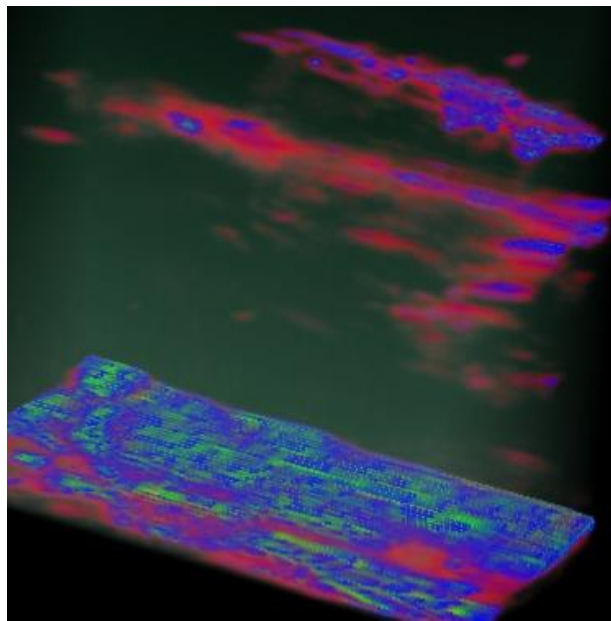
(g) Time: 180 seconds

Figure 3.12: Multiple ablation volumes at different time intervals

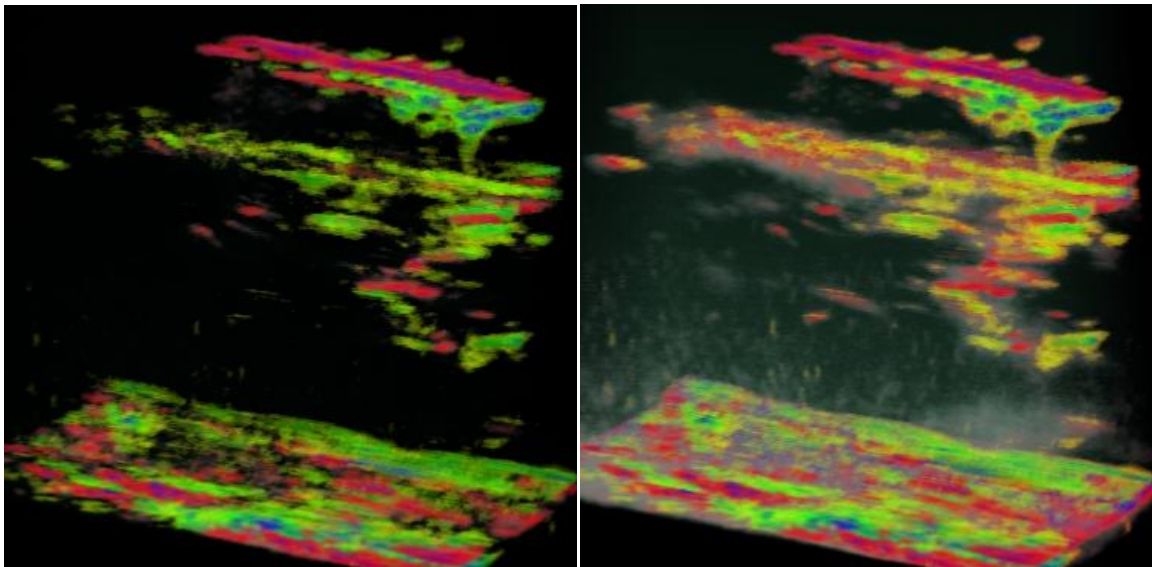
Each volume gets a unique volume ID that represents the stages of the ablation during the procedure in ascending order. The ablation sweep is not restricted for thermal ablation but can be used for any other procedure to visualize the changes occurring, for instance before and after a needle is inserted. The subtract volume module in the volume control panel helps in visualizing the features of the volume that change overtime between any 2 volumes among the set of volumes thus captured. A user can select any two volume IDs and then a new volume showing the difference between those stages is processed and visualized, highlighting the change that has occurred. Figure 3.13 shows one such sample experimental output.



(a) Image A



(b) Image B



(c) Image C = B-A (difference image)

(d) Image C superimposed on image A

Figure 3.13: Volume subtraction

3.1.2.3 Status panel

The status panel lies to the right of the sweep control. This panel does not have any interface control but is an output window to various hardware related controls. It provides the run-time state of the system and is a prominent display window for essential tasks and hardware outputs. The user gets the most up to date status and should refer to this panel first if he/she suspects any errors or issues with the system.

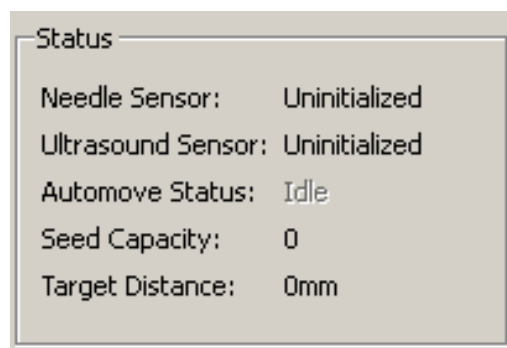


Figure 3.14: Status panel

The status messages it provides currently include the run-time state of the tracking sensors, the brachytherapy tool seed capacity, status of the auto-move control mode, distance between the virtual target and the needle tip, etc. New output status message can be added if the need is felt in future. Figure 3.14 shows the panel view.

3.1.2.4 Movement control

This panel lies exactly below the system control panel. It consists of six push buttons for 6 directions the user wants the robot to move. The 6 directions represent the typical Cartesian system orthogonal axes. This control panel can be used to move any of the two robots by toggling the control from the toolbar menu (switching from US probe robot to the needle tool holding robot). Figure 3.15 shows the panel view.

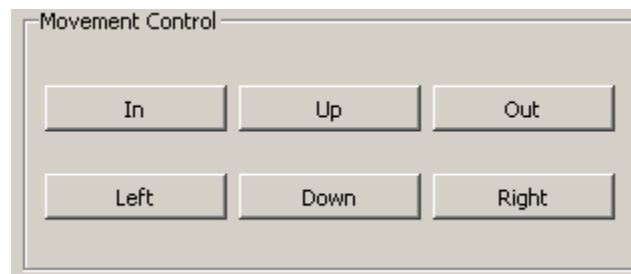


Figure 3.15: Movement control panel

3.1.2.5 Visualization control

This panel houses the generic controls for the visualization of the 3D virtual world objects. Here a user can enable or disable the visibility of the virtual needle and the needle path. Other options such as having a needle eye view (first person eye view), synchronizing the movements of the 3D volume/target (enabling real-time motion simulation of the heart beat and respiratory movements) are provided. The virtual needle is superimposed on the surgical needle (visualized in the real-time US image). Enabling or disabling the virtual needle helps in evaluating the position of the surgical needle. It compares the change in the position of the surgical needle (possibly as a result of needle bending), with respect to the position of the virtual needle. The surface/volume reconstruction renders on top of the virtual needle and provides a more clear view of the

needle deformations. New functionalities can be added if needed. Figure 3.16 shows the panel view.

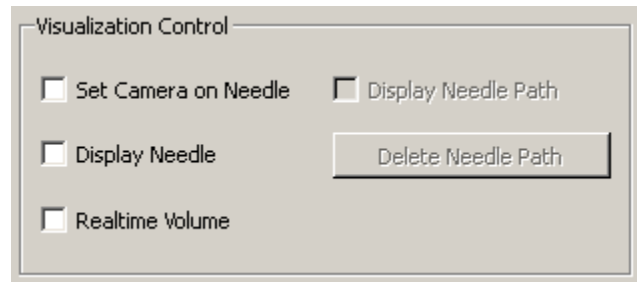


Figure 3.16: Visualization control

3.1.2.6 Surface control

This panel has the control group for the surface and region reconstruction of the volume. These options enable control over the resolution, opacity, range of the threshold filter, etc. by using the sliders provided. It also has options to enable the sub-surface and targeted sub-surface reconstruction (where a user can select the part of the image that he/she would like to be given as input for these modules). This helps to focus only on the part that is deemed to be important, makes the computation more efficient and faster. The region growing segmentation helps in determining the tumor structure. Figure 3.17 shows the view of the panel and Figure 3.18 shows various outputs that are generated by changing the surface opacity values.

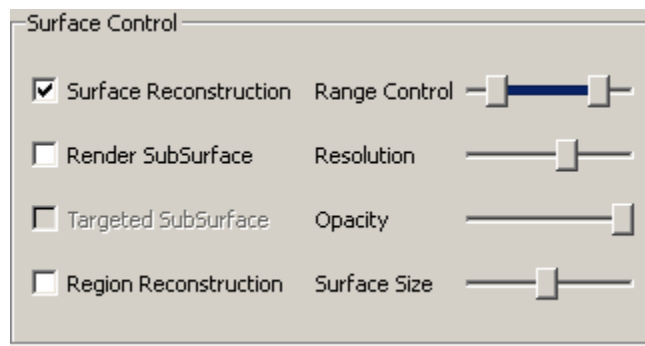


Figure 3.17: Surface control

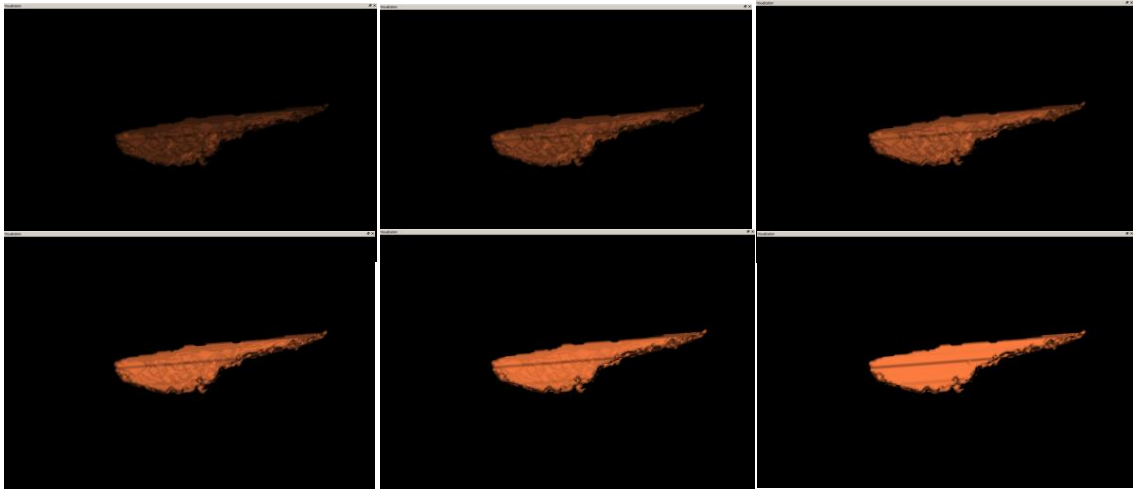


Figure 3.18: Surface opacity control

3.1.2.7 3D Volume control panel

This panel has the option to control the basic functionality for the multiple volumes that are rendered in the 3D virtual world. Here a user can make any volume (identified by its volume id), visible or invisible. He/she can control the opacity of different intensity values and make any manipulation such as applying the subtract volume filter on the volumes. In subtract volume, it asks for 2 volume IDs and then subtract one from the other to make the changes between them clearly visible. The user can delete the volumes that are no longer needed by selecting one or all of them using the GUI. Figure 3.19 below shows the panel view.

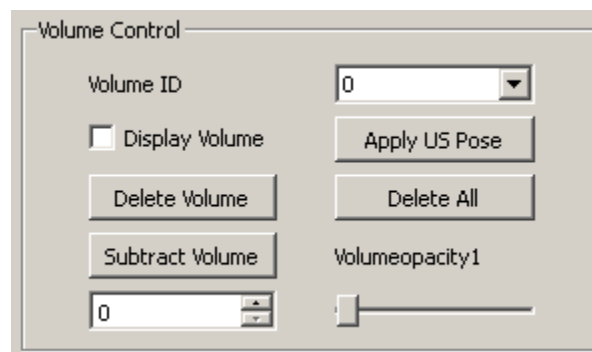


Figure 3.19: Volume control

3.1.3 Top dock (toolbar menu)

The top dock consists of the toolbar menu as shown in Figure 3.20. It consists of additional options for the InterNAV3D system. Various toggle switches are added to implement certain conditions for the system to work. The toolbar also include the help panel that provides basic overview of the software. The toolbar can be used to add additional options as needed during next iteration of software development.

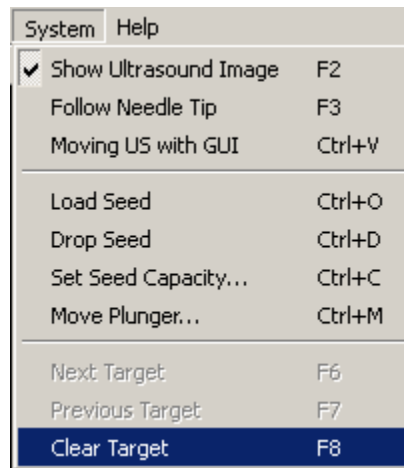


Figure 3.20: Toolbar options

3.1.4 Bottom dock (system log)

This forms the bottom dock of the system. Various important messages and outputs are shown in this window in run-time. It is a scroll window that keeps a log of all the actions performed by the user and the output messages returned from the system. It also helps in diagnosing the software (while it is in development mode) by appending the debug output to the system messages. Figure 3.21 shows a typical log window at system initialization.

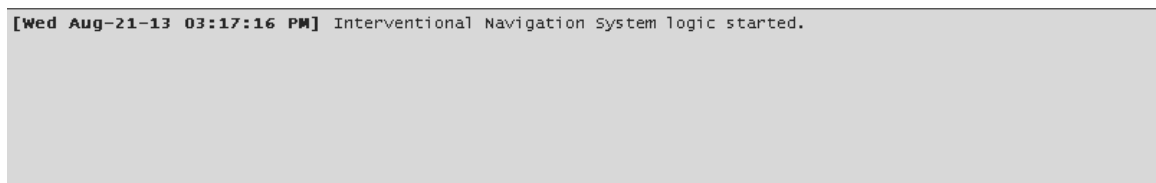


Figure 3.21: System log

3.2 Modules and working

Various modules to aid visualization and to apply image analysis have been integrated with the InterNAV3D system. This section describes the functionalities rendered by those modules and the corresponding benefits.

3.2.1 Virtual needle and path projection

The 3D virtual world displays several objects that mimic the real world surgical tools (present in the surgical site). The needle tool (a biopsy needle, a brachytherapy needle or an ablation needle) can be rendered in the 3D virtual world by tracking them with an electromagnetic sensor. Using the pivot calibration (described in Chapter 4), these tools are calibrated for getting the position of the tip and the orientation of the needle.

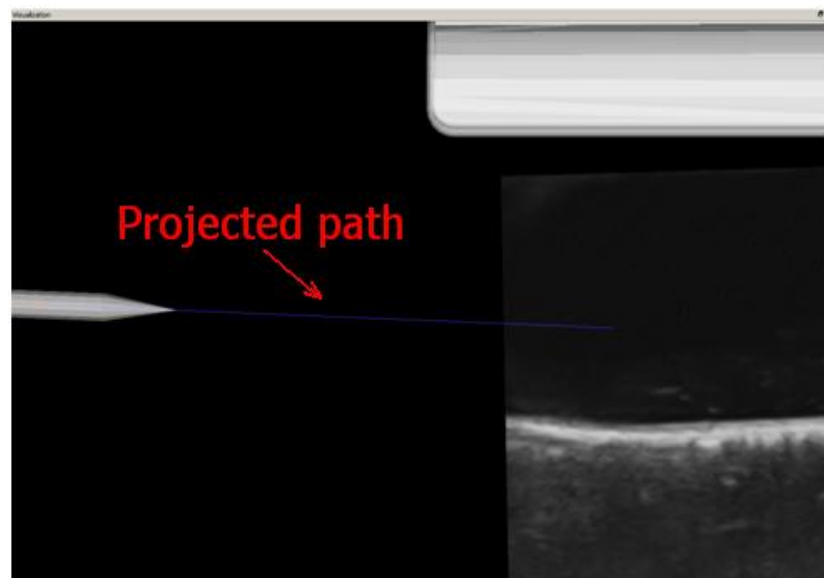


Figure 3.22: Needle path projection

The needle tool is continuously tracked and rendered in real-time in 3D world. Figure 3.22 shows a virtual radiofrequency ablation tool rendered in the 3D world with needle path projection. The virtual tip projection thus implemented, extends the needle tip, so as to show where the tip is going to hit if the needle is maneuvered straight along the axis of the needle tool. This acts as a generic pointer to align the needle tip before actually puncturing the tissue to move in by aligning itself with the target. Thus, it helps

to possibly hit the target in single puncture and avoids potential tissue damage that might arise due to pivoting of the needle tip while it is inside the tissue. The real insertion however can never be predicted to occur in a straight path as the needle might bend due to the forces exerted on its tip by the tissue. The flexibility of the needle, effects of friction (while insertion), tip geometry and the possible non-uniform stiffness of the tissue can cause this unwanted effect [99]–[101]. This module considers these consequences and adds the needle path that takes into account the most recent needle tip positions and displays an updated needle path projection of the needle bending. This updated path projection guides in determining the error caused due to the needle deflection and assists in re-orienting the needle so that it hits the target. Figure 3.23 shows the initial needle path projection and the updated needle path projection. The yellow spheres are the most recent needle tip positions. The initial path is represented by a yellow line and the updated one by a blue line. It can be observed from the image that the blue line represents the direction where the needle is heading (by visualizing the path created by yellow spheres).

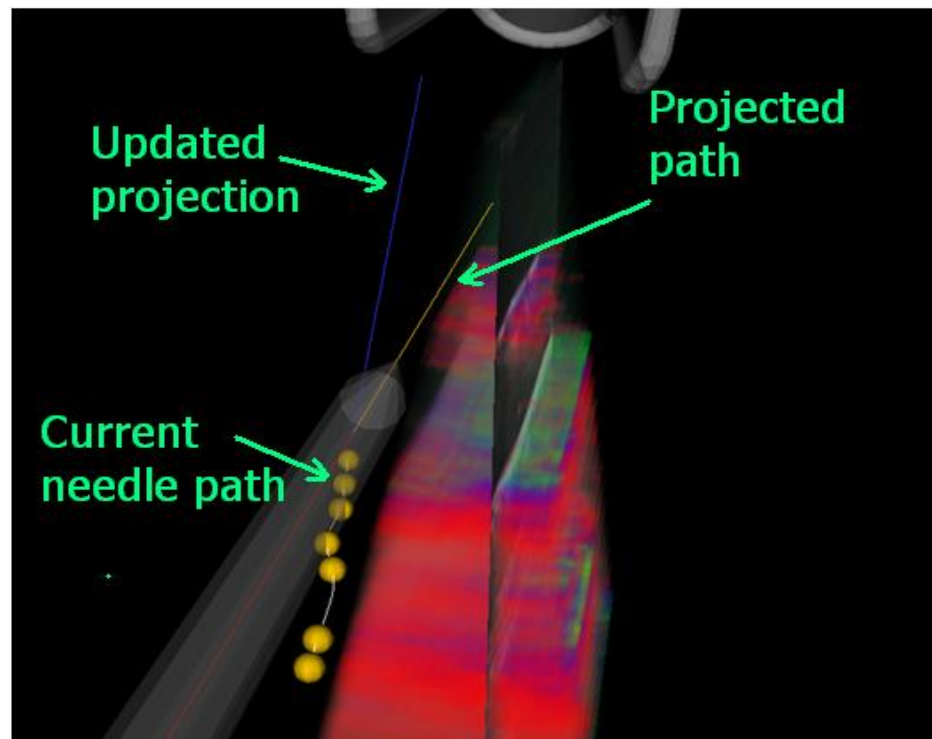
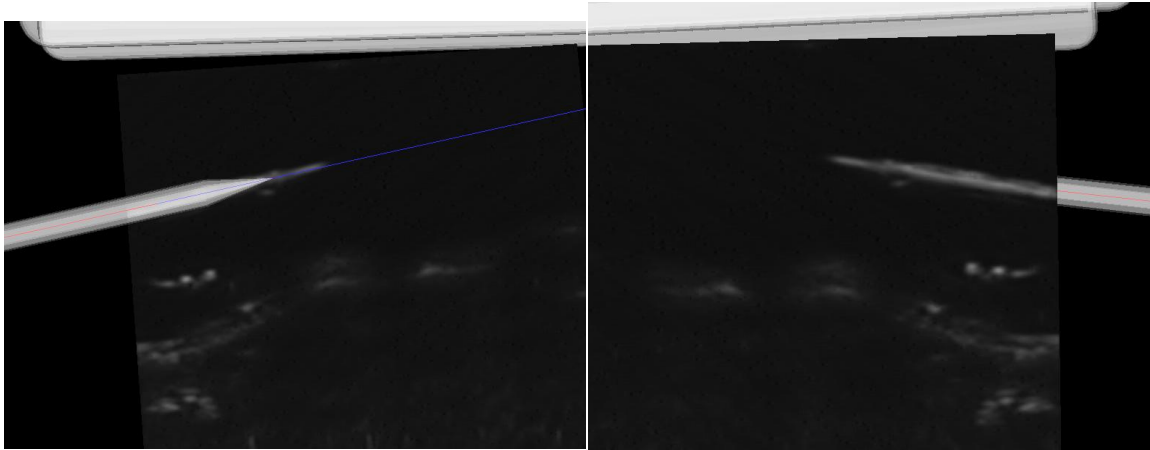


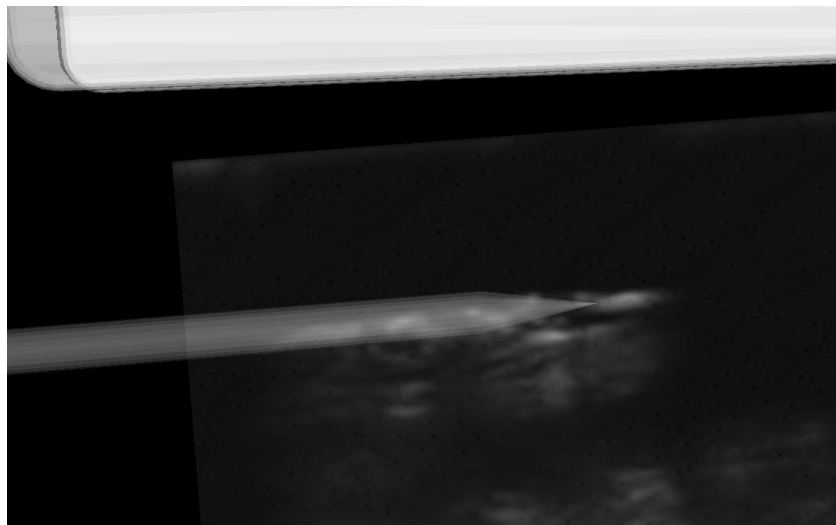
Figure 3.23: Needle updated path projection

The virtual needle rendered is the STL object of the sleeve designed for the needle (brachytherapy or ablation tool). These sleeves were designed in Solidworks (3D CAD software) and act as an interface between the tool holder on robot and the tool. Most of the sleeves have a compartment for enclosing the electromagnetic sensor. STL objects for different needles have been integrated in the InterNAV3D library to render the virtual needle tool as close as possible to the surgical tool.



(a) From the front

(b) From the back



(c) Needle STL made translucent to visualize the underlying needle (US image)

Figure 3.24: Needle STL superimposed on the US image

The length of the needle projection can be changed if needed in the software settings. The needle STL object and the virtual paths can be rendered invisible and/or their opacity can be changed if required. This functionality assists in investigating the trueness of the needle tip position by comparing them with the 3D volume and the real-time 2D US image overlay as shown in Figure 3.24.

3.2.2 Current needle path visualization

The path of the needle tip depends on several factors. It is not always possible to determine if it is going to move as anticipated. The reasons may be the needle deflection (caused due to irregular tissue stiffness or the design of the needle tip), error at the pivot point (movements at the trocar), or the irregular movements by the passive joints of the robot. The needle's path can be a simple curve completely confined on a 2D image plane to a complex curve that requires multiple image planes (or a 3D structure to confine in).

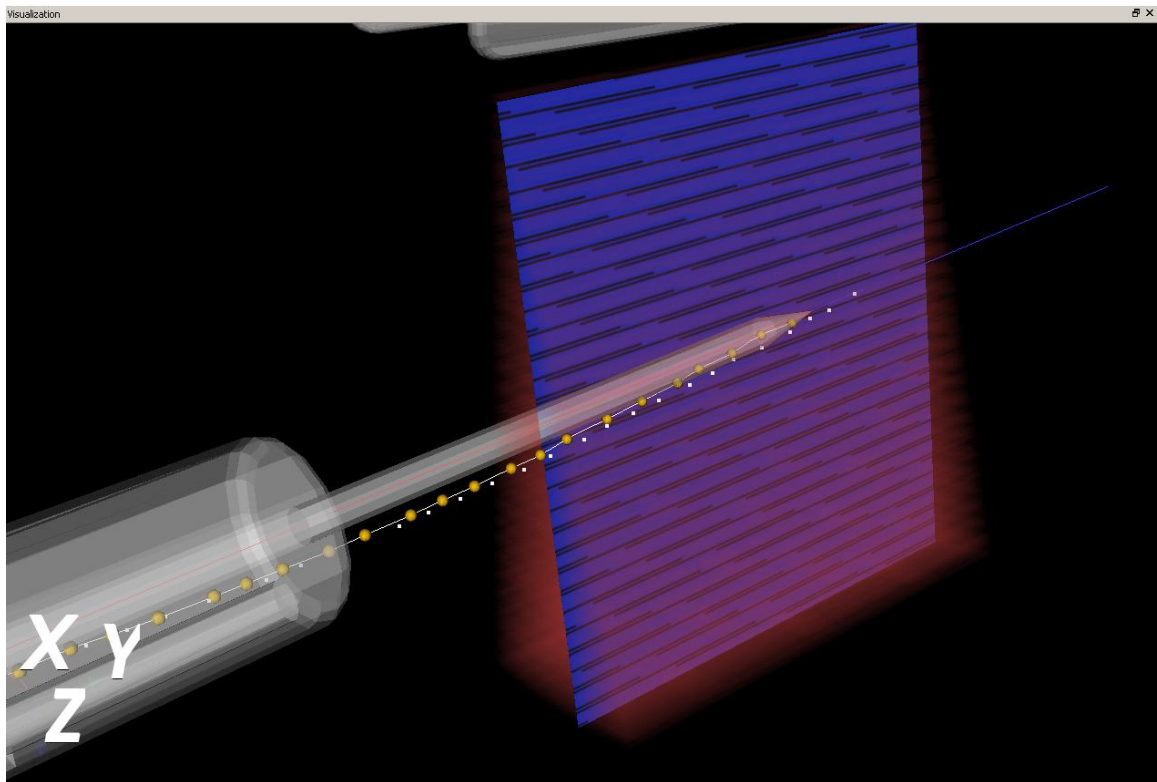


Figure 3.25: Current needle path

Having a 3D visualization of the current needle path helps in determining the changes occurring over a specified duration of time and accordingly improves the visualization of the path the needle is going to take. The current needle path visualization module keeps a history of all the points the needle tip has taken and fits a spline as shown in Figure 3.25. Needle path also helps to retract the needle along the same path as that it was inserted in, so that tissue damage can be kept to a minimum.

3.2.3 Needle path prediction

As discussed in previous section, it is not always possible to make the needle move in a straight line. The robots, AESOP and ZEUS, used in the InterNAV3D system have 2 passive joints that helps to reduce the stress at the trocar point, but it affects the path that the needle tip is going to take. A calibration path prediction method was designed in the system that records the history of the needle tip points while it is moving straight inside the surgical site. Using this history, it estimates the path that the needle would take. The path is rendered on the 3D world using the white dots as shown in Figure 3.26.

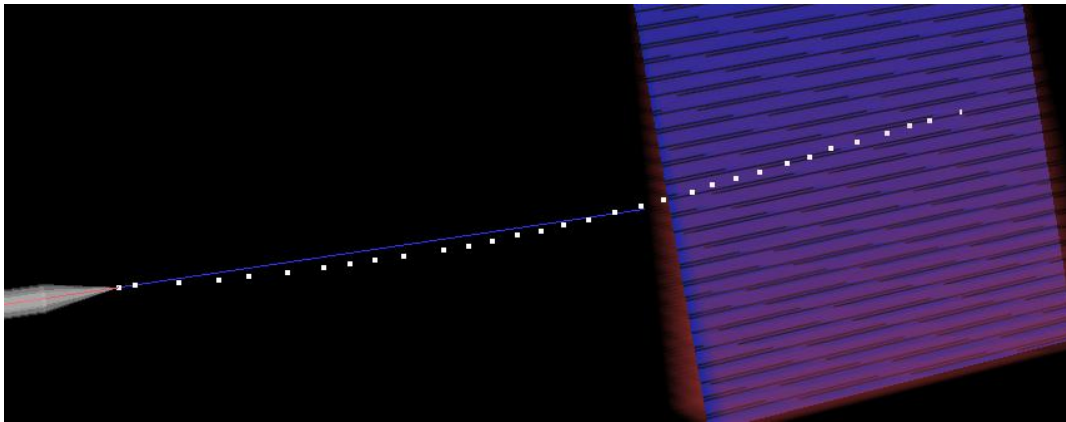
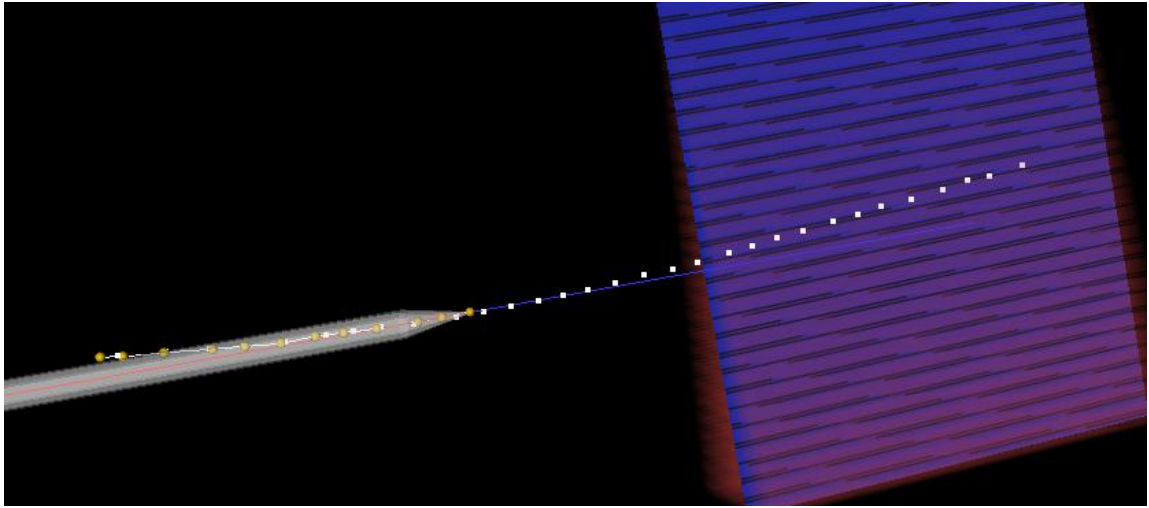
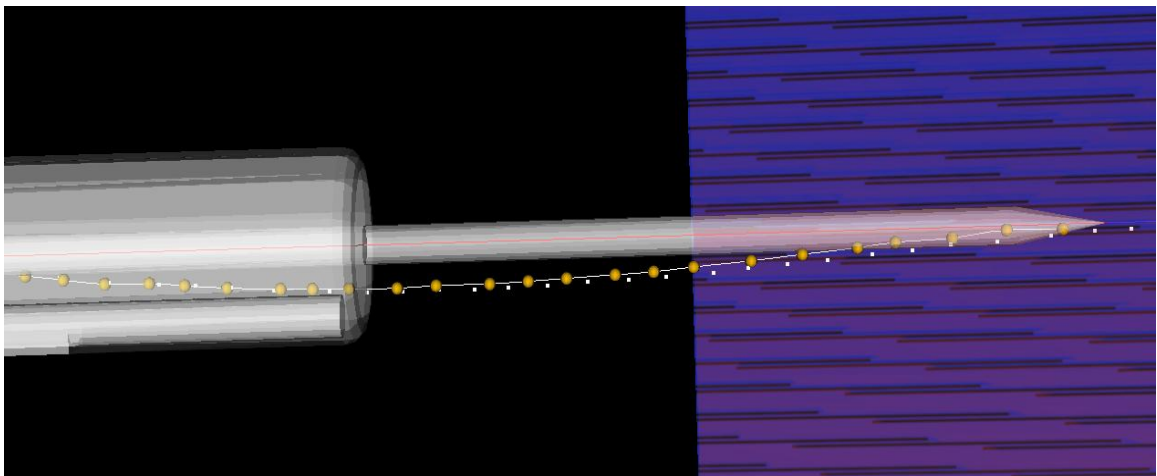


Figure 3.26: Needle path prediction

With the change in orientation, the path updates itself to show the new path the needle would take. The user can use this information to orient the needle so that the path would lie as close as possible to the target. Once the needle is oriented, the needle can be moved straight in and the user can visualize the path the needle takes and the path this module predicted.



(a) Initial stage



(b) Final stage

Figure 3.27: Needle path prediction with the current needle path

Figure 3.27 shows the closeness of the paths in one such test insertion using this module. The blue line indicates the path projection, the white squared dotted line is the path prediction and the yellow round dotted line is the run-time needle path.

3.2.4 Virtual US probe and the real-time 2D US image

As mentioned earlier, a 6-DOF electromagnetic sensor is attached on the US probe. The resulting information obtained from the sensor is used to render the virtual US probe (STL object of an enclosing sleeve) and the 2D US image plane in the 3D virtual world. These virtual objects update their position and orientation in real-time and mimics the motion of the real-world US probe. Figure 3.28 shows the virtual US probe along with the 2D image rendered below it. This image which is rendered in 3D space overlaps on the volumes that are captured and rendered in the same space. The US image can be moved all over the volume to understand the features that are lying in the image by visualizing on 3D reconstruct of the sweep. This provides essential information and helps to detect the various vital attributes such as the needle tip, the tumor shape and size etc. which are very hard to determine by querying just the 2D image plane.

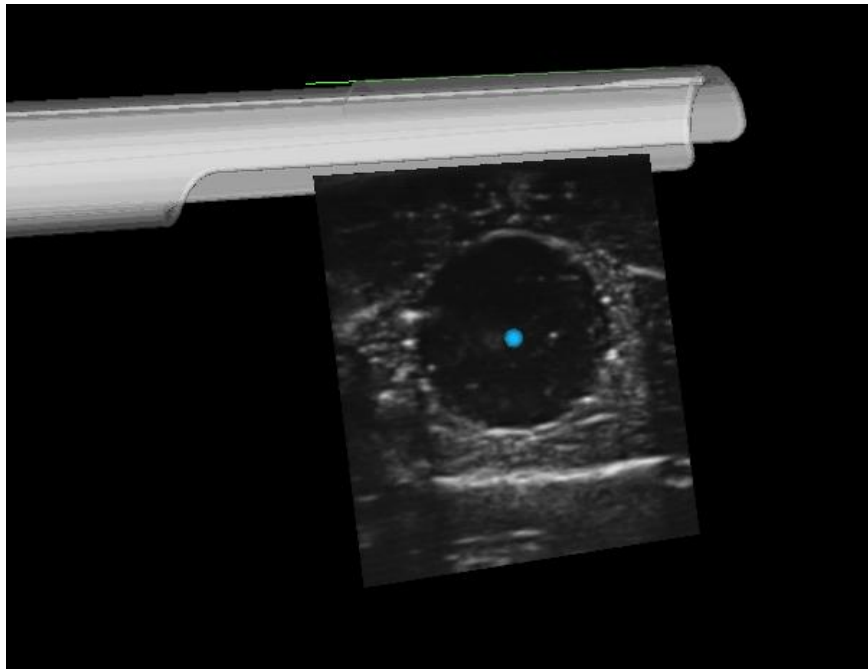


Figure 3.28: US probe and the 2D US image rendered in 3D space

Figure 3.29 shows a 2D US image rendered on top of the virtual 3D volume. The volume and the image can be seen in sync with the physical attributes observed in the image.

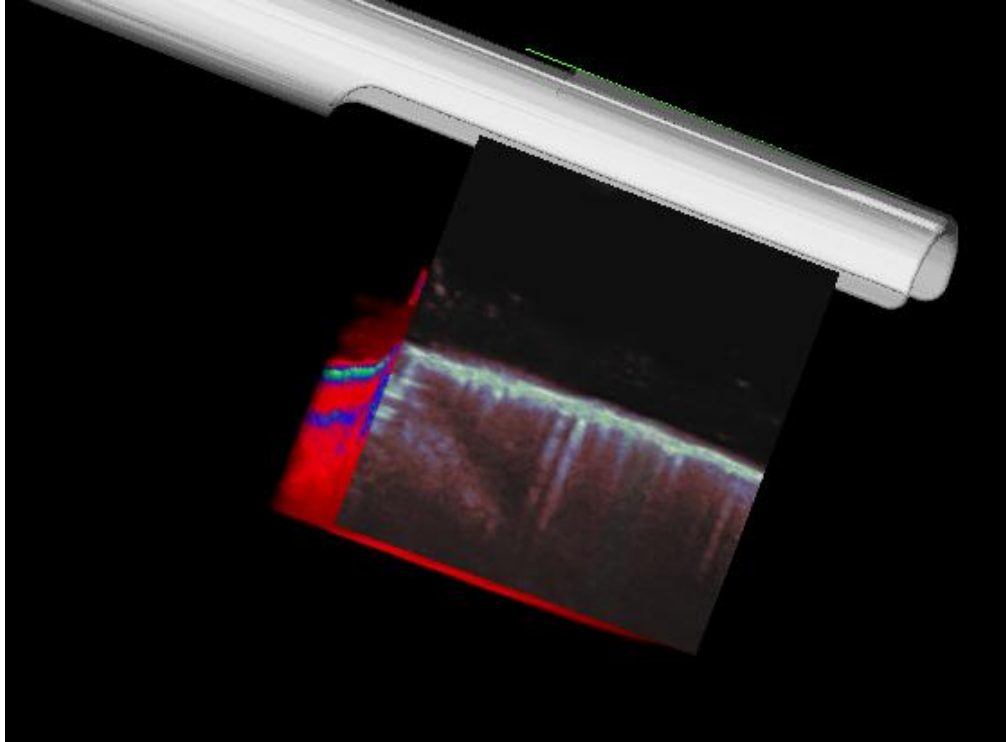
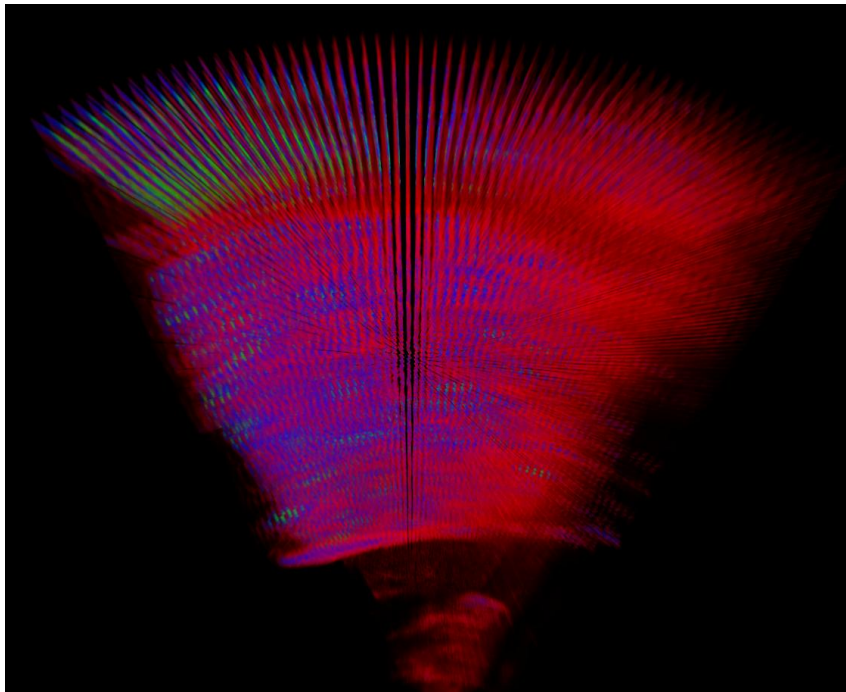
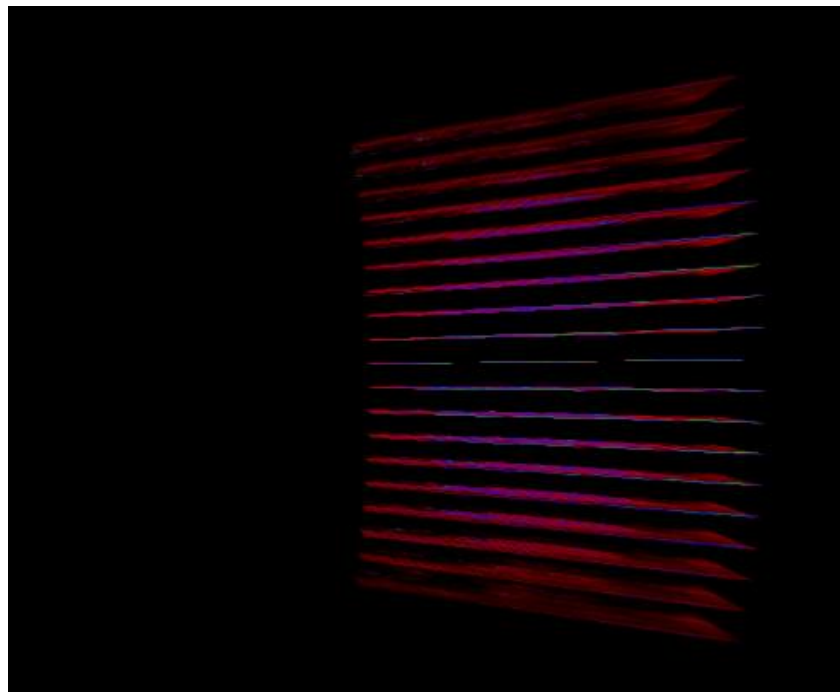


Figure 3.29: US image superimposed on a volume

Having the 6-DOF sensor, the roll of the US probe can also be visualized as well. Figure 3.30 (a) shows the US images grabbed after being rotated about its axis for a round sweep. Figure 3.30 (b) shows the image capture mode for the flat sweep method.



(a) Round sweep model



(b) Flat sweep model

Figure 3.30: Image capture model

The visibility of the 2D US image can be toggled to compare the features in the underlying volume and to avoid the occlusion caused by the image hindering the visibility of other objects in the scene. This helps in detecting occluded objects in the virtual world without moving the real world US probe.

3.2.5 US video output window, target selection and visualization

The left dock top window has the real-time US video stream. This can be used to select the targets for the 3D virtual world. As the US probe sweeps a particular region, the user must identify appropriate points of interest using the physical artifacts such as a vein bifurcation, center of the tumor etc. Figure 3.31 displays a target selected in the US video output window and the corresponding target highlighted by blue sphere in the 3D virtual world.

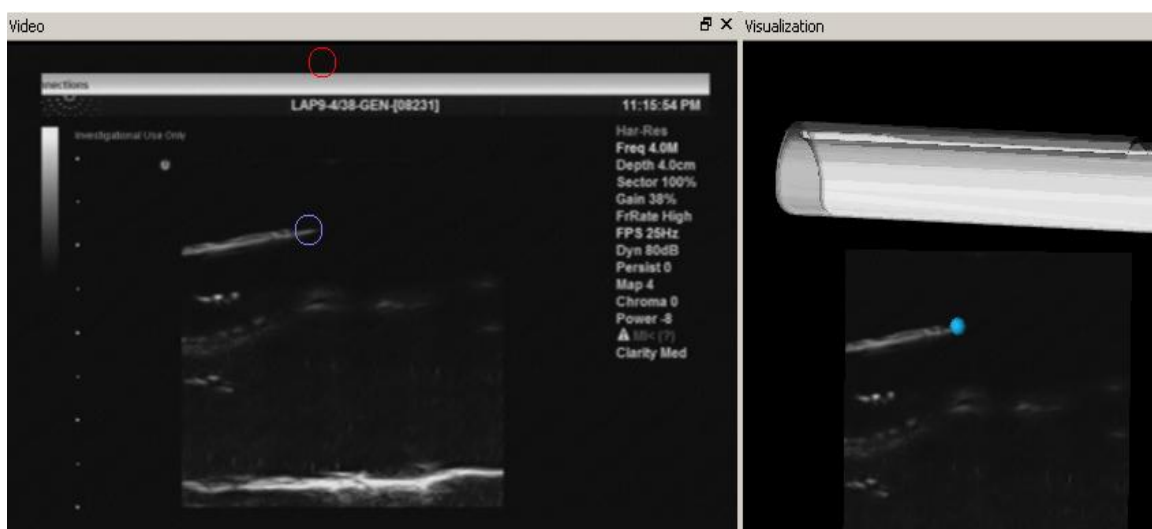


Figure 3.31: Target selection and visualization

As soon as a target is selected, the distance of the target from the needle tool tip is calculated and displayed in the status panel. This value updates constantly when the needle navigation is in progress. When the motion of the surgical site is subjected to virtual objects, it is hard for the user to select a target on the moving objects; this is why the US video output window is used to select the target as it not subjected to any induced motion.

3.2.6 Volume rendering and opacity transfer

InterNAV3D has the capability to add multiple volumes and render a complete sweep of the surgical site. New volume can be grabbed using different sweep methods as described earlier. For every new volume grabbed and rendered, a unique volume ID is tagged to distinguish it from other volumes. For each volume a pre-specified or adaptive intensity and piecewise opacity transfer function is applied, to select and color the various gray scale levels and to change its opacity to the levels specified [91], [102], [103]. Many times a specific region of an image has some unique common quality; for instance, the intensity value can distinguish a specific entity such as the tumor, tumor edge, the needle etc. This module provides control over displaying only the part of the 3D volume that is considered appropriate for better feature recognition and visualization. By controlling opacity values, only certain intensity range voxels are displayed and visualized. Figure 3.32 shows a volume rendering and opacity control output. Each image represents the same volume. The different intensity values are represented by different hue values (colors). The images shown here use different opacity values to make certain aspects of the image looks opaque or invisible (transparent).

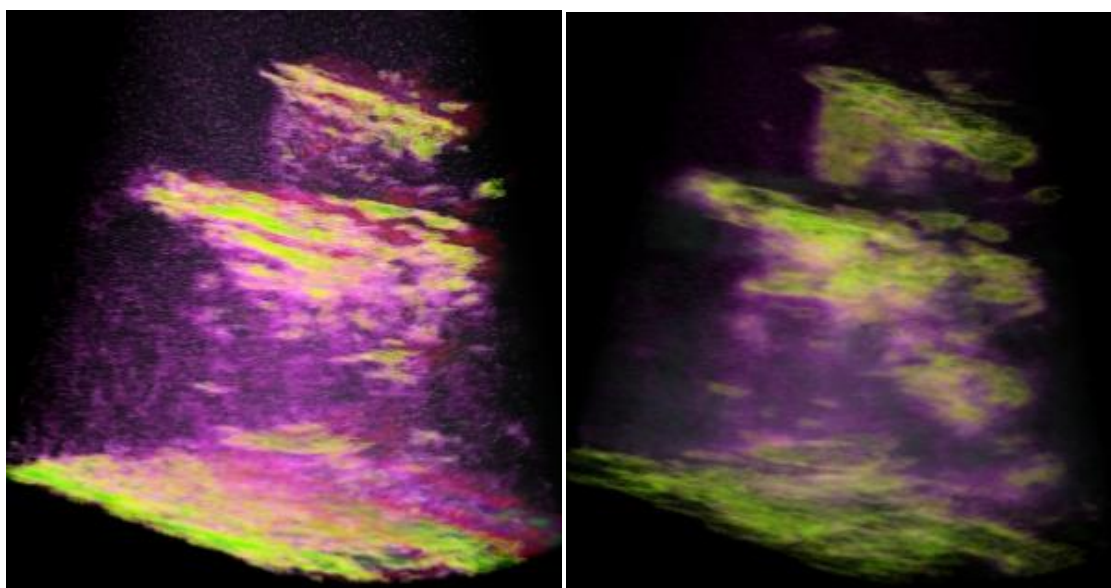


Image (a)

Image (b)

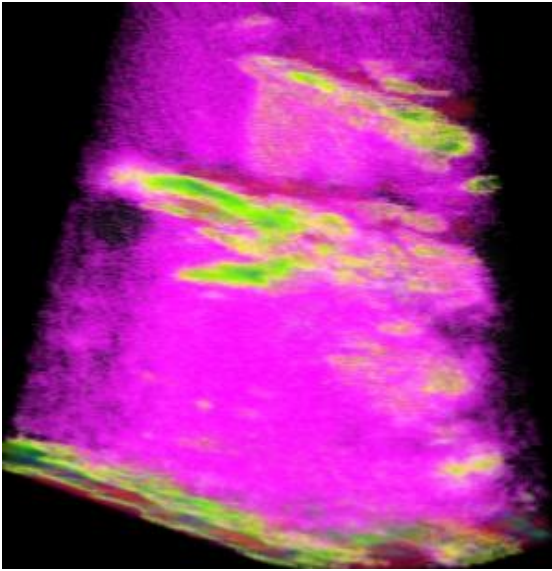


Image (c)

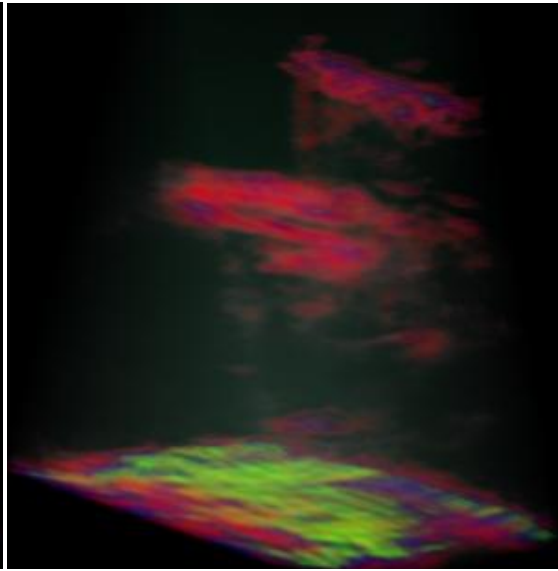


Image (d)

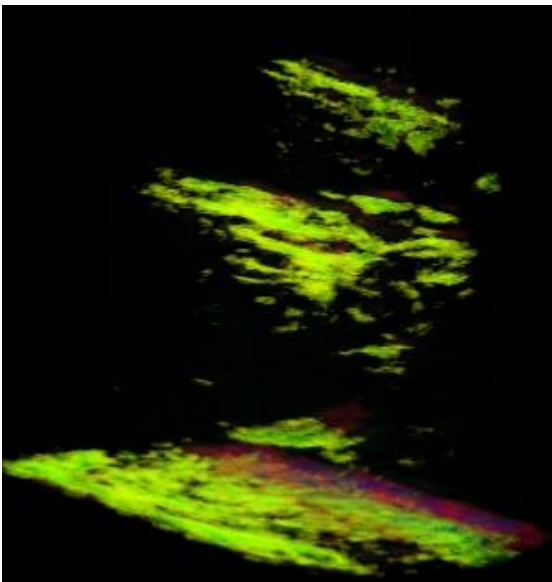


Image (e)

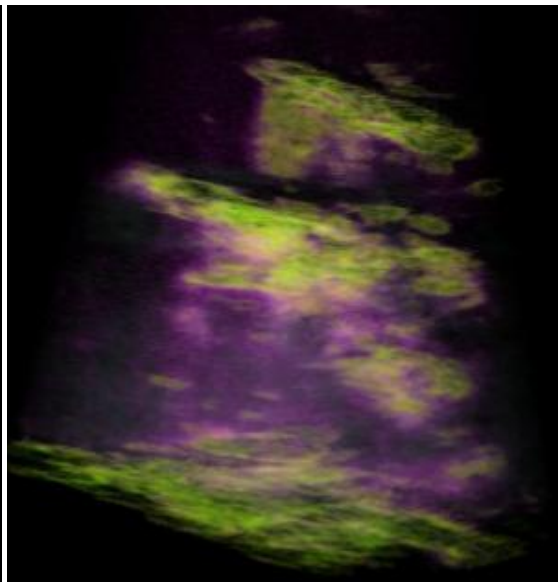


Image (f)

Figure 3.32: Opacity transfer function

3.2.7 Surface rendering and sub-surface reconstruction

Surface rendering is one of the important modules developed to help figure out the shape of the tumor in 3D space. A surface is a bounding region in 3D space that can completely encompass physical artifacts such as a needle, a vein, a tumor etc. The module in InterNAV3D takes binary image files as input. These image files are obtained by passing the US image files through a series of image processing filters such as image thresholding, morphological operations, smoothing etc. The surface panel has options to select the range of intensities to be used in the process by the help of a dual slider interface. The morphological operations and other filters help to clean up the data for the next step where surface reconstruction takes place. The method used for extracting the iso-surface from the 3D image volume is the marching cubes method which is one of the most commonly used and efficient methods [104]–[106]. A built-in VTK function (for marching cubes) was utilized to get the results. A typical surface reconstruction example showing a segmented needle and part of the underlying test-bed is shown in Figure 3.33.

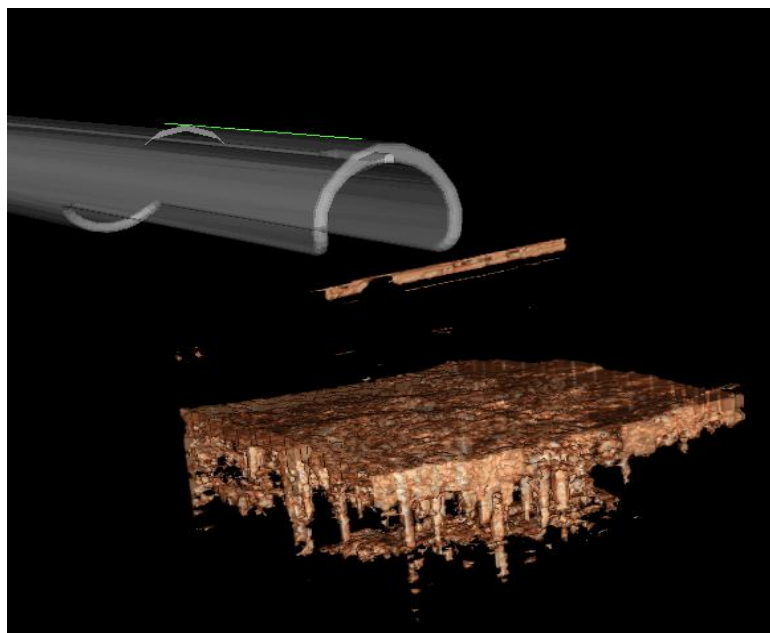


Figure 3.33: Surface reconstruction

The surfaces thus formed are always superimposed on the 3D volume so as to get better cognitive understanding of the surgical site as shown in Figure 3.34.

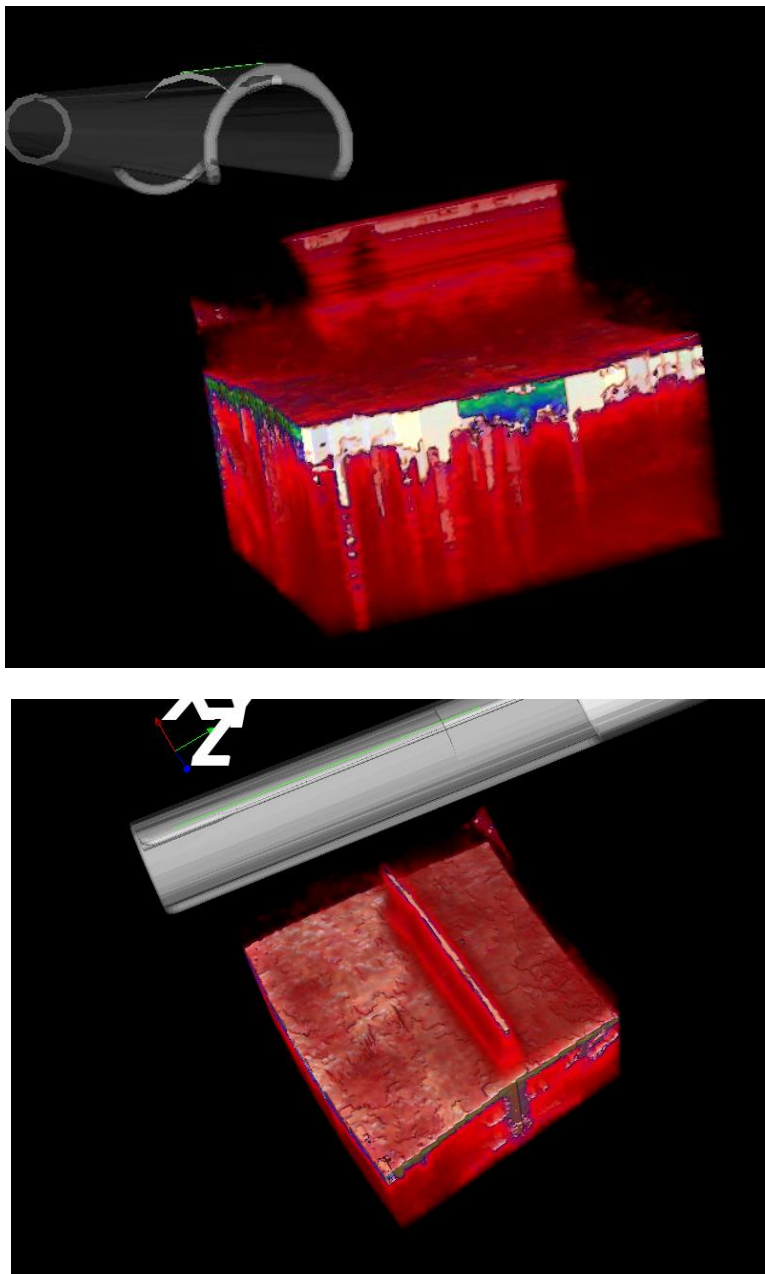


Figure 3.34: Surface reconstruction superimposed over volume

The opacity of the reconstructed surface can also be altered so that a 3D volume can be looked through the surface for hidden features. The surface visibility can be toggled so that either a complete volume or a complete surface reconstruction output is visible at any particular instant. Physical artifacts can be compared among the virtual objects by toggling their visibility or opacity. By default InterNAV3D performs surface

reconstructions of the complete 3D volume. However, a certain region (henceforth mentioned as “bounding box”) can be selected manually or determined automatically (using software), so that the focus is laid only on the area of interest as shown in Figure 3.35. The position of the bounding box is determined by the option provided by the user (either a selected target location or the software computed needle tip location).

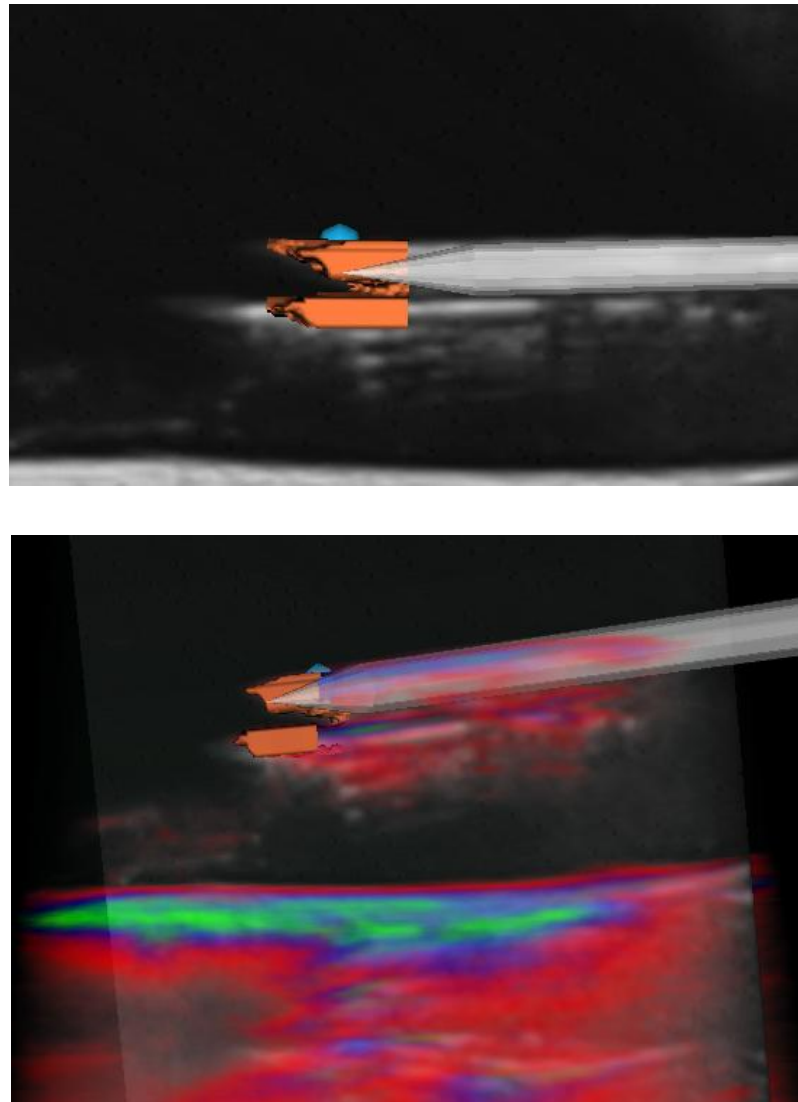


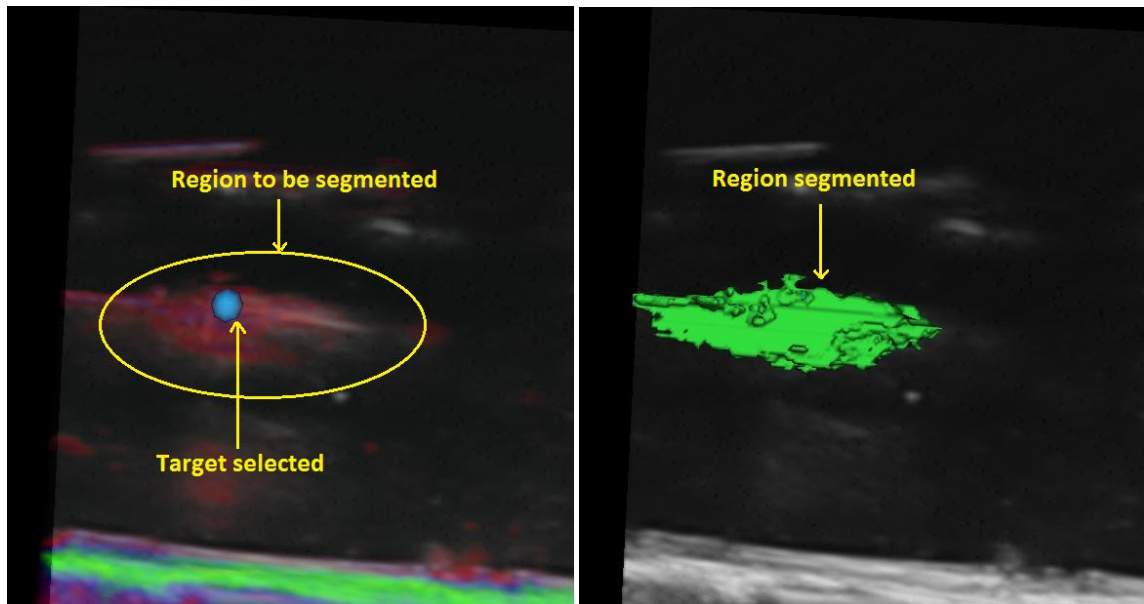
Figure 3.35: Sub-surface reconstruction

This region is processed and searched to locate needle tip by visualizing the surface reconstruction (the bounding box can be imagined as the range of the space where the needle tip is most likely to be found). To achieve efficiency and to make the system

computationally faster, a method to reduce the resolution of the surface and to change the size of the bounding box of the surface is devised and implemented. These options help in the scenarios where the user does not know if the needle tip has reached the target, due to the needle deflection or a similar reason.

3.2.8 Region reconstruction

Region reconstruction is a region growing algorithm implemented as a module in InterNAV3D. It is an image processing based segmentation procedure. Depending on the images, it is possible to segment particular regions of interest by selecting certain points (termed as seeds) within the region. These seeds satisfy the properties of the segmented region. Using these seeds as the guidance/instantiation point, a region can be segmented where all the neighboring pixels/voxels of the region satisfy certain condition (such as grayscale value, hue value). Multiple iterations can be performed and each satisfying pixel/voxel is tagged as a point residing within the region or outside the region.



(a) Seed selection

(b) Region growing reconstruction

Figure 3.36: Region reconstruction

Tagging is continued till specified iterations are completed or till all the points are classified. The tagged pixels/voxels form a region that shares a common culture of

aspects and is the desired segmented part of the image. This method can be used to segment any artifact such as a needle or a tumor by selecting the points within the suspected region using the interface. Figure 3.36 shows a typical region reconstruction output.

3.2.9 Motion simulation

In a real surgical scenario for a lung cancer treatment, most of the time there is a residual motion in the surgical site due to respiratory motion of contralateral lung and/or due to the heart beat. In such conditions it is very hard to hit a target using an interface that does not account for motion. A motion simulation option which enables 3D objects in the virtual reality world to mimic the motion of the surgical site has been implemented in InterNAV3D. This option computes the motion of the surgical site by getting the electromagnetic sensor values from the sensor attached to the US probe which moves in sync with the movements of the surface of the lung being imaged. This motion is then added to the 3D volume and other relevant objects in the virtual world. The target, if selected, can also be moved in sync with the virtual volume. This feature helps in the needle maneuvering while the surgical site is under the influence of external motion.

3.2.10 Needle navigation

This module is derived from the older version of InterNAV. Once the target is selected, the task is to maneuver the needle to the target and hit it. For this, proper orientation and alignment of the needle tool is necessary to travel to the target. Initially, a target is selected by the user. The distance of the needle tool tip to the target is calculated and displayed on the user interface status panel which provides an estimate to the user of how much the needle motion would be needed. The option of auto-move calculates the projection of the target on the plane perpendicular to the needle tool axis and passing through the needle tip so that an easy estimate of the orientation can be done. Once the tool is correctly oriented, the interface can be used to maneuver the tool inside the surgical site to reach the target automatically or manually using the robot movement control buttons from the interface panel. A needle tip eye view method from the previous InterNAV version was customized and implemented that assumes the camera of the 3D

virtual world to be set at the needle tip point. This provides a needle eye view as shown in Figure 3.37. This helps in improved feature recognition of the surgical site. Suggestive directions are rendered on the window while the needle is maneuvered manually which eases the target hitting process.

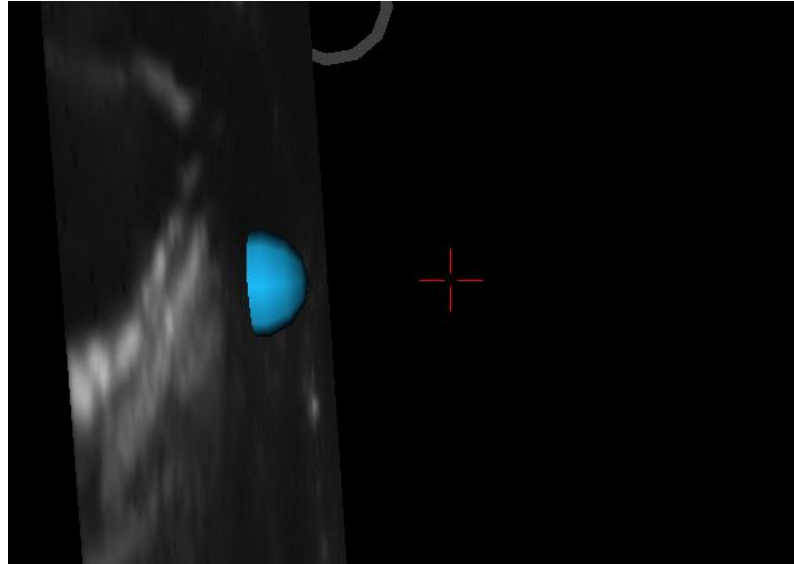


Figure 3.37: Needle eye view

3.2.11 Camera movements and additional windows

The camera is the view port through which the surgical site is viewed. The VTK library allows changing the location of camera by use of mouse movements. Various options such as zooming in or out, translating a scene, changing the orientation of the view etc. can be done with ease. Multiple viewports to visualize the image from the 3 orthogonal axis directions can be implemented. A 3D slicer that slices the 3D volume in 3 orthogonal directions has been implemented as shown in the Figure 3.38. At the same time an oblique re-slice module was implemented which allows the user to slice and visualize cross sections of the volume across any orientation as shown in Figure 3.39.

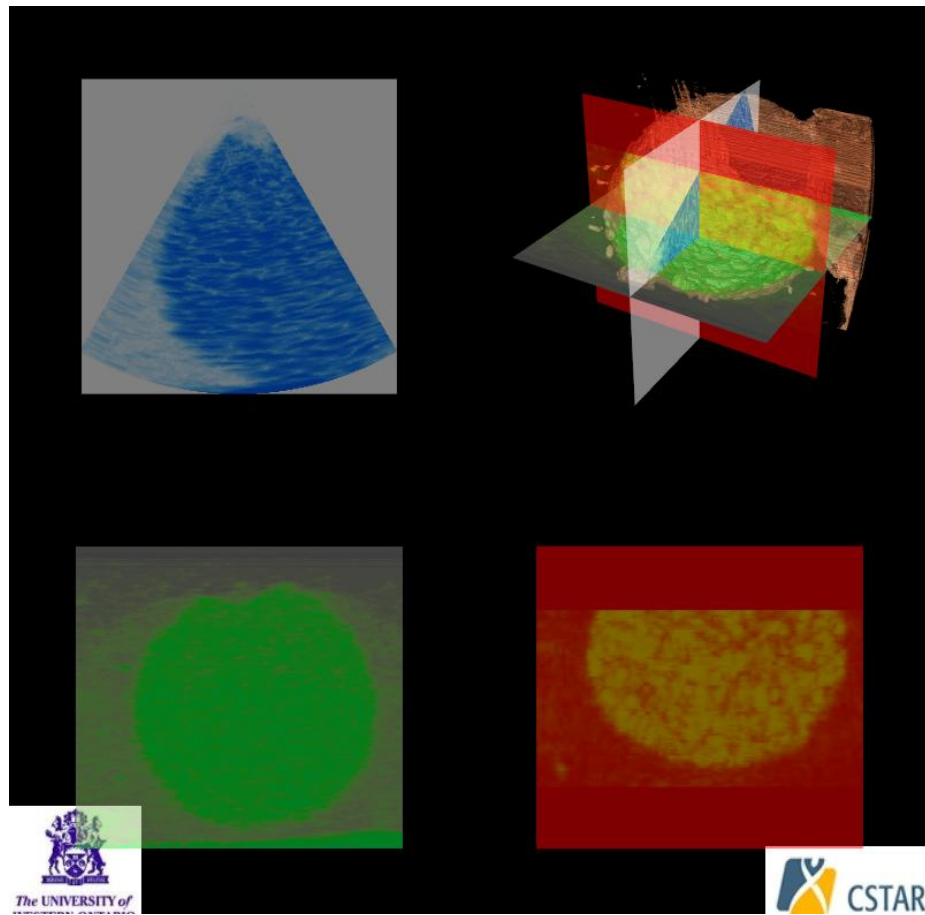


Figure 3.38: Three orthogonal views

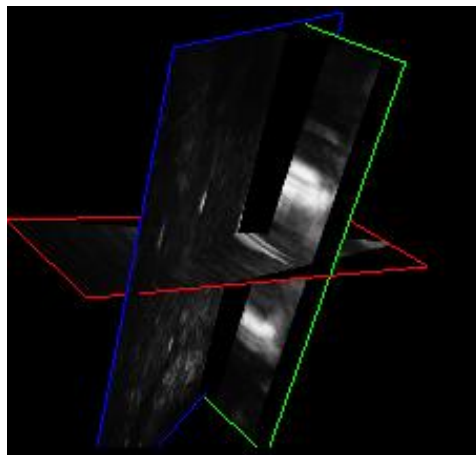


Figure 3.39: Oblique re-slices

3.3 Remarks

The complete user interface of InterNAV3D has been described and individual functionalities of the implemented modules are explained in detail. The interface design was implemented using Qt software tool and can be modified with ease. The most important benefit of the interface design is in its framework. As all the important panels are divided in the dock windows, they can be undocked to form a separate entity window for better control. These windows can then be rendered separately on different screens of the system (if multiple screens are connected). It would thus provide with a better, enhanced view and easy control in the surgical room. The size of these screens can be modified in run-time as well.

Chapter 4

4 Experimental Overview

This chapter contains a detailed explanation of the experimental setup and the calibrations performed for the InterNav3D system. The initial section focuses on the design and construction of various components manufactured during the development of the system, the experimental test-bed used for evaluating the system and the calibrations needed (in order to get the system working). The latter section describes the logic behind the experiments and assesses the entire system based on the results obtained.

4.1 Experimental test-bed

The experimental setup consists of the robots ZEUS and AESOP used to hold and maneuver the US probe and the needle respectively. Electromagnetic trackers were attached to both the tools and calibrated to retrieve real-time information of their orientation and position in the surgical workspace. These robots have two passive joints (DOFs) at the end effector (discussed in Chapter 2). The surgical tools thus mounted on these robots required a fixed pivot point for proper placement and alignment in the workspace (to orient in a specified direction). For the *in-vivo* experiments, the pivot point lies within its respective trocar; however for the *ex-vivo* experiments, a physical setup was needed (to imitate the trocar/pivot point).

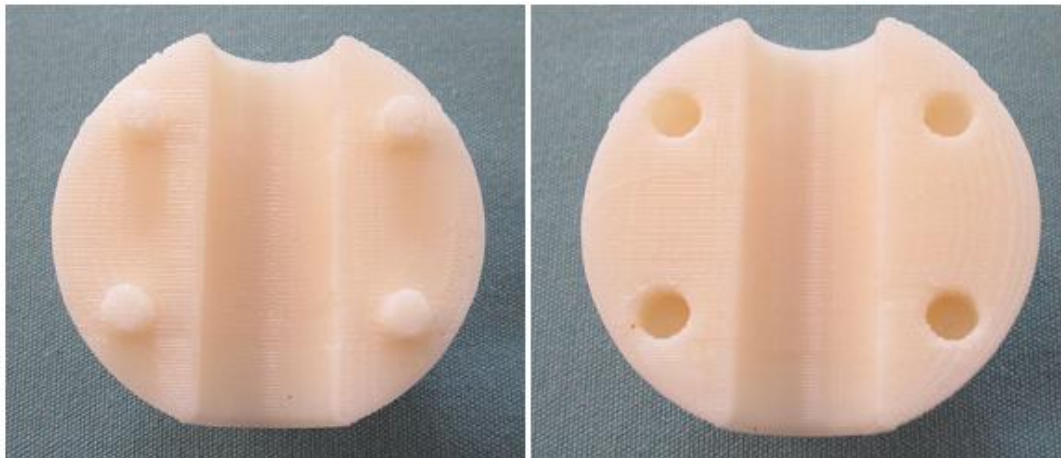


Figure 4.1: Ball and socket joint (semi-spheres)

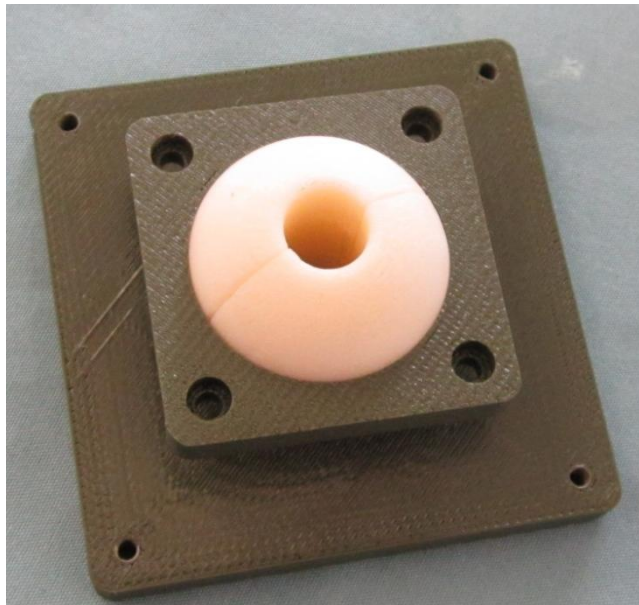


Figure 4.2: Ball and socket joint (attached)

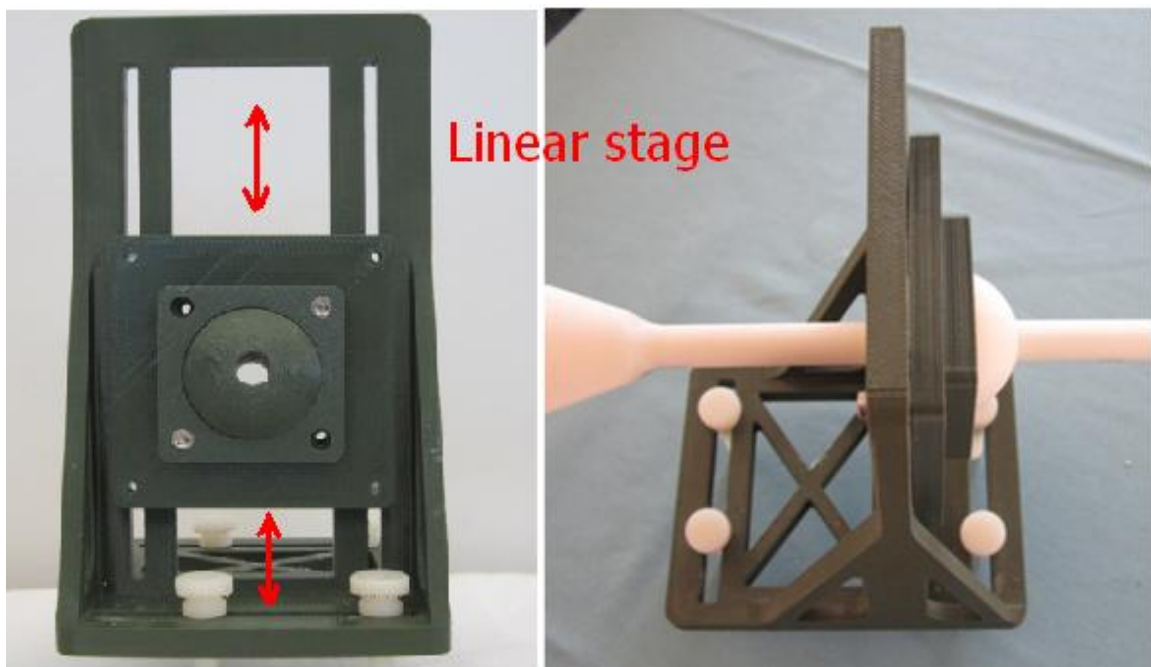


Figure 4.3: Linear stage

Solidworks was used to design a pivot point that could work for numerous surgical scenarios. It consists of a ball and socket joint as shown in Figure 4.1 and Figure 4.2. It is able to move freely and is suspended on a vertical linear stage as shown in Figure 4.3.

A wooden board was used as the test-bed to attach the linear stages (both for the US probe and the needle). It had a pre-specified set of locations that allowed for the vertical stage to be connected and moved in the horizontal direction. Most of the parts were designed in Solidworks and manufactured in a 3D printer. Figure 4.4 provides the view of the test-bed with the needle and the US probe attached to the robots and passing through their respective pivot points.

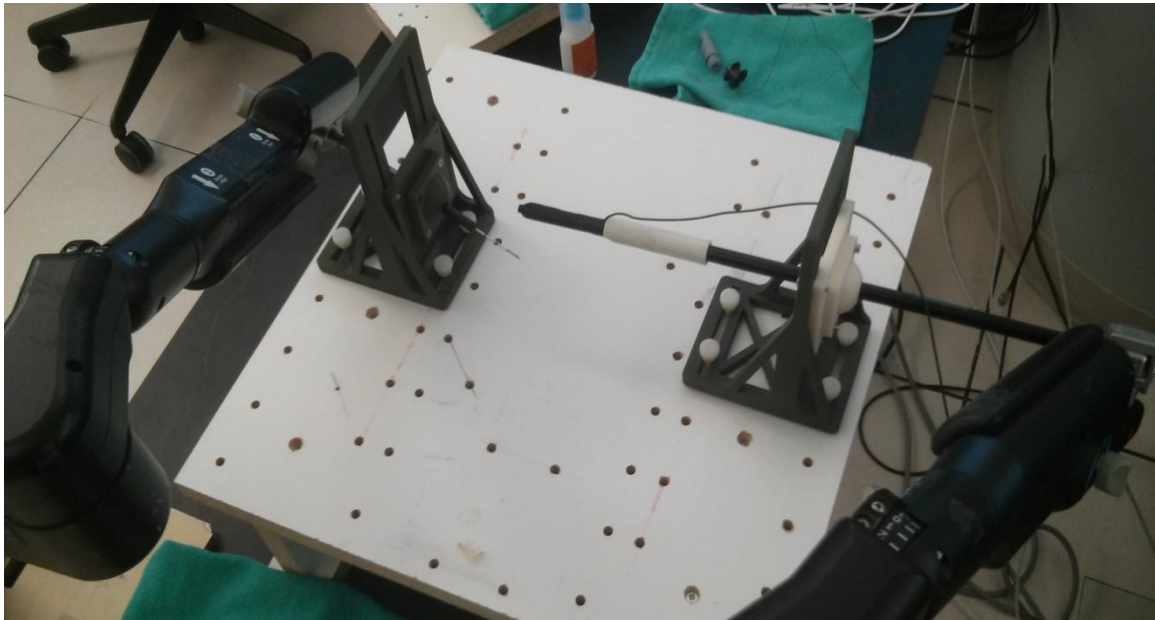


Figure 4.4: Entire test-bed

Physical sleeves to attach the electromagnetic tracker and to connect the tools with the respective end effectors were designed and implemented. Chapter 2 discussed some of the designed sleeves. Appendix-A provides the Solidworks design of the manufactured sleeves, the test-bed and in effect represents their evolution history.

The electromagnetic field generator for position tracking was placed below the surgical workspace, both in *in-vivo* and *ex-vivo* scenarios. The rest of the system as described in Chapter 2 was implemented for the experiments.

4.1.1 Motion induction

To imitate cardiac and/or respiratory motion for the *ex-vivo* test-bed, a motion induction system consisting of an inflatable structure/balloon (an elastic glove in this case) with an air pump mechanism was integrated. Figure 4.5 illustrates the apparatus that pumps the compressed air in the balloon to inflate it.



Figure 4.5: Air pump mechanism

A solenoid mechanism controls the duty cycle and frequency of the compressed air that can be changed by a graphical user interface. A valve is used to control the amount and rate of air that needs to be released through the balloon for deflating it. This system was developed in CSTAR for another project and was customized to be used as a

phantom test machine to imitate heart/lung movements. This architecture helps to represent the motion that happens in real surgical scenarios due to respiration of the contralateral lung and cardiac motion. The exact motion that occurs in a real surgical scenario might be highly variable and different from the motion generated by the setup (depending on the location of the target, extent of lung deflation and the change in frequency of motion). However, this setup was used to demonstrate that several types and/or frequencies of motion can be visualized in the InterNav3D software system. Needle maneuvering and target hitting becomes intuitive when such motion is being visualized as it represents the behavior of the surgical site. Figure 4.6 shows the motion inducing system. The top part shows two images when the phantom is deflated and inflated and the bottom image shows the components used.

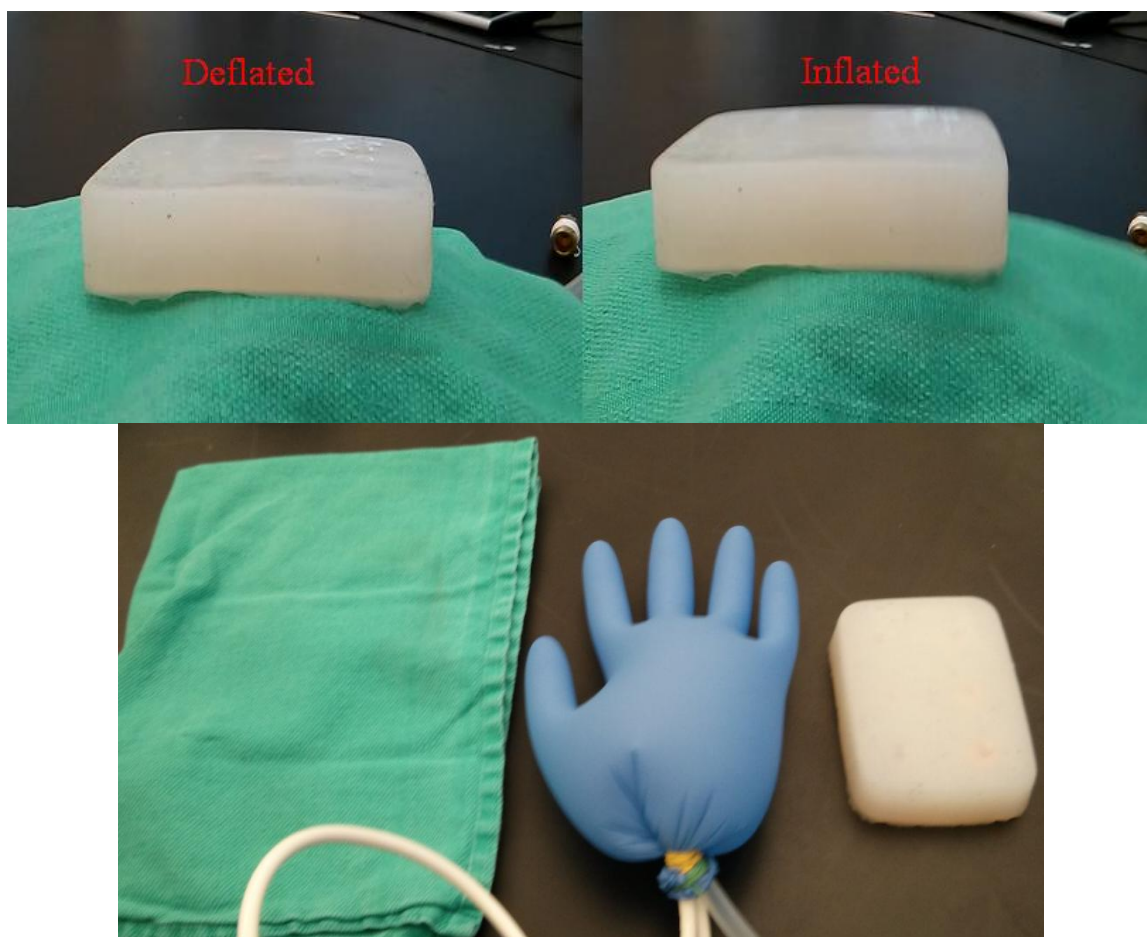


Figure 4.6: Motion inducing system

It is important to understand how the volumes are formed and what errors, if any, are present. For applying any type of volume information to the system, it is essential to know the location of individual 2D images within the 3D volume. Due to the high dexterity of motion, achievable by using the robotic arm, different methods of image capturing modes such as rotational sweep, palpation sweep are possible. The robotic arms used (AESOP & ZEUS) and their kinematic model, were described in Chapter 2. In this section, an algorithm to convert the set of 2D images to 3D volume for a particular image capturing mode is described. Figure 4.7 shows a typical rotational sweep volume capture mode. An ideal case where the various mechanical drawbacks such as backlash and resolution limits are null or negligible is considered for the simplicity of explanation. The following method was used for a rotational sweep volume reconstruction. Here we have real-time information of the location of the image slices in space by the use of a calibration method (the method is discussed in a later section).

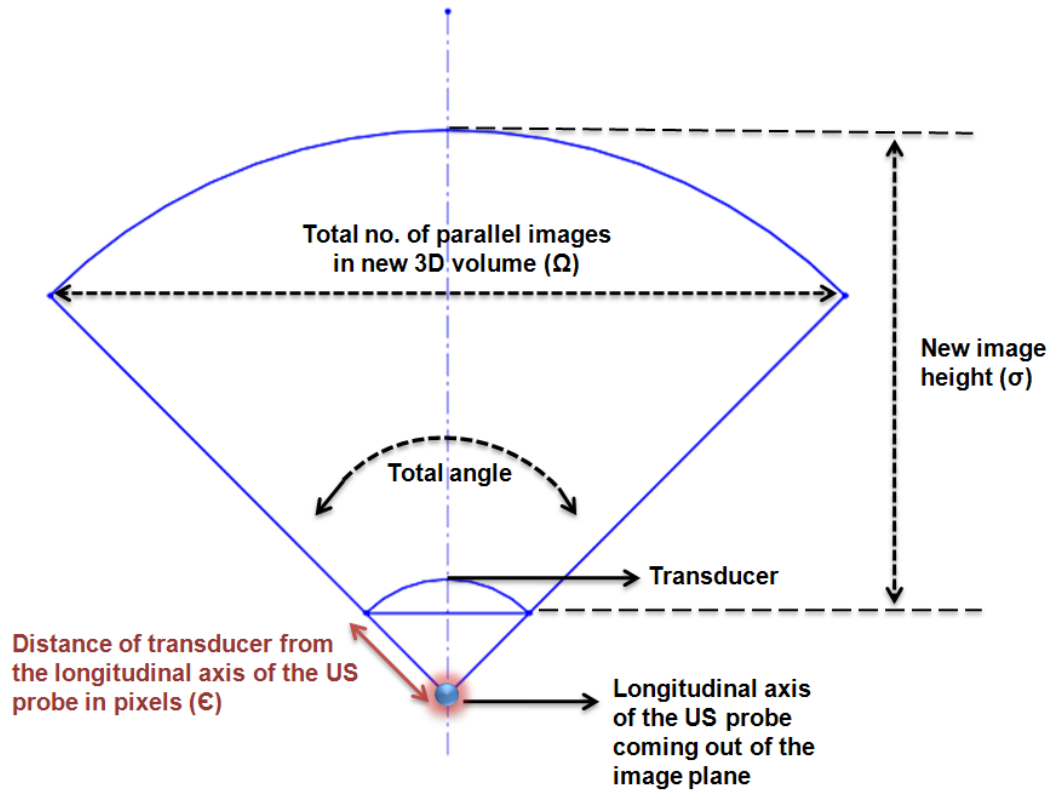


Figure 4.7: Rotational sweep capture model

The user needs to select the number of image samples that he/she wishes to capture and the difference of angle between successive images. Multiplying those provides the total angle that the transducer is going to move around its longitudinal axis (for rotational sweep). The image resolution is pre-decided and the ratio of pixels to physical distance (pixels/mm) is calculated (by the calibration process discussed later).

The problem statement now is to convert the group of images captured during a sweep procedure into a series of parallel images (for construction of a 3D volume). The model for constructing the 3D volume out of the 2D image sequence for a rotational sweep method is explained below.

The following are the known values:

α = the step-angle (angular gap between successive 2D images) in degrees,

β = number of images captured,

M = image height in pixels,

N = image width in pixels,

R = ratio of pixels to physical unit (pixels/mm); the value of R is calculated by a calibration process described later in this chapter,

ϵ = distance of transducer from the longitudinal axis of the US probe in mm.

Now, the total angle of rotation = $\alpha * (\beta - 1)$

Distance of the transducer from the longitudinal axis of the US probe in pixels = $R * \epsilon$

Size of the 3D image buffer V_{old} (to store the grabbed images)

$$V_{old} = [M, N, \beta]$$

Total number of parallel images Ω in the new volume

$$\Omega = 2 * (M + (R * \epsilon)) * \sin\left(\frac{\alpha(\beta - 1)}{2}\right) + 1$$

New image height σ for V_{new}

$$\sigma = \left(R * \epsilon * \left(1 - \cos\left(\frac{\alpha(\beta - 1)}{2}\right) \right) + M \right)$$

Size of the new 3D volume V_{new} is $[\sigma, N, \Omega]$

$$V_{new} = \left[\left(R * \epsilon * \left(1 - \cos\left(\frac{\alpha(\beta - 1)}{2}\right) \right) + M \right), N, \left(2 * (M + (R * \epsilon)) * \sin\left(\frac{\alpha(\beta - 1)}{2}\right) + 1 \right) \right]$$

A correlation is needed to transfer the 2D images to the 3D volume. Solving for the following values provide a one-to-one relationship between the angle and the slice number of the image

$$X_1 = -\theta, X_2 = \theta; Y_1 = 1, Y_2 = \beta$$

The slope m can be calculated as

$$m = \frac{(Y_2 - Y_1)}{(X_2 - X_1)}$$

The constant b in the linear equation is

$$b = 1 + \left(m * \left(\frac{\alpha(\beta - 1)}{2} \right) \right)$$

Once the relationship is obtained, a one-to-one correspondence to transfer the pixel values from V_{old} to V_{new} is performed.

*For radius τ from $(\phi + 1)$ to ω and angle δ from $-\theta$ to θ with step values $v = 1.075 - \sin(\sqrt[3]{\tau} * 12)$ (calculated from experiments)*

$$x = \left((M + (R * \epsilon)) * \sin \left(\frac{\alpha(\beta - 1)}{2} \right) \right) + 1 + \tau \sin(\delta);$$

$$y = \tau \cos(\delta) - R * \epsilon * \cos \left(\frac{\alpha(\beta - 1)}{2} \right);$$

$$\varepsilon = 1 + m \left(\delta + \left(\frac{\alpha(\beta - 1)}{2} \right) \right);$$

$$\Psi = \tau - (R * \epsilon);$$

$$V_{new}(y, N, x) = V_{old}(\Psi, N, \varepsilon)$$

For the conversion of the 2D images to 3D images, a nearest-neighbor interpolation was used. Figure 4.8 shows a scatter plot visualization of the interpolation method. It can be observed that as the radius and angle increase, the information needed to fill in the gaps between successive images increases. The higher the resolution of the sweep method (lower the step-angle), the better is the quality of the reconstructed 3D volume. However, a higher memory is needed to store the large data-set of images which in turn increases the computational time for processing the images. Thus, a trade-off exists and inherently depends on the need of the application. The option that allows the user to choose the resolution of the sweep method is implemented. Appropriate programming code was generated which takes care of mapping all the pixels from one coordinate space to the other coordinate space. The sweep model for the straight flat sweep method was also implemented.

It is important to mention here that for the rotational sweep method, the step-angle can be controlled easily and the radius of the sweep is constant (original image height). However, in case of the straight flat sweep, the radius of rotation (the length of the transducer from the pivot point) can change before any sweep and due to this uncertainty, computing the resolution of the image capturing mode becomes unintuitive. To overcome this drawback, a method to use the electromagnetic sensor feedback to calculate the degree of rotation and the radius of the sweep method was devised and implemented.

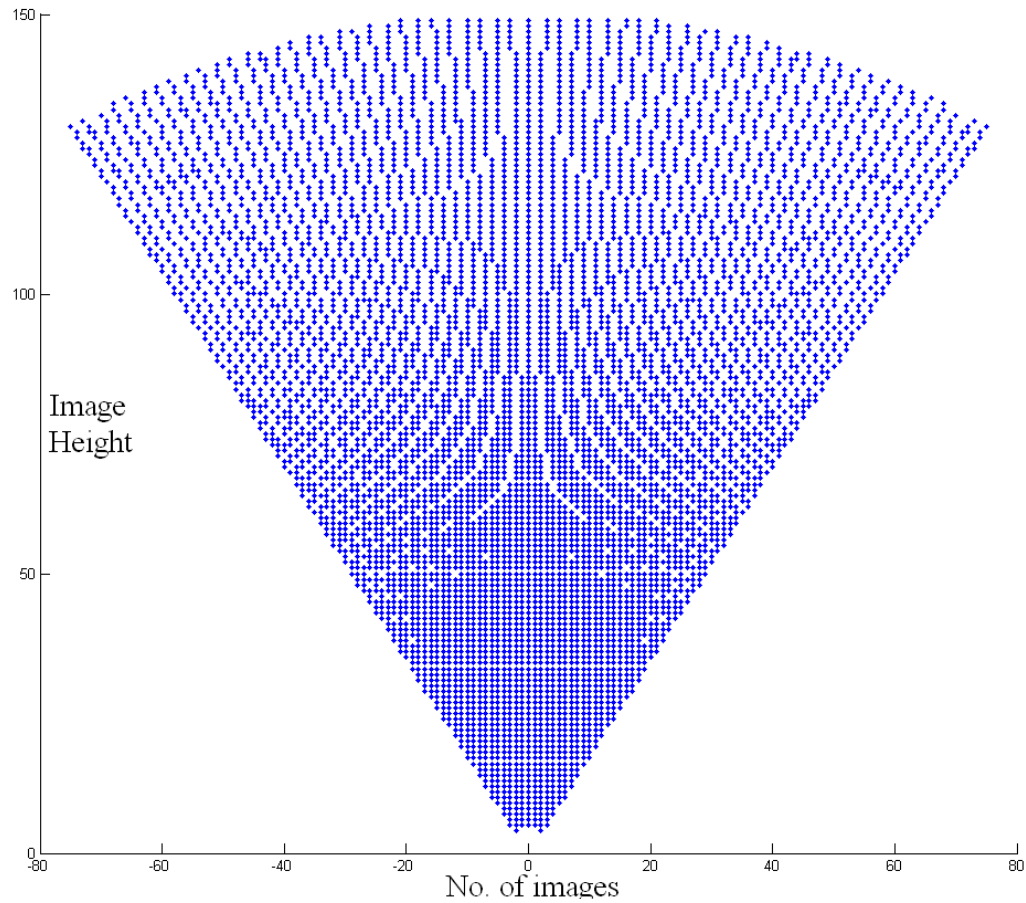


Figure 4.8 Scatter plot for 2D to 3D image conversion

4.2 Calibration

For proper working of the entire system, various calibrations were needed. These calibrations help to get the accurate information from the surgical system in real-time and assist in improving the accuracy of the results of the experiments performed.

4.2.1 Needle tool tip calibration

An electromagnetic tracker is required to retrieve the information of the position and the orientation of the needle in the experimental workspace. A needle sleeve to enclose the needle and attach it to the robot end-effector was designed. This sleeve incorporates an empty notch that was used to affix the electromagnetic sensor. The notch was designed such that the electromagnetic sensor is oriented in the best way possible parallel to the needle axis; however, it cannot be guaranteed that the needle axis and the electromagnetic

sensor's axis align perfectly as required. Hence, a calibration method was devised to evaluate this difference and compensate for the error. Once the calibration is applied, the location of every point of the needle in the workspace can be computed.

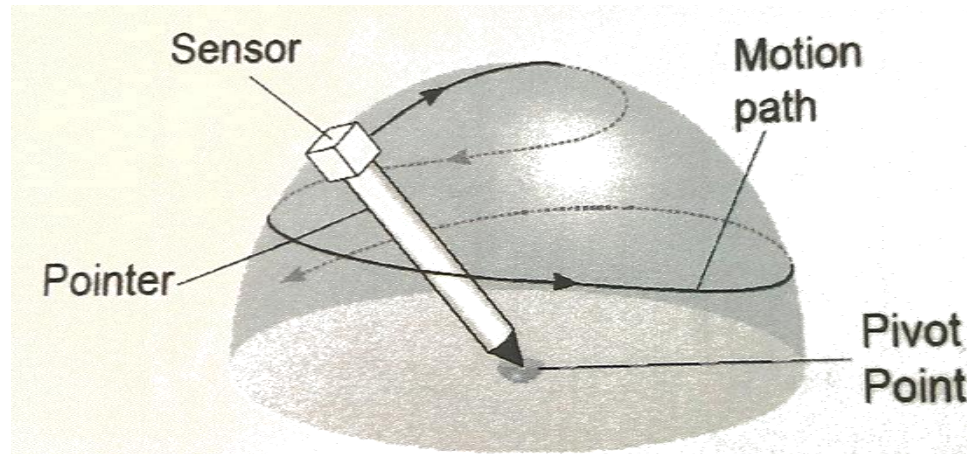


Figure 4.9: Pivot tool-tip calibration

The calibration method described here comes as an interface application tool with the software package of NDI's Aurora electromagnetic tracking system. Before the calibration is applied, it is very important to ensure that the sensor is attached to the tool body as a rigid extension (such that the relative motion between them is zero). Once it is taken care of, the interface application tool can be used for calibration. The application tool asks for the pivot instrument (in this case, the needle) to be pivoted by its end point on a rigid platform. The complete body is then moved to and fro around the tip in different orientations with the fixed pivot point so that enough sample data is captured for the required calculations as shown in Figure 4.9. This data is then processed to estimate a local transformation matrix that transforms the position and orientation of the sensor to the tip of the needle. The accuracy of the calibration can be evaluated by using the interface designed for InterNav3D.

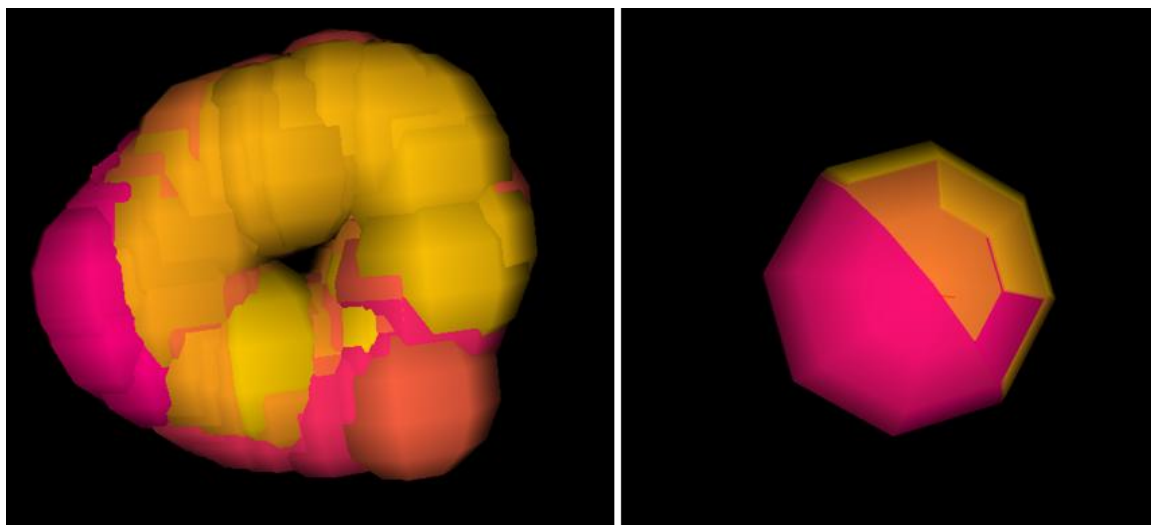


Figure 4.10: Needle tip calibration

In this interface, a calibrated needle tool is moved along its longitudinal axis. At every step of the motion, a point (sphere) is rendered at the needle tip. If an error exists, the group of points forms a ring like structure as shown on the left in Figure 4.10 which means the needle is not calibrated properly. Different color represents different spheres (needle tip points) at different time interval. The radius of the ring thus formed represents the extent of the error. In this case, a re-calibration is performed by the pivot calibration method or a manual calibration using the visualization toolkit. A typical successful calibration process output is shown on the right in Figure 4.10 and the values of the same in Figure 4.11.

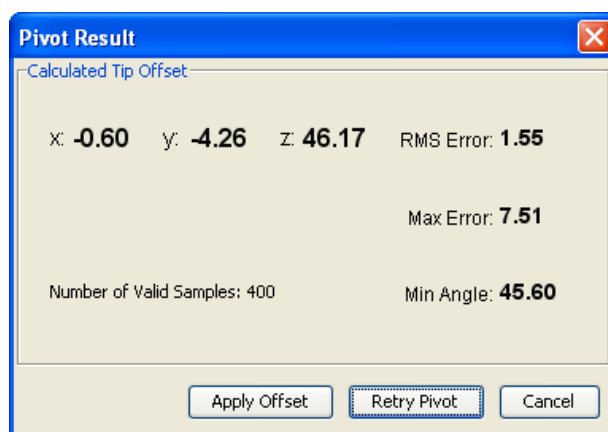


Figure 4.11: Pivot calibration values

4.2.2 US image calibration

Knowing the location of the US image plane in the workspace is crucial to derive the 3D volumes (by grabbing a series of images). For instance, in the rotational sweep method the US probe is rotated around its longitudinal axis. The information about the roll is important in order to know the angular gap between successive images. Hence, a 6-DOF electromagnetic sensor is placed on the US probe for retrieving the roll information.

A calibration is required to map the US image plane with the electromagnetic sensor. As described in Chapter 2, a 6-DOF sensor is placed on the surface of the US probe and affixed by shrink wrap. To reduce the calibration errors, it is very important to ensure that the sensor axis stays parallel to the US probe's longitudinal axis. The sensor needs to be installed such that the relative motion between the US image plane and the sensor is zero. Thus, a rigid transformation can be applied to calculate the location of the pixels lying on the image plane in a 3D virtual space. A calibration system to get this information is developed as a software tool within InterNav3D.

For formulating an equation of any plane lying in 3D space, we need at least 3 non-collinear points. The objective is to calculate a transformation matrix that would take care of rotation, translation and scaling for transforming one plane to the other plane in space. For the sake of explanation, let us consider an example. The plane *A* is an image plane initialized at the origin and lies completely within the *x-y* plane. The electromagnetic sensor orients its local longitudinal axis with the *z* axis of the workspace. Plane *B* is the US image rendered in space with respect to the electromagnetic sensor. The transformation from plane *A* to plane *B* is the solution required. It is important to note that scaling is an essential parameter in this scenario since the image rendered in virtual space of Aurora electromagnetic tracker converts the pixels into the physical world unit (mm). In short, a pixel to physical space ratio needs to be estimated. In the process of calibration a specific tool such as a needle, which was calibrated by the pivot calibration method, is used as an input device. The information obtained from the sensor provides the location of the needle tip in 3D space of the Aurora electromagnetic tracker.



Figure 4.12: US image plane calibration

An agar cube is used as the medium for the US imaging. The US probe that needs to be calibrated with the attached electromagnetic sensor is used to image the agar cube. The needle is inserted into the agar cube as shown in Figure 4.12 and visualized on the 2D US image plane. As soon as the needle tip is visualized in the image, the position value at the location of the needle tip is recorded (from the Aurora electromagnetic tracker). The corresponding pixel location on the 2D US image plane is stored as well. This step is repeated for at least 3 different non-collinear points on the image plane (the process can be repeated for multiple locations to gain a better accuracy in calibration). The group of points thus obtained is used to form a plane that is the best fit for the points. Three random non-collinear points completely lying in the image plane are selected to fill a matrix A whereas the corresponding pixel locations on the 2D image plane are used to fill a matrix B . Now both the matrices consist of three different points related by an unknown local transformation as shown in Figure 4.13.

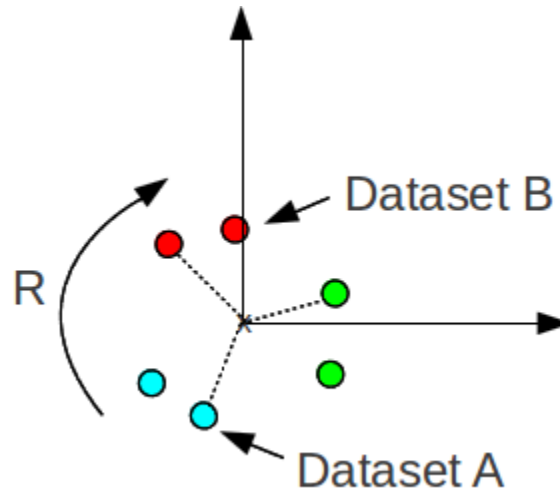


Figure 4.13: Calculating dataset transformation

This information is then run through an algorithm that calculates the transformation matrix M . This matrix concatenates the rotation matrix information R and scaling information S . The equation can thus be simplified as shown below:

$$B = R * S * A + T$$

where B and A are the two 3×3 matrices containing the information of the three selected points. Matrices R , S and T consist of the rotation, scaling and translation information respectively. Before further calculations, we need to calculate the scaling information S . The resolution of the 3D image is kept proportional along the three orthogonal axes; thus the scaling information S is the same for all the directions and hence is a scalar value for this scenario. The scaling information is computed by evaluating the ratio of the distances among the 3 points in dataset A with respect to dataset B . Once the scaling information is obtained, two matrices R and T remain to be computed.

$$B = R * S * A + T \text{ can be written as } B = R * C + T$$

where C is the multiplication output of scalar S and matrix A . The overall equation can be simplified by removing the translation parameter. For this, the centroid for both the point sets is computed and then the complete image frame is shifted so that the centroid becomes the origin. The new matrices thus formed are B' and C' respectively. Thus, both

the images now share a common origin and the only unknown that remains is the matrix R .

$$B' = R * C'$$

The equation for the matrices can be solved as follows:

Post multiplying by C inverse on both sides gives

$$B' * C'^{-1} = R * C' * C'^{-1}$$

$$B' * C'^{-1} = R * I = R$$

Thus the matrix R is computed. There is however an issue of singularity where the matrix A^{-1} cannot be computed. In such a scenario, the singular value decomposition (SVD) [ref: Matrix Computations, Golub and Van Loan] is used.

SVD decomposes a given matrix E of size $(m \times n)$ with $m \geq n$ into a product of 3 matrices such that

$$E = U * W * V^T$$

where $U^T * U = V^T * V = V * V^T = I_n$ and $W = \text{diag}(\sigma_1, \dots, \sigma_n)$.

The matrix U consists of n eigenvectors associated with the n largest eigenvalues of $E * E^T$, and the matrix V consists of the orthonormalized eigenvectors of $E^T * E$. The diagonal elements of W are the non-negative square roots of the eigenvalues of $E^T * E$ called singular values in descending order [107].

$$[U, W, V] = \text{SVD}(E)$$

The matrix E here is the covariance matrix computed as

$$E = B' * C'^T$$

After decomposing the matrix E into U , W , and V , the rotation matrix R can be computed as

$$R = V * U^T$$

Vtkmath, an inbuilt library of VTK was used to compute the SVD. Using the decomposition matrix, the rotation matrix R is calculated and the only unknown that needs to be calculated is the translation matrix T which is computed as

$$T = -R * \text{centroid } C + \text{centroid } B$$

Thus, the calibration of the US image plane is obtained. The calibration method developed is very easy to use and can be implemented any time when InterNav3D is running (in case rigidity is lost due to any reason.)

Table 4.1 shows a typical calibration value obtained during the calibration procedure.

Table 4.1: US image calibration value

Parameter	Rotation	Translation	Scaling
X	25.70	2.39	0.132
Y	93.60	-1.04	0.132
Z	-11.20	18.45	0.132

4.2.3 Robotic calibration

The AESOP and ZEUS robotic arms were used for the experiments performed in evaluating the InterNav3D system. The control system of the robot was implemented in the previous version of InterNav. While performing several experiments, it was found out that the needle tip does not always moves in a straight line. This could be a combination of the effect of the passive joints at the end effector of the robot, the uneven tissue or the

non-uniform needle tip. Thus, errors were introduced in the needle insertion procedure. The InterNav3D was developed on the premise to utilize as much information as possible from the behavior of the system components to its advantage so that the complete procedure could be performed intuitively by reducing the operational time and maximizing the efficiency. From the use and analysis of the previous system, it was realized that a significant amount of time was taken by the user in orienting the needle (several times an entire procedure). This also caused trauma to the tissue. One way to compensate for this was to use the kinematics of the robot arm for improving the needle maneuvering but this depends on the location of the pivot point and the robot base. Usually in a clinical procedure, it is hard to determine those points prior to the procedure, due to the unpredictability of the patient's orientation and location of the lung once it is collapsed. Hence, a calibration process was developed that takes into account the behavior of the needle during an insertion procedure and then uses that information for subsequent insertions to predict the path the needle tip will take. This method assists in efficiently moving the needle towards the target. The user is able to visualize the path that the needle is taking and determine if any manual intervention is needed (if and when the needle tip deviates from the predicted path and determine the extent of the deviation). This calibration process is described as a module in Chapter 3.

To test the calibrations and compensations thus applied, phantoms were used and imaged to visualize their 3D volumes. The corresponding artifacts in the physical and virtual world were detected and tested with the distance and orientation to evaluate the accuracy of the system. Figure 4.14 shows the different phantoms used.

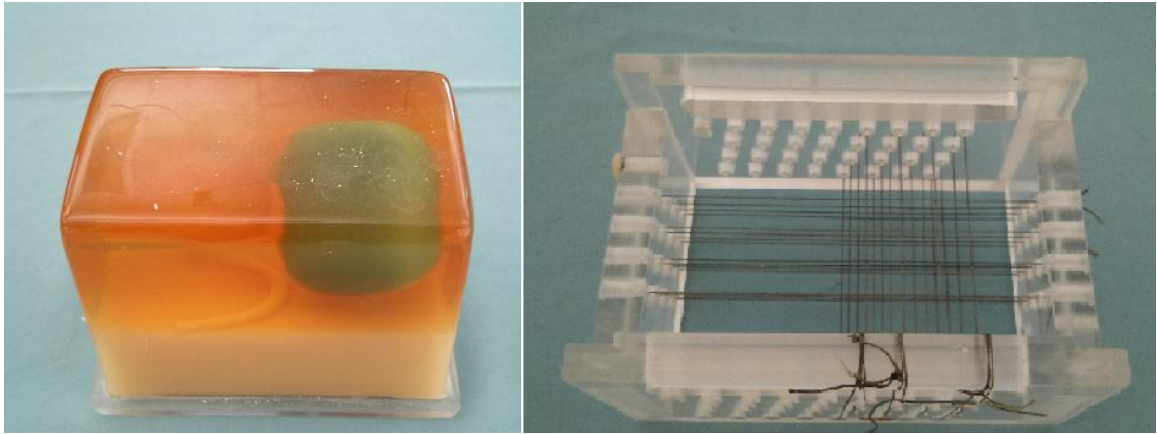


Figure 4.14: Phantoms used to evaluate calibrations

On the right of the figure is a linear mesh of strings with a fixed distance and angle between successive strings. On the left is a prostate phantom that was imaged to get the virtual physical target. Figure 4.15 shows the physical setup for conducting phantom tests. Figure 4.16 shows the reconstructed version of a phantom whose artifacts were detected and measured in the software to coordinate them to their real physical world distances. Table 4.2 shows the result. For the linear string cage, the measurements of the determined joint locations (string crossover) and the corresponding angle between the successive layers of strings were found to be very close to the real-world values. For the other phantom, the shape was determined and the location of the target that was selected in physical space was matched to the one in the virtual space and the results obtained proved that the rendering and the calibration system were working accurately as needed.

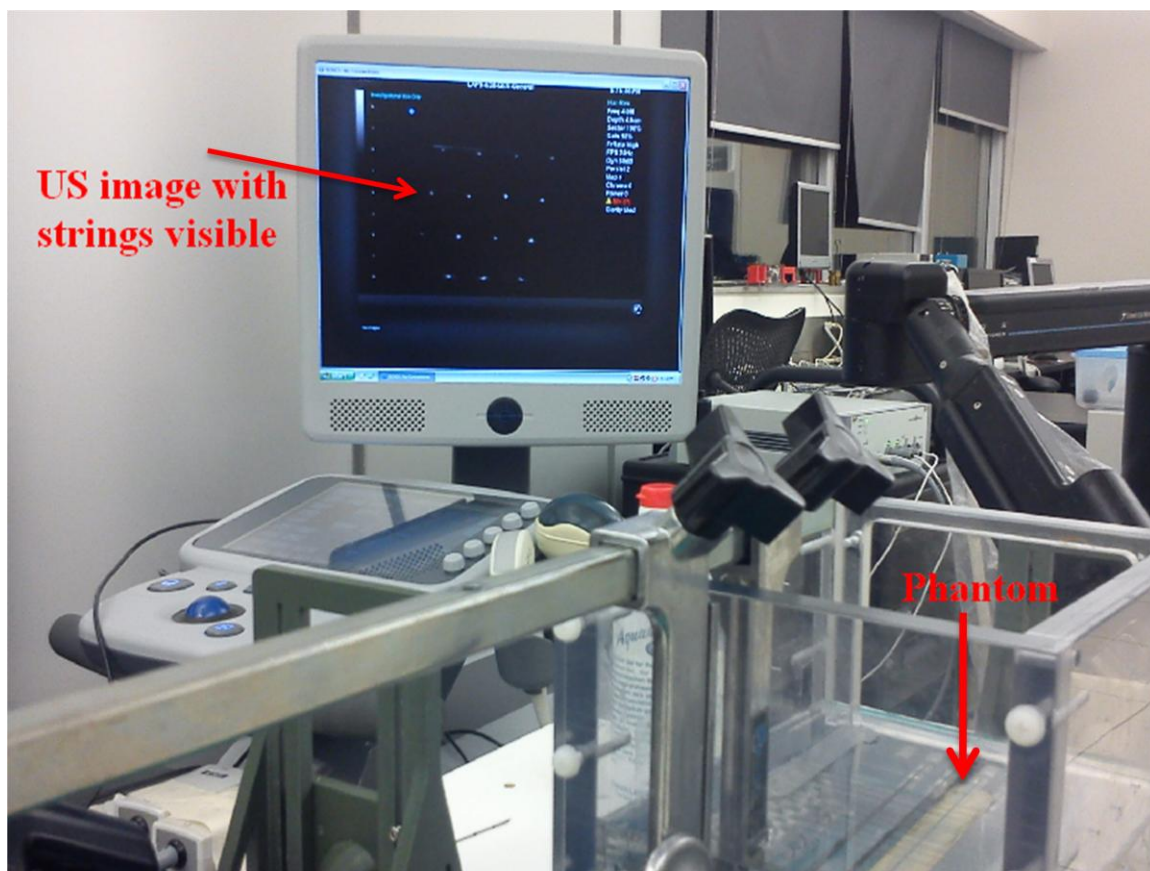


Figure 4.15: Evaluating the calibration using a phantom

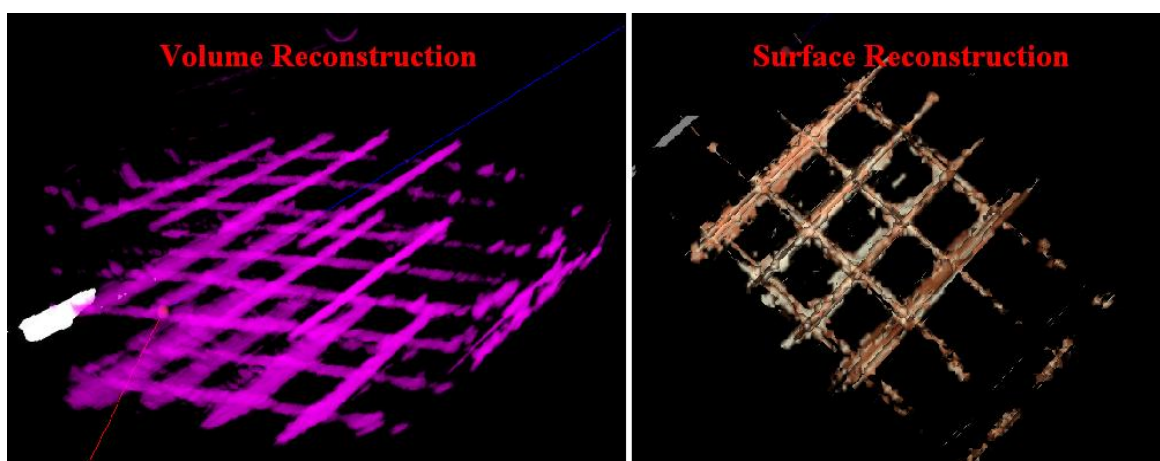


Figure 4.16: Phantom volume and surface reconstruction

Table 4.2: Evaluating the calibration

	Mean	Median	Mode	Std. deviation
String cross-over distance¹ (10mm)	9.95	9.9	9.9	0.216
Angular distance (14.03)	13.955	14.015	14.2	0.2678

4.3 Experiments and validations

The experiments were designed to demonstrate the enhancements of InterNAV3D made on top of its predecessor (InterNAV), the ability of the interface to tackle the problems that could arise in a surgical procedure and to showcase the benefits of the implemented modules. Experiments were also performed, both *ex vivo* and *in vivo*, to demonstrate the potential of the system to be applied for minimally invasive interventions.

All the experiments, except for the volume estimation experiment in section 4.3.3 and the *in vivo* experiments in section 4.3.6, were performed by 10 different test subjects. This group consisted of people who had previously used the InterNAV system and those who were completely new to the InterNAV/InterNAV3D environment. The test subjects were allowed to have 2 trial runs prior to conducting the experiments to get them acquainted with the system. Every test subject performed the experiment 3 times. For section 4.3.3, the InterNAV3D software was used to perform 30 iterations for evaluating the system. On the other hand for section 4.3.6, the *in vivo* experiments were performed

¹ The values are computed by InterNAV3D software by detecting the intersection points of the string. It showcases the functionality of InterNAV3D to represent the 3D volume and surface reconstruction accurately.

by an expert clinician who had previous experience using the InterNAV and InterNAV3D systems.

Following are some of the difficulties that were encountered when using InterNAV:

- InterNAV visualized the surgical site with the help of a 2D image plane rendered in a 3D workspace. This helped to visualize the location of target in space but was not able to perceive the structure of the tumor
- The visualization window provided the needle eye view (as if the camera is set at the needle tip). Although this improved certain aspects of the procedure, it was restrictive as far as user interaction is concerned.
- The knowledge of the orientation of the needle with respect to the surgical space was not possible due to the limited visibility (visualized only 2D image plane). Also, the tools to visualize the needle bending and to localize the needle tip during an insertion procedure were lacking.
- The image of the US was rendered directly in the virtual world. No provision for enhancing the images was present.
- The targets were rendered in the virtual world depending on the location selected by the user. In the case that the real physical target moves, the virtual target was not able to follow it.

The development of InterNAV3D started by overcoming the above drawbacks and with time, it also implemented additional modules for enhancing the overall architecture of the system. Some of the difficulties discussed below were also addressed in the development of the system.

- Simulating the motion of the surgical space in the 3D virtual world elements.
- Detecting and determining needle bending and the needle tip (-ability to detect deflection in 3D).

- Advanced needle insertion with the help of the developed modules and needle retraction.

Different image processing techniques such as image thresholding, histogram equalization, morphological operations, edge detection etc. were used to determine the physical artifacts present in the images. Noise removal and image softening/sharpening techniques were also employed to enhance the images. Different experiments that were performed to evaluate the system are described below.

4.3.1 Needle bending

This experiment was designed to showcase the capability of the system to accurately represent possible needle flexing during a needle insertion procedure and to determine the capability to approximate the needle tip location.

4.3.1.1 Design

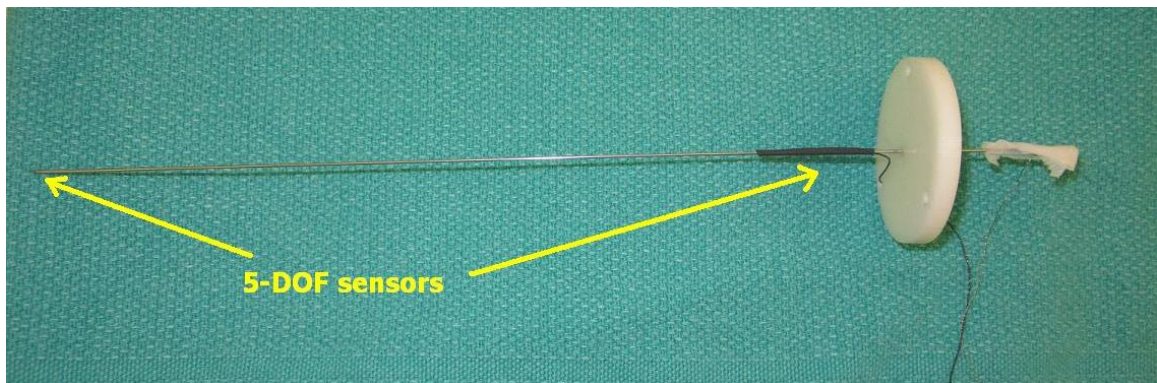


Figure 4.17: Needle with two 5-DOF sensors attached

A 22 gauge brachytherapy needle was used for this experiment as shown in Figure 4.17. A 5-DOF electromagnetic sensor was placed at the tip of the needle which provided the real-time position and orientation information of the needle tip in the real surgical space. Another 5-DOF sensor was placed at the base of the needle to represent the un-flexed axis of the needle (original axis of needle). The needle was inserted in phantoms (agar cubes and liver tissue). The US probe, with a 6-DOF sensor attached, was used for imaging. The aim of the experiment was to image the phantom, construct 3D volumes

and then identify the needle to determine and verify possible needle deflection and position of the needle tip. The 5-DOF sensor positioned at the needle tip is used for evaluating the results.

4.3.1.2 Evaluation

Multiple needle insertions were performed in the phantom and approximate needle tip locations were estimated. Figure 4.18 shows a needle insertion procedure. Figure 4.19 shows the 3D view of one of the experimental trials. Table 4.3 provides the results obtained.

The location of the needle tip was calculated and recorded using the shape detected in the 3D visualization world by the assistance of the built-in modules and the position of the tracker attached to the base of the needle². Simultaneously, the electromagnetic tracker at the needle tip is queried for the position. The difference between the two locations is the error in measurement.

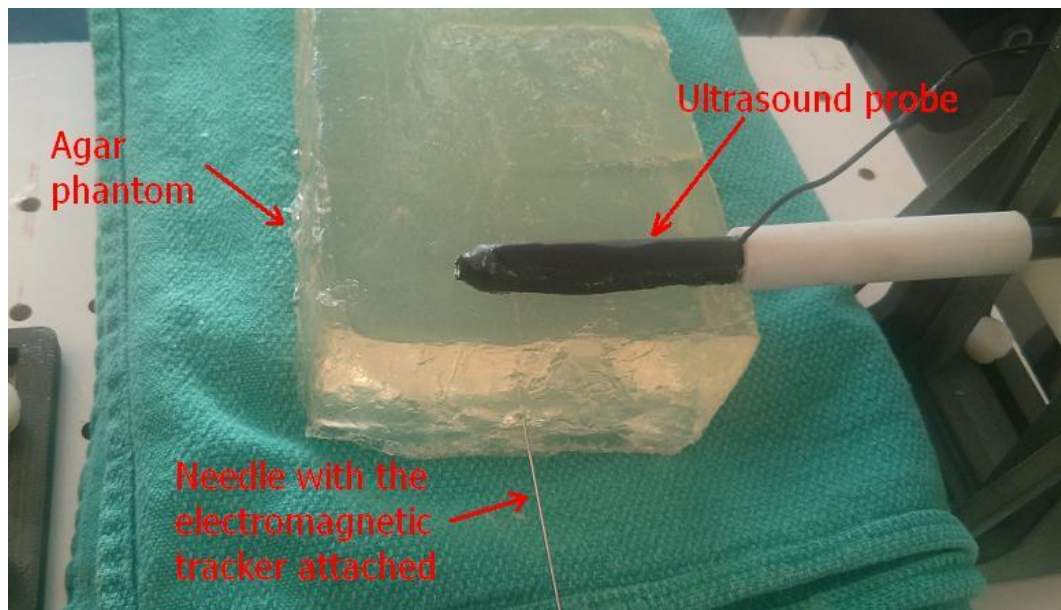


Figure 4.18: Experimental setup for evaluating needle bending

² The electromagnetic tracker at the base of the needle gives a projected path where the needle should have been heading

The InterNAV3D system was able to reproduce the bending structure of the needle in the virtual world. It represented the shape correctly and the user was able to determine the needle tip easily and accurately with a mean error less than a millimeter.

Table 4.3: Error analysis (needle tip detection)

	Mean	Median	Mode	Std. deviation
Error (mm)³	0.97	0.9	0.9	0.19

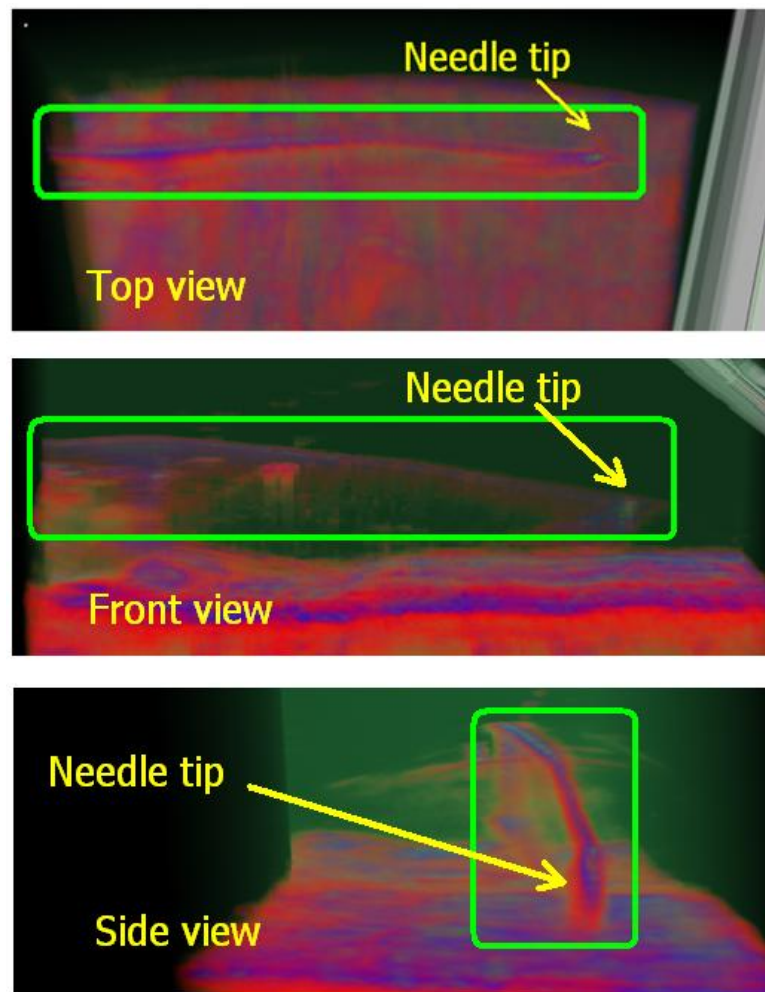


Figure 4.19: Needle bending visualization and tip detection in the 3D virtual world

³ Distance between the estimated needle tip and the electromagnetic tracker location

4.3.2 Needle maneuvering

This experiment was performed to demonstrate the advantages of InterNAV3D over its predecessor as compared to the time, number of attempts to re-maneuver/reorienting and the distance travelled by the needle tip towards the target in needle insertion procedures. The results help to evaluate the benefit of the needle path projection and prediction module for needle maneuvering. The aim is to demonstrate that by using the path history of the needle and by applying the prediction model of the needle's behavior, it can be maneuvered easily and intuitively towards the target.

4.3.2.1 Design

In this experiment, the users were allowed to familiarize themselves with the software interface and to run trials before the experiment. The aim is to orient the needle and maneuver it to the random target locations selected by the software. Time, distance and numbers of attempts to reorient the needle and the needle tip locations (at every 1 mm of travel interval) during the insertion procedure were recorded. Once the user feels that he/she has reached the target, the timer is stopped and all the collected information is saved through the software interface.

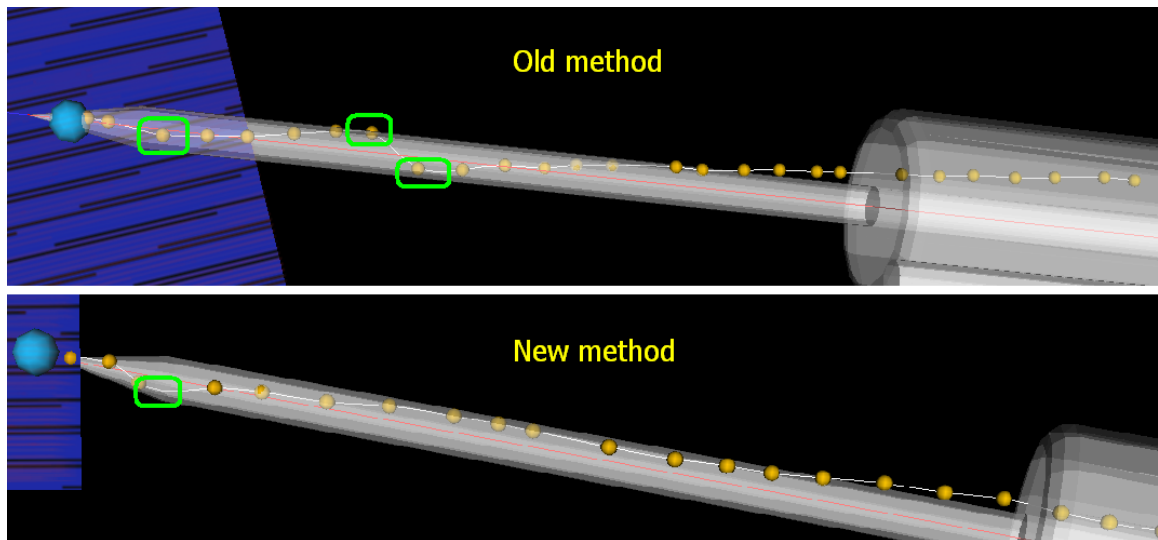


Figure 4.20: Needle insertion with and without the assistance of the developed modules

The experiments were performed in the needle-eye view mode of the predecessor software and the 3D-visualization mode of InterNAV3D with the assistance of needle path prediction and current needle path visualization. Figure 4.20 compares a typical insertion procedure with (new method) and without (old method) the assistance of the developed modules. The points where the needle had to re-maneuver are highlighted by the green boxes. The needle path that was predicted was formed by utilizing the path history of the needle (from prior insertions). It is important to mention here that if a needle bending model is developed, the software is able to implement it in the 3D visualization window and helps to achieve accurate needle insertions and target hitting.

4.3.2.2 Evaluation

It was observed that with the help of the modules, the number of attempts to re-align/reorient the needle during the needle insertion procedure reduced as compared to the method without any assistance. The needle paths were observed to be smooth and directed towards the target during the use of the needle maneuvering modules which were implemented in InterNAV3D.

Figure 4.21 shows the needle paths rendered in 3D space for multiple insertions performed by a user. Each unique colored line represents a different track of insertion performed by a user. The lines are the actual path of the needle tip during an insertion procedure. The needle paths obtained without the assistance from the built-in modules have often the movements to re-align the needle which showcases the damage caused to tissue. The new method on the other hand, provides a better and intuitive way to maneuver the needle as it tries to make re-aligning and re-maneuvering minimum by using the path projection and path prediction widget. Figure 4.22 shows the needle path for the insertion procedure which had assistance of the built-in needle maneuvering modules. The amount of needle reorientations can be clearly seen to be lowered. Table 4.4 shows the experimental analysis. It can be observed that though the duration of procedure increased with the help of the modules, the number of maneuvering attempts required and the total distance traversed for a fixed target distance were reduced. This helps to reduce the trauma caused to the tissue.

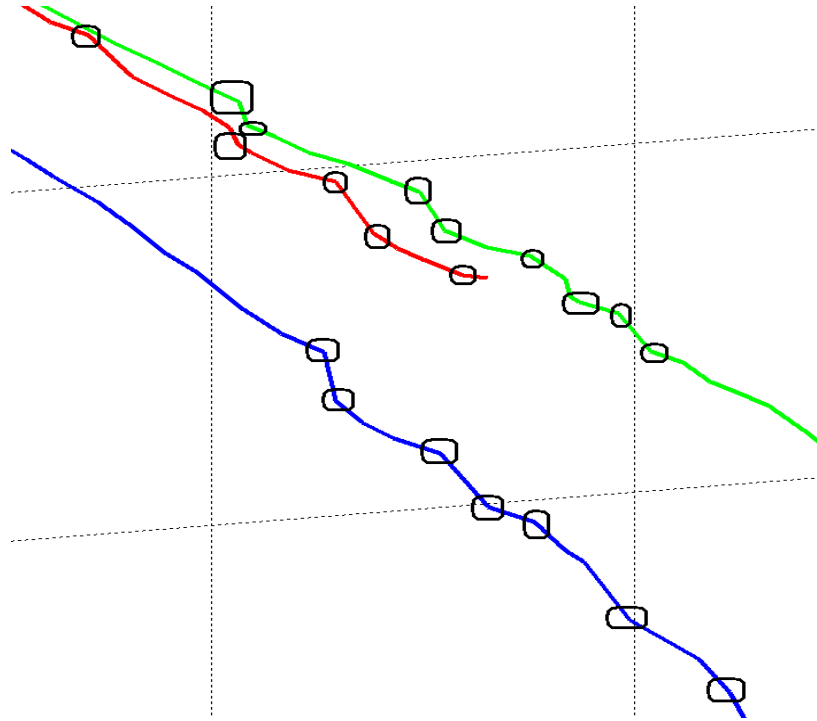


Figure 4.21: Re-orientation during an insertion procedure without the assistance of the built-in modules (displayed within the boxes)

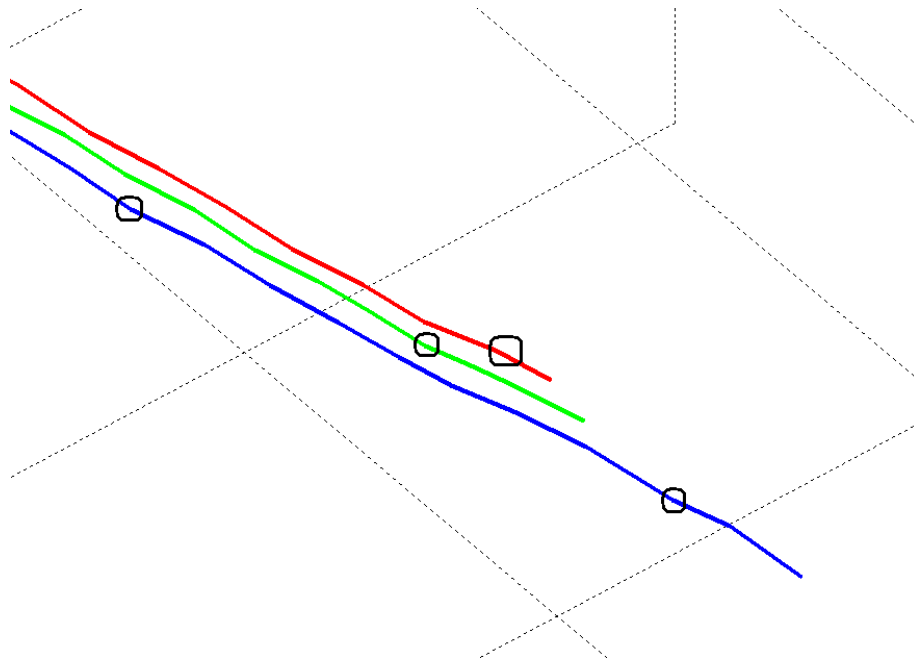


Figure 4.22: Re-orientation during an insertion procedure with the assistance of the built-in modules (displayed within the boxes)

Table 4.4: Needle maneuvering experimental analysis

	Mean	Median	Mode	Std. deviation	Worst reading	Best reading
Old method (no. of re-manuevering attempts)	4.4	4.5	5	0.699206	5	3
New method (no. of re-manuevering attempts)	1.9	2	2	0.567646	3	1
Old method (procedural duration) seconds	97.9	98.5	NA	13.06777	120	75
New method (procedural duration) seconds	117.6	117.5	115	17.25753	145	88
Old method (distance traversed) 70 mm	75.9	75.5	73	2.282786	79	73
New method (distance traversed) 70 mm	72.5	72.5	72	1.080123	74	71

4.3.3 Tumor detection and reconstruction

This experiment was performed to evaluate the 3D reconstruction feature of the InterNAV3D and to showcase the benefits in perceiving the tumors and the targets in 3D space.

4.3.3.1 Design

Here, agar cubes were used as the phantom to mimic tissue. Spherical balls made of agar and barium powder were used as phantom tumors. Figure 4.24 shows the experimental setup.

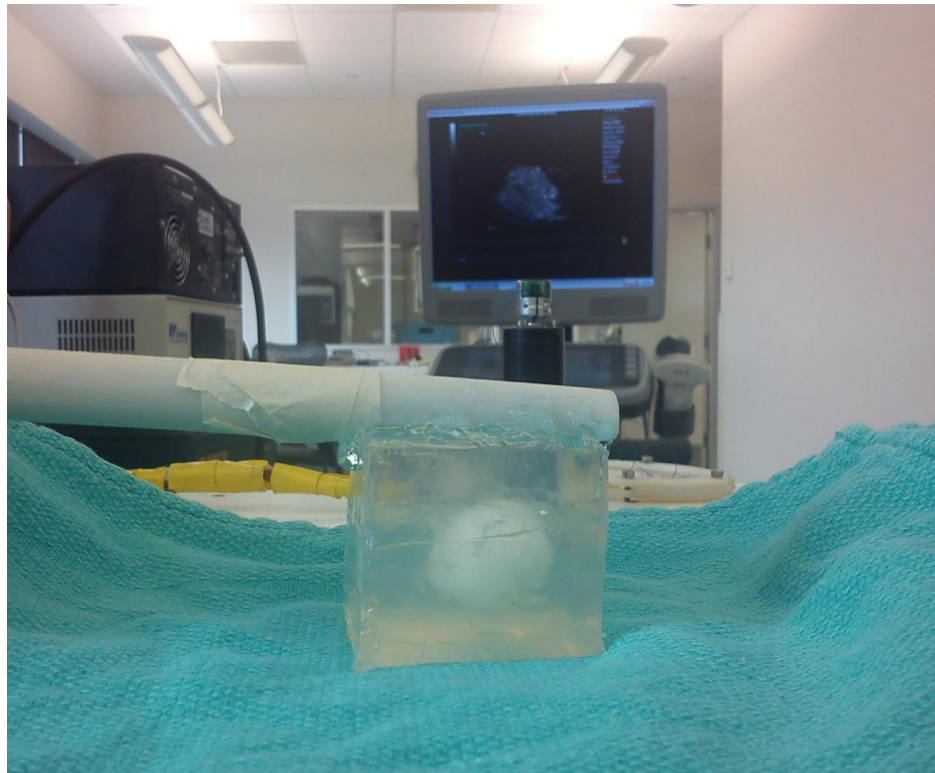


Figure 4.23: Agar sphere being imaged

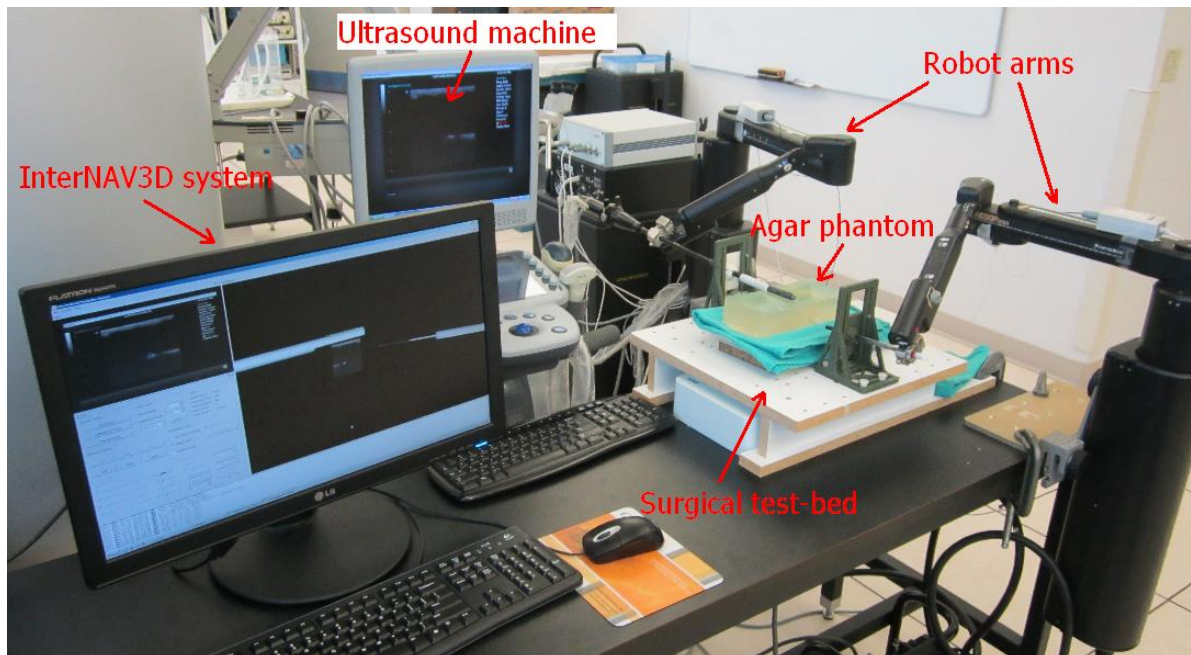


Figure 4.24: Experimental setup for 3D volume reconstruction

InterNAV3D was used to construct 3D volumes by capturing a sufficient number of images. Then the number of voxels (volume capacity) of the tumor was computed. The results were then compared with the volume capacity of the tumors. Figure 4.25 shows the volume reconstruction from one of the experiment.

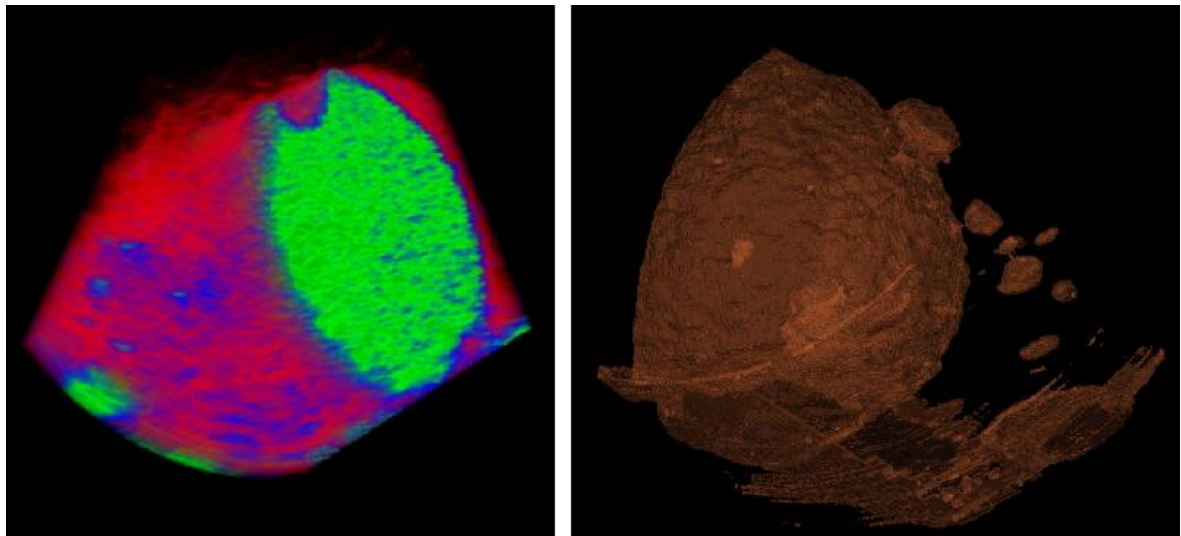


Figure 4.25: 3D volume and surface reconstruction

4.3.3.2 Evaluation

The average diameter was measured along the 3 orthogonal axes. The volume capacity was then computed using the mathematical formula (for instance volume of a sphere with radius r equals $\frac{4\pi}{3}r^3$). At the same time, the number of voxels that occupy the 3D sphere structure was calculated using the software interface. The accuracy of the system to identify the correct shape and size of the tumor was estimated. Table 4.5 shows the results obtained by performing experiments on tumors of different shapes and sizes such as cones, cubes and bars.

Table 4.5: Error analysis (3D volume reconstruction)

		Mean	Median	Mode	Std. deviation
Error	(in percentage)	5.759594	5.258314	NA	3.164669

4.3.4 Ex-vivo experiments: target selection and hitting

This experiment was designed to focus on the benefits provided by the 3D visualization and image processing modules implemented in InterNAV3D. The 3D virtual world provides a greater sense of understanding of the objects and tools present in the surgical space. The implemented image processing modules and widgets assist in enhancing the visibility of the artifacts present in the surgical space. There could be multiple tumors present in a lung. The pre-operative images provide the structure and location of the tumors in the lung. The location of the tumor, however, changes when the lung is collapsed.

For a minimally invasive intervention, it is hard for the clinician to detect the tumor based on only 2D US imaging as it generates images of a lower quality when the lung is imaged. Even if the tumor is identified, it is not easy to determine and visualize its shape. The current software helps to overcome this issue and provides a better approach

in reaching the target for brachytherapy and thermal ablation procedures with greater accuracy. Two sets of experiments were performed. One without motion and the other with induced motion on the surgical test bed. This experiment was performed to show the benefit of the system under such conditions.

4.3.4.1 Design

Figure 4.26 shows a liver being imaged. The experimental setup is similar to Figure 4.24.



Figure 4.26: *Ex-vivo* experiment

Small incisions of sufficient size were made on the tissue⁴ to place multiple phantom tumors such as agar spheres and duck gizzard (various sizes) as shown in Figure 4.27. The incision was sutured to ensure that the tumor stays within the tissue as shown in Figure 4.28.

⁴ Both lung and liver were used on different occasions for the experiments.



Figure 4.27: Phantom tumors

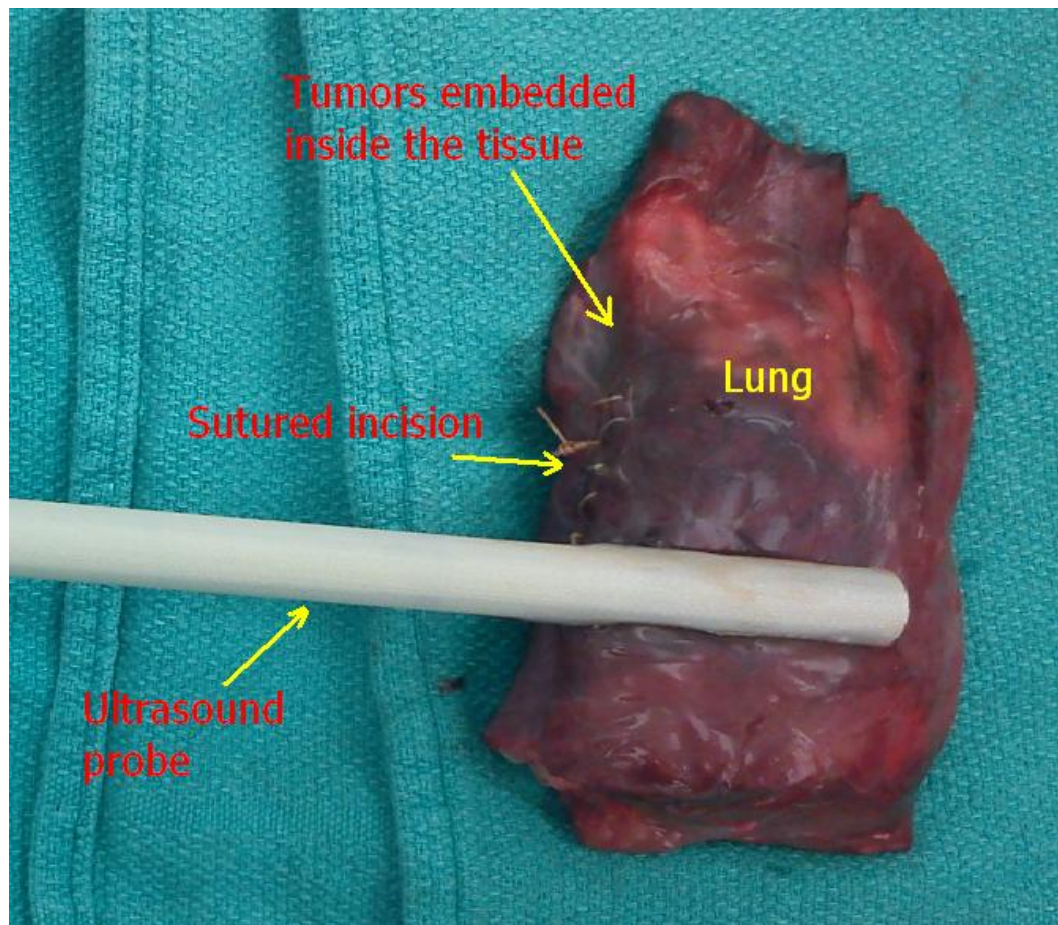


Figure 4.28: Tissue sutured after implanting tumors and being imaged by US

It was assumed that pre-operative imaging was performed which provided the required information of the number of tumors, their sizes and shape (spherical). The location of the tumors within the tissue was not provided to the user.

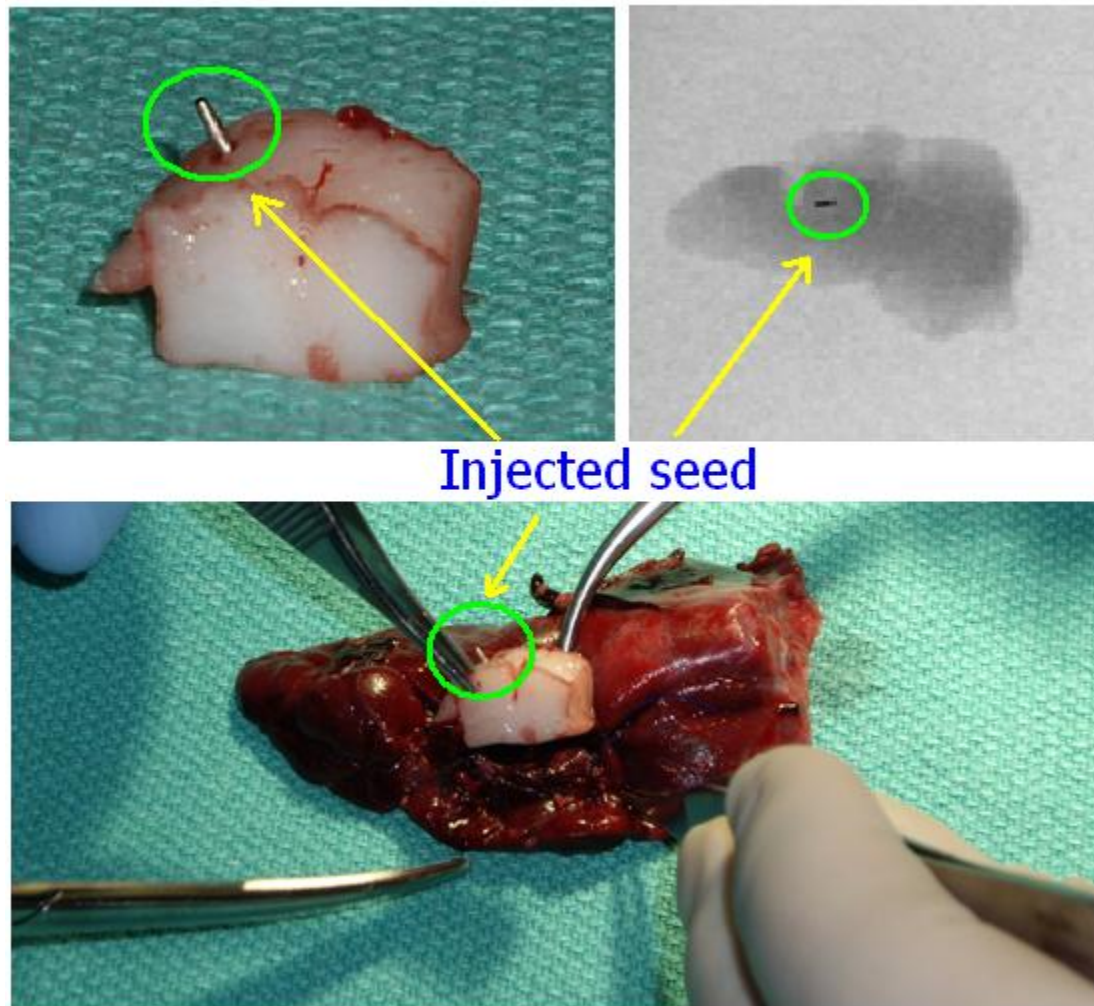


Figure 4.29: Seed missed the target using InterNAV

Previous experiments performed at CSTAR by using the InterNAV showcased the drawback of using only the 2D US imaging for determining the tumor position and shape. It was very unintuitive for a user to determine the shape and the center of the tumor (target) in 2D view. Figure 4.29 shows the output of one such experiment where the injected seed missed the target location. The user was not able to correctly determine the center of the tumor as only single perspective (one angle view) to visualize the shape of the tumor was possible.

For the current experiment, the user needs to use the functionalities provided by the software interface to determine the location of the tumor and its structure. An electromagnetic tracker was installed at the center of every tumor prior to its suturing inside the tissue as shown in Figure 4.30. The procedure allowed the use of the auto-manual mode and the various built-in modalities for target selection and visualization. The user is now supposed to image the tissue using the different sweep methods and try to detect the center of the tumor which he/she can now select as the target location. Test trials were performed to let the user familiarize with the functionalities provided in the system. Now, the user maneuvers the needle to the target and when he/she thinks that they have reached the target, the sensor readings are saved and the error is estimated. Users were asked to repeat the insertion if the needle tip was considered well off the target location (after an initial attempt) such that the needle maneuvering within the tissue was deemed dangerous. The number of attempts required to maneuver the needle per target location was recorded. Experiments were performed for both with and without induced motion (moving the surgical test bed using the motion induction system).



Figure 4.30: Electromagnetic tracker attached to the phantom tumor

4.3.4.2 Evaluation

This section evaluates the experiments performed. Figure 4.31 represents a sample volume reconstruction during one of the experiments. Determination of the shape was performed for agar tumors but it was not possible to do the same for the unknown shape of the duck gizzard. Participants were however told the total number of tumors and they were able to detect the duck gizzard. How a participant perceives such a shape is very subjective, hence they were asked to use the system to detect its structure and find out its center. 3D visualization provided an estimation of the shape and the participant was able to select his/her perceived center as the target and was able to maneuver the needle and reach it. Accuracy of the insertion (target hitting) and the number of attempts required were used to evaluate the system.

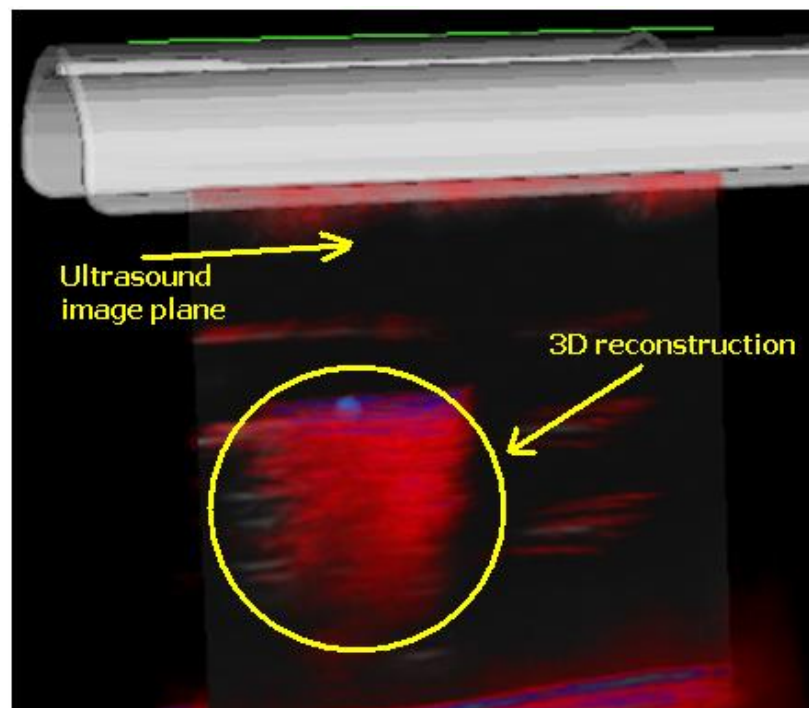


Figure 4.31: Volume reconstruction of duck gizzard

Table 4.6: Error analysis for needle target hitting

	Mean	Median	Mode	Std. deviation	Worst reading	Best reading
Without motion (mm)	0.93	0.9	1.1	0.245176	1.3	0.5
With motion (mm)	1.36	1.35	1.2	0.313404	2.0	0.8

Table 4.7: Number of insertion attempts to reach the target

	Mean	Median	Mode	Std. deviation	Worst reading	Best reading
Without motion (attempts)	1.1	1	1	0.316228	2	1
With motion (attempts)	1.2	1	1	0.421637	2	1

The experimental results show that the added motion did not greatly affect the system performance even with the induced motion. This proves that the system is capable of working in real surgical scenarios where there is usually some movement at the surgical site. The number of attempts to correctly hit the target is however slightly greater in the experiments with the induced motion.

4.3.5 Needle retraction

In InterNAV3D, a module to visualize the real-time location of the path of the needle tip during an insertion procedure is implemented. This module provides a realistic view of the behavior of the needle during its maneuvering towards the target location. While being inserted, the needle often gets deflected from the intended path due to the dynamics at the needle tip (uneven tissue stiffness, geometry of the tip, friction effects, etc.). This causes the user to take an action to realigning the needle, or retracting and reinserting (depending on the amount of flexing). This module represents the needle flexing and the reorientation, if any, done during the insertion procedure as a 3D spline rendered in the 3D virtual window. Once the target is pierced, the needle needs to be retracted. It is helpful to retract the needle along the same path as it was inserted so that tissue damage is kept to a minimum. This experiment evaluates the module by performing needle retraction for varied scenarios and presents the accuracy with which the system is capable of completing the procedure.

4.3.5.1 Design

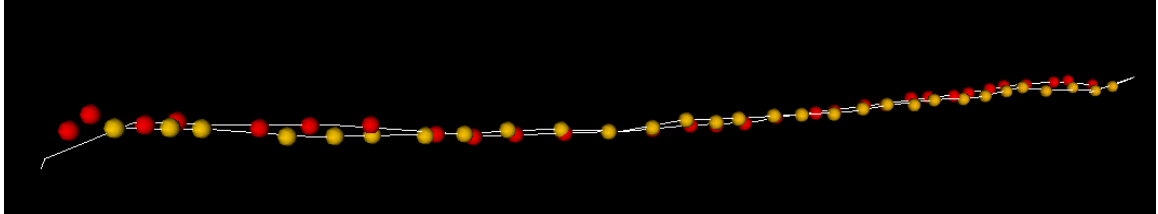
Agar cubes were used as phantoms to visualize the tissue under US. The users were provided with a target and allowed to use the system for inserting the needle to pierce the target. Once they determined that the target had been reached, they were asked to retract the needle as close as possible along the same path as they inserted the needle using the needle path history as a guide. The needle tip locations were recorded during the procedure by the software.

4.3.5.2 Evaluation

Figure 4.32 shows an example during one of the needle retraction procedures where the needle insertion path was used as a guideline to retract the needle. It represents the needle insertion path (shown by yellow spheres) and the needle retraction path (shown by red spheres). Table 4.8 provides the statistical analysis of the results.

Table 4.8: Needle retraction analysis

	Mean	Median	Mode	Std. deviation
Error (mm)	0.51	0.5	0.8	0.292309

**Figure 4.32: Needle insertion and retraction path**

The error in Table 4.8 represents the distance between the needle retraction path and the needle insertion path.

4.3.6 *In-vivo* experiments

To evaluate the system for a realistic surgical scenario, *in-vivo* experiments were performed by a clinician at CSTAR, Dr. R. Malthaner. During a surgical experiment performed by Dr. Malthaner on a porcine lung under his ethics protocol, InterNAV3D was used. Prior to the use of the system, one of the lungs was collapsed

4.3.6.1 Reaching a Target

This experiment was used to evaluate the benefits of the system in determining and reaching a specified target. An electromagnetic tracker was placed inside a spherical phantom tumor made of agar of radius 5 mm such that the tracker lies as close as possible to the center of the sphere. The tumor was placed inside the lung by making a small incision and sutured as shown in Figure 4.33.

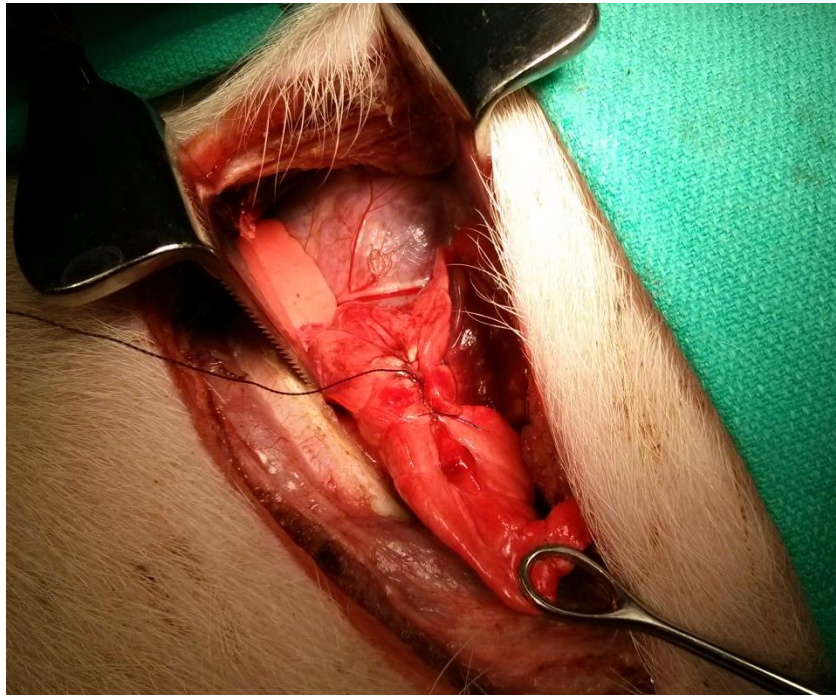


Figure 4.33: Phantom tumor with the attached electromagnetic tracker placed within the lung and sutured

Small incisions were made on the body of the animal at appropriate locations determined by the clinician to insert the laparoscopic US probe and the ablation needle for accessing the surgical site. The clinician then used the InterNAV3D system to detect the tumor and visualized the surgical site in 3D as shown in Figure 4.34. One of the unaltered 2D US image from a series of captured images is shown in Figure 4.35.

The electromagnetic tracker is visible in the image. It is important to mention here that during this procedure the lung was moving due to cardiac motion and respiratory motion of the contralateral lung. The software interface was able to simulate the motion in the 3D virtual window and the 3D volume that was created was subjected to move with the estimated motion, replicating the behavior of the surgical site. The clinician was then asked to determine the center of the tumor and select it as the target location. The target was also subjected to motion in the virtual world following the movements of the real physical world target. The ablation needle was used to pierce the tumor and reach the target.

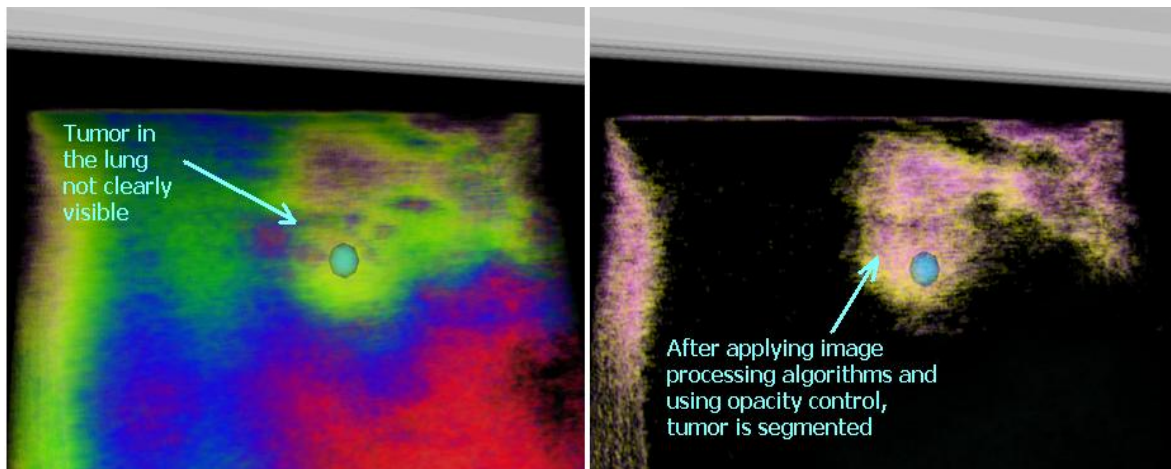


Figure 4.34: 3D reconstructed volume

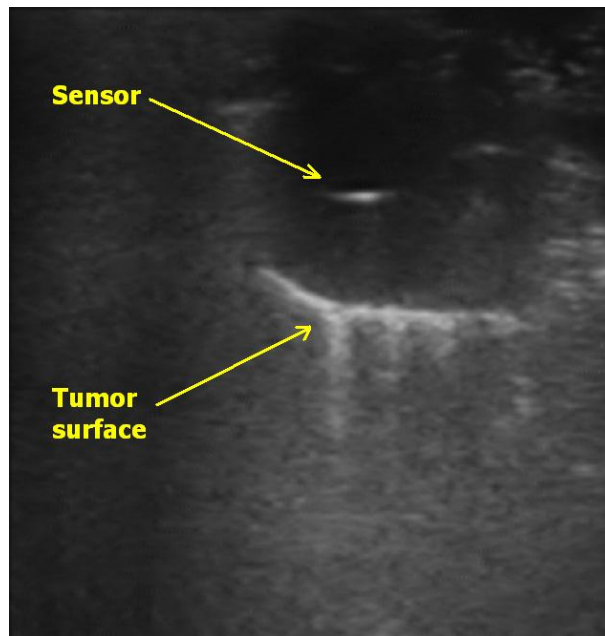


Figure 4.35: *In-vivo* 2D US image of the deflated lung

Once the clinician thought that he had reached the specified target, the difference between the location of the needle tip and the electromagnetic tracker placed within the tumor were recorded and the error was estimated. The InterNAV3D system was able to assist the clinician in determining the shape of the tumor and select the specified target.

The target was reached with an accuracy of 1.3mm determined by the calculation of the software in *in-vivo* experiment under the influence of residual motion of the heart and the contralateral lung.



Figure 4.36: *In-vivo* lung experiment (needle hitting the target)

Figure 4.36 shows the tumor divided into two halves to visualize the longitudinal groove made due to the needle insertion. The experiment was repeated with a new tumor and the clinician was able to hit the target with an accuracy of 1.4 mm.

4.3.6.2 Microwave ablation

This experiment was designed to evaluate the InterNAV3D setup to perform *in-vivo* thermal ablation. Visual feedback by continually rendering new 3D volumes at specified equal intervals was provided. The clinician was asked to select a target of his choice and maneuver the needle to it. The objective was to visualize the changes happening in the lung due to the creation of an ablation zone and to present the user with an intuitive way to determine the extent of ablation. It assists the user to modify the location of the needle in case he/she determines that a healthy part of the lung is getting ablated while insufficient ablation is performed on the cancerous region due to inaccurate probe placement or due to the effect of the motion induced on the lung (cardiac and contralateral lung motions).

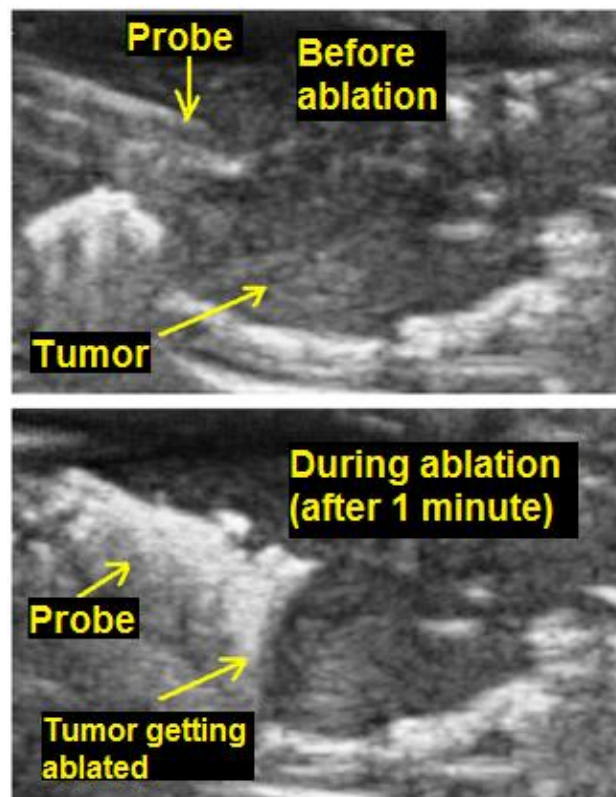


Figure 4.37: *In-vivo* thermal ablation (power 30W, microwave energy)

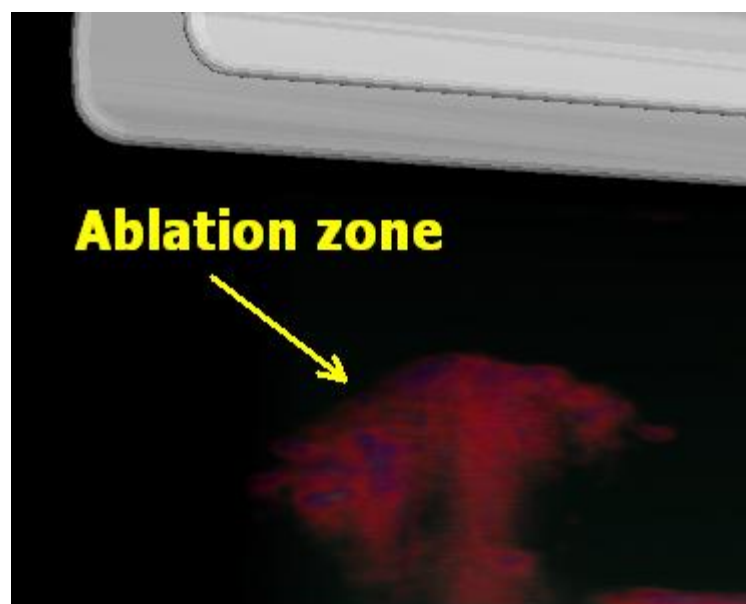


Figure 4.38: Ablation volume

Figure 4.37 shows the 2D US image of the surgical site during the procedure while Figure 4.38 shows the 3D volume generated by the round rotational sweep.



Figure 4.39: Lung (post ablation)

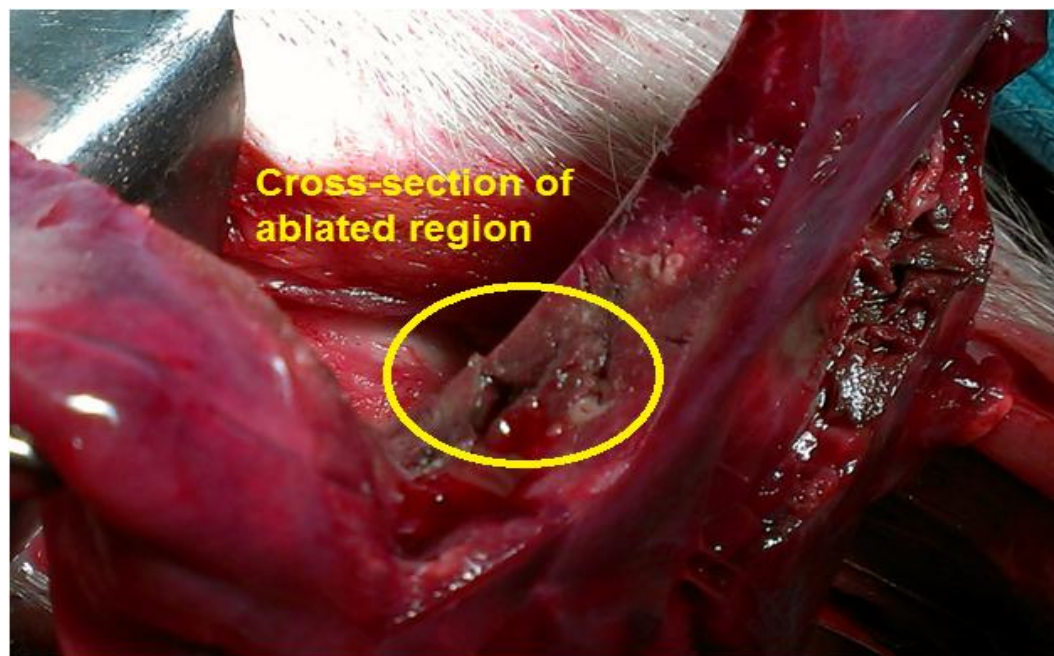


Figure 4.40: Ablation zone cut in half

The clinician was impressed with the developed tool and was able to perform ablation at the selected target location. Figure 4.39 shows the post ablation view of the lung. The lung was then cut along the ablated zone to evaluate the entirety of the procedure as shown in Figure 4.40. By evaluating the size and structure of the ablation zone, the clinician confirmed that the procedure was completed successfully.

4.4 Review

InterNAV3D provides a comprehensive system for performing minimally invasive lung cancer treatment. For the working of the system, different calibrations were performed. The system has proved to be a significant enhancement on its predecessor and also implements novel tools that help the clinician to achieve more accurate and reliable a performance. The next chapter provides concludes the thesis and discusses possible additional features for InterNAV3D.

Chapter 5

5 Summary, Conclusion and Future Work

This chapter contains a brief discussion of the main aspects of the work described in the thesis, its main conclusions and suggestions for possible future work.

5.1 Summary

InterNav3D was initiated to fulfill the important need of a comprehensive system that combines new approaches in the minimally invasive intervention techniques with the developments in medical robotics. The goal of the project was to significantly enhance the capabilities of the earlier version of InterNAV by integrating a novel visualization approach for the surgical site using advanced image processing techniques, and to improve the current scenario of lung cancer treatment (the minimally invasive approach). The new framework has been designed to deliver greater accuracy in feature recognition (characterization of the surgical site), better control of the surgical tools (by the use of the robots), and improved needle maneuvering. It helps to reduce targeting errors while achieving significantly better surgical performance (speed, time, precision of target hitting) during the procedure.

InterNav was conceived specifically for a lung cancer treatment system to implement a minimally invasive technique for brachytherapy by the use of surgical robots with assistive feedback from 2D visualization of the surgical site. InterNav3D builds on this foundation and implements a collaborative framework which capable of addressing applications such as robot-assisted tissue biopsy, radiofrequency and microwave ablation as well as low- and high-dose rate brachytherapy. It provides 3D virtual visualization of the surgical site with image processing both in online and offline modes. The system can also be applied to follow the same treatment procedures on other types of cancers such as in the liver and the prostate.

US imaging was used as the primary imaging modality for InterNav3D primarily because of its easy availability and safety, but InterNav3D is capable of using other

imaging modalities such as CT and MRI so long as an appropriate setup mechanism has been put in place to transfer real-time images to the computer for “real-time” analysis. Currently, it has been tested to work in an offline mode for CT and MRI modalities to deliver offline visualization and processing.

The use of US has its drawbacks while imaging organs such as the lung due to the presence of air in the lung. Our experience has indicated that appropriate lung deflation can significantly reduce the number of artifacts in US images and enable them to be used effectively with InterNav3D where the availability of advanced image processing capabilities helps to further enhance the images for retrieving additional information.

The introduction of 3D volumes and 3D objects provides further clarity to the visualization. The incorporated modules assist in sorting out the features that are needed to detect a tumor, a needle, veins etc. A motion simulation environment that behaves in the same way as the real physical world provides an intuitive and logical approach to relate to the actual clinical intervention.

InterNav3D involves several calibrations and modules for its successful working. An intra-procedure (run-time) calibration for determining the transformation matrix of the US image plane with respect to the electromagnetic tracking sensor attached to the US probe was developed and implemented. It allows to select different locations of the needle tip on the 2D US image plane (for different insertions), and then to correlate them with the respective electromagnetic tracking sensor values. The calibration is calculated and applied in run-time. Thus, it helps to overcome the errors that might occur due to incorrect image resolution (caused by a change in a US transducer or machine) and/or due to the relative motion between the electromagnetic tracking sensor and the US transducer. The calibration can be performed, if needed, prior to the surgical procedure. A manual registration mechanism for the 3D image volume and other imaging elements has been added, so that if at some time the physical tumor moves for any reason, the virtual tumor can be registered with it manually using the real-time US feedback.

Capturing multiple volumes and rendering them in the same 3D virtual world facilitate in developing a complete, comprehensive 3D structure of the relevant surgical

site. Image capturing modes such as a round (rotational) sweep and a flat (straight) sweep assists to gather volume information and aids in filling the vacant volume space, if any, formed during the construction of a 3D sweep. This helps in acquiring detailed information of the tissue structure and enhances its visibility (as perceived by the user) in associating the tumors found in the intraoperative 3D US images with the corresponding tumors found in pre-operative images (before the lung is collapsed). The opacity control parameters added to the volume help to control the aspects of the 3D structure that a user wants to be visible or invisible. The overlay of the surface reconstruction on the underlying 3D volume further helps in localizing the tumor within the 3D volume sweep as it segments out the surface of the tumor. This facilitates improved target selection as the complete approximate structure of the tumor is identified before the procedure is initiated. The opacity control of the reconstructed surface helps to determine the target location (when the target lies within the tumor). Different modules to help maneuver the needle towards the target are implemented. They provide the required information of the tool orientation and the target it is going to hit, thus helping to pivot the tool appropriately before insertion. As a result, any maneuvering of the needle tip inside the tissue is avoided.

A local focused image processing tool is implemented. The feedback from the electromagnetic tracker provides the most probable location of the needle tip. This information is used to focus on a very small region of an entire image (which might contain the required information), and is processed. An algorithm to auto adjust the size of the focused control structure (sub-volume) is employed. It automatically takes care of choosing the part of the volume that qualifies for processing by removing the part that does not contain any relevant information. The location of the focused control structure can also be selected manually by the user, if needed. This method of focused image processing helps to speed up the image analysis, and thus speeds up the complete procedure.

A region growing algorithm to segment out the physical structures present in the volume based on its connectivity (or inherent property) has been implemented. By default, it utilizes the information of the approximate needle tip location to segment out

the needle tool. If for any reason, the needle diverges from the proposed projected path, a manual method to select a location in the 3D volume that acts as the seed location for the algorithm is implemented. Selecting even a small portion of the said region, segments out the complete structure based on the region growing algorithm. Thus, a wider range of control is given to the user when needed, so that unexpected problems, if any, occurring during the procedure can be overcome. This module can also be used to segment out the tumor or any other physical entity in the image if required.

Different widgets to enhance the procedure of needle maneuvering by providing up-to-date information of the needle's shape and its tip location are implemented. Needle path prediction widget predicts the needle's path and guides the user to make minimum orientation changes while the needle maneuvers within the tissue. It also helps to reduce the path length and effectively the trauma to the tissue. A visualization history of the needle tip locations during an insertion procedure is provided which helps in retracting the needle along the same path (needle insertion path) to reduce trauma to the tissue. The real-time needle path projection widget uses the most recent needle tip locations to estimate the orientation of the needle tip at that particular instance. This is very helpful as the needle tip may deflect sometimes due to irregularities in the tissue stiffness and/or the irregular (e.g. bevel) shape of the needle tip. Path projection widget assists the user to update the needle orientation appropriately for ensuring accurate target hitting.

A collision detection module that provides visual information (by changing the color of the virtual objects) has been implemented. This assists the user to know the instance the needle comes in contact with the 3D volume/objects. The change in the color also helps in knowing the range of the needle tip from the target and provides a cleaner, enhanced visual approach for the user. The user can concentrate entirely on maneuvering rather than constantly checking distance values when he/she is very near the target and/or during the time when the target is reached. The collision detection tool also helps in needle retraction as it provides a visual cue when the needle tip is entirely out of the sweep volume and/or it reaches a pre-specified location.

A motion estimation and simulation module has been integrated in InterNav3D. It calculates the motion of the underlying tissue (due to respiratory motion of the contralateral lung and cardiac motion) and induces its simulation on the virtual elements present in the 3D virtual visualization. This provides a realistic “feel” of the surgical site and the user can perceive the changes occurring in the surgical site more clearly. The selected target can also be rendered with the induced motion of the surgical site and appropriate actions of the robot movement for the needle insertion can be applied.

5.2 Conclusion

From Chapters 3 and 4, it can be concluded that InterNav3D improves the visualization and perception of the physical attributes of the surgical site by presenting an intuitive and interactive virtual-reality environment. The added capability of image processing makes it more insightful in detecting the required features in the surgical site and in determining the size and shape of tumors. The motion estimation and its implementation on the virtual elements as well as the target elements make it much easier for the user to get acquainted with the real surgical site and improve the capability for reaching the targets. The needle path prediction and projection module provides useful guidance for achieving faster and accurate needle maneuvering. They assist the user to maneuver the needle to reach the target in significantly fewer attempts, thus helping to reduce tissue damage which might occur if multiple incisions are made. This serves the purpose of avoiding needle pivoting while the needle is inside the patient’s body. However, sometimes the needle needs to be pivoted to avoid certain physical entities and/or to compensate for needle bending. For this reason, the needle path history can be helpful. The visualization of the needle path history helps to retract the needle along the same path as that during insertion so that tissue damage could be kept to a minimum. The various other modules such as surface rendering, needle detection, region-growing algorithms etc. help to enhance visualization and feature recognition. These modules guides the user to correctly and intuitively understand the various attributes present in the system and assists in completing the overall procedure with ease and greater accuracy in a shorter time.

The different clinical treatment techniques such as radiofrequency and microwave ablation have been implemented. This system can also be used for biopsy of tissue under

image guidance. Modules associated with the above-mentioned techniques are integrated in the system such as ablation sweep and volume subtraction, which helps to visualize the changes happening in the tumor over time during the procedure and provide guidance through the ablation process to ensure that cancerous tissue is being ablated and damage to healthy tissue is minimized. These modules assist clinician in estimating the entirety of the ablation procedure. The volume subtraction feature helps to determine the changes between two sets of images.

The *ex-vivo* experiments performed on tissue with and without added external motion (induced heart and respiratory motion) shows that InterNav3D improves upon its predecessor for greater accuracy and repeatability. The *in-vivo* experimental results demonstrate that this system can be applied in real clinical scenarios. InterNAV3D enhances the visualization of the surgical site and helps in faster and more accurate target selection and achievement. Experiments to determine needle deflection and subsequently establishing the tip location with the assistance of 3D visualization shows the effectiveness of the system for providing enhanced and accurate analysis of needle structure during the clinical procedure. This system demonstrates benefits such as prediction of the approximate needle tip location using certain points on the needle body. The various experimental results demonstrate the advantages of the system such as determining the tissue edges and its structure, determining the changes occurring in a volume over a duration of time (for ablation), comparing multiple volumes, enhancement of the visualization and perception of the surgical site, determining needle deflection and its deformed shape etc.

The software front end developed for InterNav3D can also work in an offline mode. It can retrieve and process offline images obtained from an imaging modality such as US, CT, MRI and display them in the 3D visualization window. It can perform all the visualization and image processing tasks to enhance the visibility of specific physical entities within the images. This system, developed on open-source application tools such as VTK, ITK, Qt provides an added advantage of having a wide variety of integrating options. VTK and ITK are huge resource libraries of visualization and medical image processing based algorithms and widgets. These libraries are updated frequently and

improved by the research community. This means that InterNav3D will always be able to take advantage of implementing new application tools for enhancing the overall architecture in the future. The current system, developed on the SAW framework, provides an added impetus to future expansion by integrating new hardware and software profiles.

5.3 Drawbacks and future work

As with any research project, there is always an intention to make the system better, faster and more reliable. The current drawbacks, their possible solutions and the future developments that can enhance the usability of the InterNav3D are summarized below:

- A prominent feature that the current system lacks is accounting for tissue deformation. In the virtual world scenario though the virtual elements move in synchronous motion with the real physical elements, they lack the feature to represent the deformations happening in real-time. Depending on the type of tissue (such as the lung which is very elastic), deformations can occur and could be a consequence of the force exerted by the US transducer probe and the needle tip on the tissue while clinical procedure is being performed. These deformations need to be accounted for to get more accurate visualization. Currently, though the target motion is simulated in the visualization world, errors can occur as deformation is not accounted for. The presence of real-time 2D US image feedback helps to realize the real-time location of the target (as the tissue deformation is visualized in the 2D US image plane).
- Another important feature that can be integrated in the system could be to improve the speed of the procedure. Currently a major portion of the rendering time is consumed by the underlying image enhancing algorithm. The complete system could be made more efficient by speeding up the image processing modules. Addition of one or more GPUs could provide the processing power needed to significantly speed up the processing for 3D images.

- Motion compensation: Currently, the system estimates the tissue motion and visualizes it in the virtual world. The same information could be used by the robot to reduce errors as a result of the motion by compensating for them by its motion. The surgical tool can be synchronized with the estimated motion. Therefore, as the tool moves with the motion of the tissue, the relative motion between the target and the tool tip would effectively be close to zero. This would help the user to gain better control while hitting the target as he/she would not have to worry about moving the surgical tool synchronously with the target.
- Advanced image processing: This could include more advanced image processing tools to the system module to guide surgeon in determining boundaries of tumors more accurately. A rigorous tumor localization mechanism for lung cancer treatment is needed which would make the entire procedure much faster and easier to be performed under US imaging. Certain techniques such as elastography and minimally invasive palpation could provide approaches to achieve this [108], [109].
- Integration of ROS: ROS (Robot Operating System) is an application layer that was developed to incorporate the control of all robot-based systems, devices and application tools under one software framework. ROS helps in communicating with other similar systems more intuitively. Integrating SAW with ROS will add an extra layer of the latest tools that will enhance the development of the entire system (due to the huge resource library provided by ROS).
- Quite often clinicians find it difficult to determine the locations of tumors in a minimally invasive procedure. The tissue deformation which occurs due to collapsing of lung makes it harder to correlate tumor information from the pre-operative image to that in the intra-operative image since the position of the tumors can change. A probabilistic model which correlates tissue deformation in the lung during its respiratory motion with the deformation occurring when it is collapsed in a clinical setting can help narrow down the tumor locations. Implementing such a model in the current system will speed up the procedure

time. The same information can also be used to enhance the visualization showing the concurrent tissue deformation that is occurring in the surgical site due to respiratory motion of the contralateral lung and the heart motion.

- Simulation environment: Addition of a simulation environment that could train the clinician for the procedure would be helpful. By developing a model to simulate an intra-operative surgical scenario using the pre-operative imaging would help the surgeon to get acquainted with the surgical site and practice before the real procedure. This will improve his/her surgical skills and help reduce errors when he/she performs the real surgery.

Bibliography

- [1] Statistics Canada, “Canadian Cancer Statistics Special topic: Liver cancer,” Toronto, ON, 2013.
- [2] A. L. Trejos, A. W. Lin, S. Mohan, H. Bassan, C. Edirisinghe, R. V. Patel, C. Lewis, E. Yu, A. Fenster, and R. A. Malthaner, “MIRA V: An integrated system for minimally invasive robot-assisted lung brachytherapy,” *Robot. Autom.* 2008. *ICRA 2008. IEEE Int. Conf.*, pp. 2982–2987, May 2008.
- [3] A. L. Trejos, A. W. Lin, M. P. Pytel, R. V. Patel, and R. A. Malthaner, “Robot-assisted minimally invasive lung brachytherapy,” *Int. J. Med. Robot. Comput. Assist. Surg.*, vol. 3, no. 1, pp. 41–51, Mar. 2007.
- [4] A. Patriciu, D. Petrisor, M. Muntener, D. Mazilu, M. Schar, D. Stoianovici, and M. Schär, “Automatic brachytherapy seed placement under MRI guidance.,” *Biomed. Eng. IEEE Trans.*, vol. 54, no. 8, pp. 1499–1506, Aug. 2007.
- [5] B. S. Hilaris and D. A. Mastoras, “Contemporary brachytherapy approaches in non-small-cell lung cancer,” *J. Surg. Oncol.*, vol. 69, no. 4, pp. 258–264, Dec. 1998.
- [6] P. N. Mathur, E. Edell, T. Sutedja, and J.-M. Vergnon, “Treatment of early stage non-small cell lung cancer,” *CHEST J.*, vol. 123, no. 1_suppl, p. 176S–180S, Jan. 2003.
- [7] C. Aygun, S. Weiner, A. Scariato, D. Spearman, and L. Stark, “Treatment of non-small cell lung cancer with external beam radiotherapy and high dose rate brachytherapy,” *Int. J. Radiat. Oncol.*, vol. 23, no. 1, pp. 127–132, 1992.
- [8] R. Lencioni, L. Crocetti, R. Cioni, A. Mussi, G. Fontanini, M. Ambroggi, C. Franchini, D. Cioni, O. Fanucchi, R. Gemignani, R. Baldassarri, C. A. Angeletti, and C. Bartolozzi, “Radiofrequency Ablation of Lung Malignancies: Where Do We Stand?,” *Cardiovasc. Intervent. Radiol.*, vol. 27, no. 63–6, pp. 581–590, 2004.

- [9] T. Baère, “Lung Tumor Radiofrequency Ablation: Where Do We Stand?,” *Cardiovasc. Intervent. Radiol.*, vol. 34, no. 2, pp. 241–251, Apr. 2011.
- [10] G. Carrafiello, M. Mangini, I. Bernardi, F. Fontana, G. Dionigi, S. Cuffari, A. Imperatori, D. Laganà, and C. Fugazzola, “Microwave ablation therapy for treating primary and secondary lung tumours: technical note,” *Radiol. Med.*, vol. 115, no. 6, pp. 962–974, Sep. 2010.
- [11] X. D. Zhou and Z. Y. Tang, “Cryotherapy for primary liver cancer,” *Semin. Surg. Oncol.*, vol. 14, no. 2, pp. 171–4, Mar. 1998.
- [12] L. M. Mir and B. Rubinsky, “Treatment of cancer with cryochemotherapy,” no. October 2001, pp. 1658–1660, 2002.
- [13] K. Furuse, M. Fukuoka, H. Kato, T. Horai, K. Kubota, N. Kodama, Y. Kusunoki, N. Takifuji, T. Okunaka, and C. Konaka, “A prospective phase II study on photodynamic therapy with photofrin II for centrally located early-stage lung cancer. The Japan Lung Cancer Photodynamic Therapy Study Group,” *J. Clin. Oncol.*, vol. 11, no. 10, pp. 1852–1857, 1993.
- [14] D. E. J. G. J. Dolmans, D. Fukumura, and R. K. Jain, “Photodynamic therapy for cancer,” *Nat. Rev. Cancer*, vol. 3, no. 5, pp. 375–80, May 2003.
- [15] E. C. White, M. R. Kamrava, J. Demarco, S.-J. Park, P.-C. Wang, O. Kayode, M. L. Steinberg, and D. J. Demanes, “High-Dose-Rate Prostate Brachytherapy Consistently Results in High Quality Dosimetry,” *Int. J. Radiat. Oncol. Biol. Phys.*, no. 310, pp. 1–6, May 2012.
- [16] T. P. Rutten, J. M. Lawson, and L. G. Marcu, “Treatment technique evolution and dosimetry trends over seven years of low dose rate prostate brachytherapy at an Australian institution,” *Phys. Med.*, pp. 1–9, Sep. 2012.
- [17] A. D’Amico, R. Cormack, C. Tempany, S. Kumar, G. Topulos, H. Kooy, and C. N. Coleman, “Real-time magnetic resonance image-guided interstitial

- brachytherapy in the treatment of select patients with clinically localized prostate cancer,” *Int. J. Radiat. Oncol.*, vol. 42, no. 3, pp. 507–515, Oct. 1998.
- [18] J. a Escobar-Sacristán, J. I. Granda-Orive, T. Gutiérrez Jiménez, J. M. Delgado, a Rodero Baños, and R. Saez Valls, “Endobronchial brachytherapy in the treatment of malignant lung tumours,” *Eur. Respir. J.*, vol. 24, no. 3, pp. 348–52, Sep. 2004.
- [19] M. Taulelle, B. Chauvet, P. Vincent, C. Félix-Faure, B. Buciarelli, R. Garcia, Y. Brewer, and F. Reboul, “High dose rate endobronchial brachytherapy: results and complications in 189 patients,” *Eur. Respir. J.*, vol. 11, no. 1, pp. 162–168, Jan. 1998.
- [20] A. G. Villanueva, T. C. Lo, and J. F. Beamis Jr, “Endobronchial brachytherapy,” *Clin. Chest Med.*, vol. 16, no. 3, p. 445, 1995.
- [21] W. Lee, B. D. T. Daly, T. A. Dipetrillo, D. M. Morelli, A. C. Neuschatz, J. Morr, and M. J. Rivard, “Limited Resection for Non – Small Cell Lung Cancer: Observed Local Control With Implantation of I-125 AM NP FM AC AT FR RH AS LT LS HO,” 2003.
- [22] B. S. Hilaris and N. Martini, “The current state of intraoperative interstitial brachytherapy in lung cancer,” *Int. J. Radiat. Oncol.*, vol. 15, no. 6, pp. 1347–1354, Dec. 1988.
- [23] R. T. Heelan, B. S. Hilaris, L. L. Anderson, D. Nori, N. Martini, R. C. Watson, J. F. Caravelli, and L. A. Linares, “Lung tumors: percutaneous implantation of I-125 sources with CT treatment planning,” *Radiology*, vol. 164, no. 3, pp. 735–740, Sep. 1987.
- [24] M. D. Chan, D. E. Dupuy, W. W. Mayo-Smith, T. Ng, and T. a DiPetrillo, “Combined radiofrequency ablation and high-dose rate brachytherapy for early-stage non-small-cell lung cancer,” *Brachytherapy*, vol. 10, no. 3, pp. 253–9, 2011.
- [25] S. J. DiBiase, K. Hosseinzadeh, R. P. Gullapalli, S. C. Jacobs, M. J. Naslund, G. N. Sklar, R. B. Alexander, and C. Yu, “Magnetic resonance spectroscopic

- imaging-guided brachytherapy for localized prostate cancer.,” *Int. J. Radiat. Oncol. Biol. Phys.*, vol. 52, no. 2, pp. 429–38, Feb. 2002.
- [26] A. Y. C. Fung, “C-Arm imaging for brachytherapy source reconstruction: Geometrical accuracy,” *Med. Phys.*, vol. 29, no. 5, p. 724, 2002.
- [27] A. V D’AMICO, R. CORMACK, S. KUMAR, and C. M. TEMPANY, “Real-time magnetic resonance imaging-guided brachytherapy in the treatment of selected patients with clinically localized prostate cancer,” *J. Endourol.*, vol. 14, no. 4, pp. 367–370, 2000.
- [28] W. C. Chen, J. Katcher, C. Nunez, A. M. Tirgan, and R. J. Ellis, “Radioactive seed migration after transperineal interstitial prostate brachytherapy and associated development of small-cell lung cancer.,” *Brachytherapy*, vol. 11, no. 5, pp. 354–8, 2012.
- [29] A. X. Zhu, K. E. Wallner, G. P. Frivold, D. Ferry, K. R. Jutzy, and G. P. Foster, “Prostate brachytherapy seed migration to the right coronary artery associated with an acute myocardial infarction.,” *Brachytherapy*, vol. 5, no. 4, pp. 262–5, 2006.
- [30] H. O. Badwan, A. E. Shanahan, M. a Adams, T. G. Shanahan, P. W. Mueller, S. J. Markwell, and T. H. Tarter, “AnchorSeed for the reduction of source movement in prostate brachytherapy with the Mick applicator implant technique.,” *Brachytherapy*, vol. 9, no. 1, pp. 23–6, 2010.
- [31] T. Zhang and R. Patel, “Optimization-based dosimetry planning for brachytherapy.,” *Conf. Proc. IEEE Eng. Med. Biol. Soc.*, vol. 2011, no. i, pp. 5569–72, Jan. 2011.
- [32] S. H. Okazawa, R. Ebrahimi, J. Chuang, R. N. Rohling, and S. E. Salcudean, “Methods for segmenting curved needles in ultrasound images.,” *Med. Image Anal.*, vol. 10, no. 3, pp. 330–42, Jun. 2006.

- [33] P. M. Novotny, J. a Stoll, N. V Vasilyev, P. J. del Nido, P. E. Dupont, T. E. Zickler, and R. D. Howe, "GPU based real-time instrument tracking with three-dimensional ultrasound.," *Med. Image Anal.*, vol. 11, no. 5, pp. 458–64, Oct. 2007.
- [34] D. E. Dupuy and S. N. Goldberg, "Image-guided radiofrequency tumor ablation: challenges and opportunities--part II.," *J. Vasc. Interv. Radiol.*, vol. 12, no. 10, pp. 1135–48, Oct. 2001.
- [35] O. R. Brook, M. Mendiratta-Lala, D. Brennan, B. Siewert, S. Faintuch, and S. N. Goldberg, "Imaging findings after radiofrequency ablation of adrenal tumors.," *AJR. Am. J. Roentgenol.*, vol. 196, no. 2, pp. 382–8, Feb. 2011.
- [36] D. E. Dupuy, "Image-guided Thermal Ablation of Lung Malignancies," *Radiology*, vol. 260, no. 3, pp. 633–655, 2011.
- [37] C. L. Brace, "Radiofrequency and microwave ablation of the liver, lung, kidney, and bone: what are the differences?," *Curr. Probl. Diagn. Radiol.*, vol. 38, no. 3, pp. 135–43, 2009.
- [38] A. S. Wright, L. A. Sampson, T. F. Warner, D. M. Mahvi, and F. T. Lee, "Radiology Radiofrequency versus Microwave Ablation in a Hepatic Porcine Model 1," no. 4, 2005.
- [39] F. A. Shepherd, R. J. Ginsberg, G. A. Patterson, W. K. Evans, and R. Feld, "A prospective study of adjuvant surgical resection after chemotherapy for limited small cell lung cancer. A University of Toronto Lung Oncology Group study.," *J. Thorac. Cardiovasc. Surg.*, vol. 97, no. 2, pp. 177–186, Feb. 1989.
- [40] J. L. Navia and D. M. Cosgrove III, "Minimally invasive mitral valve operations," *Ann. Thorac. Surg.*, vol. 62, no. 5, pp. 1542–1544, Nov. 1996.
- [41] G. Belfiore, G. Moggio, E. Tedeschi, M. Greco, R. Cioffi, F. Cincotti, and R. Rossi, "CT-Guided Radiofrequency Ablation: A Potential Complementary Therapy for Patients with Unresectable Primary Lung Cancer—A Preliminary

- Report of 33 Patients,” *Am. J. Roentgenol.*, vol. 183, no. 4, pp. 1003–1011, Oct. 2004.
- [42] D. E. Dupuy, R. J. Zagoria, W. Akerley, W. W. Mayo-Smith, P. V Kavanagh, and H. Safran, “Percutaneous Radiofrequency Ablation of Malignancies in the Lung,” *Am. J. Roentgenol.*, vol. 174, no. 1, pp. 57–59, Jan. 2000.
- [43] D. E. Dupuy, “Science to Practice: Microwave Ablation Compared with Radiofrequency Ablation in Lung Tissue – Is Microwave Not Just for Popcorn Anymore?,” *Radiology*, vol. 251, no. 3, pp. 617–618, 2009.
- [44] J. C. Chen, J. a Moriarty, J. a Derbyshire, R. D. Peters, J. Trachtenberg, S. D. Bell, J. Doyle, R. Arrelano, G. a Wright, R. M. Henkelman, R. S. Hinks, S. Y. Lok, a Toi, and W. Kucharczyk, “Prostate cancer: MR imaging and thermometry during microwave thermal ablation-initial experience.,” *Radiology*, vol. 214, no. 1, pp. 290–7, Jan. 2000.
- [45] W. Wein, S. Brunke, A. Khamene, M. R. Callstrom, and N. Navab, “Automatic CT-ultrasound registration for diagnostic imaging and image-guided intervention,” *Med. Image Anal.*, vol. 12, no. 5, pp. 577–585, Oct. 2008.
- [46] A. Krieger, R. C. Susil, C. Menard, J. a Coleman, G. Fichtinger, E. Atalar, L. L. Whitcomb, and C. Ménard, “Design of a novel MRI compatible manipulator for image guided prostate interventions,” *Biomed. Eng. IEEE Trans.*, vol. 52, no. 2, pp. 306–313, Feb. 2005.
- [47] S. W. Gould, G. Lamb, D. Lomax, W. Gedroyc, and a Darzi, “Interventional MR-guided excisional biopsy of breast lesions,” *J. Magn. Reson. Imaging*, vol. 8, no. 1, pp. 26–30, 1998.
- [48] R. P. Burns, “Image-guided breast biopsy,” *Am. J. Surg.*, vol. 173, no. 1, pp. 9–11, Jan. 1997.
- [49] M. A. Mauro, *Image-guided interventions*, vol. 2. Elsevier Health Sciences, 2008.

- [50] J. Bodner, H. Wykypiel, A. Greiner, W. Kirchmayr, M. C. Freund, R. Margreiter, and T. Schmid, "Early experience with robot-assisted surgery for mediastinal masses," *Ann. Thorac. Surg.*, vol. 78, no. 1, pp. 259–265, Jul. 2004.
- [51] M. Tavakoli, R. V Patel, and M. Moallem, "Haptic interaction in robot-assisted endoscopic surgery: a sensorized end-effector," *Int. J. Med. Robot. Comput. Assist. Surg.*, vol. 1, no. 2, pp. 53–63, 2005.
- [52] J. Rosen, M. Lum, M. Sinanan, and B. Hannaford, "Raven: Developing a Surgical Robot from a Concept to a Transatlantic Teleoperation Experiment," in *Surgical Robotics SE - 8*, J. Rosen, B. Hannaford, and R. M. Satava, Eds. Boston, MA: Springer US, 2011, pp. 159–197.
- [53] M. Shi, H. Liu, and G. Tao, "A stereo-fluoroscopic image-guided robotic biopsy scheme," *Control Syst. Technol. IEEE Trans.*, vol. 10, no. 3, pp. 309–317, 2002.
- [54] W. H. H. Chapman Iii, R. J. Albrecht, V. B. Kim, J. A. Young, and W. R. Chitwood Jr, "Computer-Assisted Laparoscopic Splenectomy with the da VinciTM Surgical Robot," *J. Laparoendosc. Adv. Surg. Tech.*, vol. 12, no. 3, pp. 155–159, 2002.
- [55] J. Bodner, H. Wykypiel, G. Wetscher, and T. Schmid, "First experiences with the da VinciTM operating robot in thoracic surgery," *Eur. J. Cardio-Thoracic Surg.*, vol. 25, no. 5, pp. 844–851, May 2004.
- [56] L. W. W. Nifong, V. F. Chu, B. M. M. Bailey, D. M. Maziarz, V. L. Sorrell, D. Holbert, W. R. Chitwood, and W. R. Chitwood Jr, "Robotic mitral valve repair: experience with the da Vinci system," *Ann. Thorac. Surg.*, vol. 75, no. 2, pp. 438–443, Feb. 2003.
- [57] K. Cleary and C. Nguyen, "State of the art in surgical robotics: Clinical applications and technology challenges," *Comput. Aided Surg.*, vol. 6, no. 6, pp. 312–328, Jan. 2001.

- [58] R. D. Howe and Y. Matsuoka, "Robotics for surgery," *Annu. Rev. Biomed. Eng.*, vol. 1, no. 1, pp. 211–240, Jan. 1999.
- [59] J. Rosen, B. Hannaford, and R. M. Satava, *Surgical robotics: systems, applications, and visions*. Springer, 2011.
- [60] M. L. Brachytherapy, A. L. Trejos, R. Patel, and R. Malthaner, "A Device for Robot-Assisted," *Proc. 2006 IEEE Int. Conf. Robot. Autom.*, no. May, pp. 4187–4192, 2006.
- [61] H. S. Bassan, "DESIGN , CONSTRUCTION AND CONTROL OF A MICRO MANIPULATOR FOR PROSTATE BRACHYTHERAPY," University of Western Ontario, 2007.
- [62] E. Yu, C. Lewis, A. Luisa Trejos, R. V. Patel, and R. A. Malthaner, "Lung Cancer Brachytherapy: Robotics-Assisted Minimally Invasive Approach," *Curr. Respir. Med. Rev.*, vol. 7, no. 5, pp. 340–353, Oct. 2011.
- [63] "NDI Aurora." [Online]. Available: <http://www.ndigital.com/medical/aurora.php>.
- [64] "Ultrasonix sonixtouch." [Online]. Available: <http://www.ultrasonix.com/ultrasound-systems/sonixtouch>.
- [65] S. Hughes, "Medical ultrasound imaging," *Phys. Educ.*, vol. 36, no. 6, pp. 468–475, Nov. 2001.
- [66] W. D. Middleton, A. B. Kurtz, and B. S. Hertzberg, *Ultrasound: the requisites*. Mosby St. Louis, 2004.
- [67] L. Zagsebski, "Essentials of Ultrasound Physics by," p. 5.
- [68] F. W. Kremkau and G. A. W. Gooding, *Diagnostic ultrasound: principles and instruments*. WB Saunders Philadelphia, PA, 1998.
- [69] R. W. Cootney, "Ultrasound Imaging: Principles and Applications in Rodent Research," *ILAR J.*, vol. 42, no. 3, pp. 233–247, Jan. 2001.

- [70] G. Kossoff and D. S. Eng, "Basic Physics and Imaging Characteristics of Ultrasound," pp. 134–142, 2000.
- [71] A. Goldstein, "Overview of the physics of US.," *Radiographics*, vol. 13, pp. 701–704, 1993.
- [72] C. J. Harvey, J. M. Pilcher, R. J. Eckersley, M. J. K. Blomley, and D. O. Cosgrove, "Advances in ultrasound.," *Clin. Radiol.*, vol. 57, no. 3, pp. 157–177, Mar. 2002.
- [73] B. J. Wood, H. Zhang, A. Durrani, N. Glossop, S. Ranjan, D. Lindisch, E. Levy, F. Banovac, J. Borgert, S. Krueger, J. Kruecker, A. Viswanathan, and K. Cleary, "Navigation with electromagnetic tracking for interventional radiology procedures: a feasibility study.," *J. Vasc. Interv. Radiol.*, vol. 16, no. 4, pp. 493–505, Apr. 2005.
- [74] a Schneider, H. Hautmann, H. Barfuss, T. Pinkau, F. Peltz, H. Feussner, and a Wichert, "Real-time image tracking of a flexible bronchoscope," *Int. Congr. Ser.*, vol. 1268, pp. 753–757, Jun. 2004.
- [75] J. Harms, H. Feussner, M. Baumgartner, A. Schneider, M. Donhauser, and G. Wessels, "Three-dimensional navigated laparoscopic ultrasonography," *Surg. Endosc.*, vol. 15, no. 12, pp. 1459–1462, Dec. 2001.
- [76] M. Kleemann, P. Hildebrand, M. Birth, and H. P. Bruch, "Laparoscopic ultrasound navigation in liver surgery: technical aspects and accuracy," *Surg. Endosc. Other Interv. Tech.*, vol. 20, no. 5, pp. 726–729, May 2006.
- [77] N. D. Glossop, K. Cleary, and F. Banovac, "Needle tracking using the aurora magnetic position sensor," *CAOS*, 2002.
- [78] J. Kuipers, "OBJECT TRACKING AND ORIENTATION," Feb. 1975.
- [79] F. H. Raab, E. B. Blood, T. O. Steiner, and H. R. Jones, "Magnetic Position and Orientation Tracking System," *Aerosp. Electron. Syst. IEEE Trans.*, vol. AES-15, no. 5, pp. 709–718, 1979.

- [80] A. M. J. Bull and A. A. Amis, "Accuracy of an electromagnetic tracking device," *J. Biomech.*, vol. 30, no. 8, pp. 857–858, 1997.
- [81] M. A. Nixon, B. C. McCallum, W. R. Fright, and N. B. Price, "The effects of metals and interfering fields on electromagnetic trackers," *Presence Teleoperators Virtual Environ.*, vol. 7, no. 2, pp. 204–218, 1998.
- [82] S. E. Butner, S. Member, and M. Ghodoussi, "Transforming a Surgical Robot for Human Telesurgery," *Robot. Autom. IEEE Trans.*, vol. 19, no. 5, pp. 818–824, 2003.
- [83] A. Austad, O. J. Elle, and J. S. Røtnes, "Computer-aided planning of trocar placement and robot settings in robot-assisted surgery," *Int. Congr. Ser.*, vol. 1230, no. 0, pp. 1020–1026, Jun. 2001.
- [84] T. Ortmaier and G. Hirzinger, "Cartesian control issues for minimally invasive robot surgery," in *Proceedings. 2000 IEEE/RSJ International Conference on Intelligent Robots and Systems (IROS 2000) (Cat. No.00CH37113)*, 2000, vol. 1, pp. 565–571.
- [85] J. Cornell, O. J. Elle, W. Ali, and E. Samset, "Improving Cartesian Position Accuracy of a Telesurgical Robot," *Ind. Electron. 2008. ISIE 2008. IEEE Int. Symp.*, pp. 1261–1266, 2008.
- [86] "Matrox Vio," *manual*. Matrox Imaging, pp. 2–4, 2006.
- [87] A. Deguet, R. Kumar, R. Taylor, and P. Kazanzides, "The cisst libraries for computer assisted intervention systems," *MIDAS J Syst Arch. Comput Assist Interv*, pp. 1–8, 2008.
- [88] B. Vagvolgyi, S. DiMaio, A. Deguet, P. Kazanzides, R. Kumar, C. Hasser, and R. Taylor, "The surgical assistant workstation," in *Proc MICCAI Workshop: Systems and Architectures for Computer Assisted Interventions*, 2008, pp. 1–8.

- [89] J. Young, H. Elhawary, and A. Popovic, "Integration of a Robotic Arm with the Surgical Assistant Workstation Software Framework," pp. 1–6, 2011.
- [90] W. J. Schroeder, K. M. Martin, and W. E. Lorensen, "The design and implementation of an object-oriented toolkit for 3D graphics and visualization," *Proc. Seventh Annu. IEEE Vis.* '96, pp. 93–100,.
- [91] W. J. Schroeder and L. S. Avila, "Visualizing with VTK: A Tutorial," no. October, pp. 20–27, 2000.
- [92] W. Schroeder, "The ITK Software Guide Second Edition Updated for ITK version 2.4," 2005.
- [93] T. S. Yoo, M. J. Ackerman, W. E. Lorensen, W. Schroeder, V. Chalana, S. Aylward, D. Metaxas, and R. Whitaker, "Engineering and algorithm design for an image processing Api: a technical report on ITK--the Insight Toolkit.," *Stud. Health Technol. Inform.*, vol. 85, pp. 586–92, Jan. 2002.
- [94] T. S. Yoo, *Insight into images: principles and practice for segmentation, registration, and image analysis*, vol. 203. AK Peters Wellesley^ eMassachusetts Massachusetts, 2004.
- [95] W. D. D'Souza, R. R. Meyer, B. R. Thomadsen, and M. C. Ferris, "An iterative sequential mixed-integer approach to automated prostate brachytherapy treatment plan optimization.," *Phys. Med. Biol.*, vol. 46, no. 2, pp. 297–322, Feb. 2001.
- [96] S. Nag, J. P. Ciezki, R. Cormack, S. Doggett, K. DeWyngaert, G. K. Edmundson, R. G. Stock, N. N. Stone, Y. Yu, and M. J. Zelefsky, "Intraoperative planning and evaluation of permanent prostate brachytherapy: Report of the American Brachytherapy Society," *Int. J. Radiat. Oncol.*, vol. 51, no. 5, pp. 1422–1430, Dec. 2001.
- [97] E. M. Messing, J. B. Y. Zhang, D. J. Rubens, R. A. Brasacchio, J. G. Strang, A. Soni, M. C. Schell, P. G. Okunieff, and Y. Yu, "Intraoperative optimized inverse

- planning for prostate brachytherapy: early experience,” *Int. J. Radiat. Oncol.*, vol. 44, no. 4, pp. 801–808, Jul. 1999.
- [98] S. Senan, F. J. Lagerwaard, C. de Pan, D. Sipkema, S. A. Burgers, and L. H. P. Murrer, “A CT-assisted method of dosimetry in brachytherapy of lung cancer,” *Radiother. Oncol.*, vol. 55, no. 1, pp. 75–80, Apr. 2000.
- [99] G. Wan, Z. Wei, L. Gardi, D. B. Downey, and A. Fenster, “Brachytherapy needle deflection evaluation and correction,” *Med. Phys.*, vol. 32, no. 4, p. 902, 2005.
- [100] N. Abolhassani and R. V Patel, “Deflection of a Flexible Needle during Insertion into Soft Tissue,” *Eng. Med. Biol. Soc. 2006. EMBS '06. 28th Annu. Int. Conf. IEEE*, vol. 1, pp. 3858–3861, Jan. 2006.
- [101] M. D. O’Leary, C. Simone, T. Washio, K. Yoshinaka, A. M. Okamura, and C. Sirnane, “Robotic needle insertion: effects of friction and needle geometry,” *Robot. Autom. 2003. Proceedings. ICRA '03. IEEE Int. Conf.*, vol. 2, pp. 1774–1780 vol.2, 2003.
- [102] P. T. Johnson, D. G. Heath, D. F. Bliss, B. Cabral, and E. K. Fishman, “Three-dimensional CT: real-time interactive volume rendering,” *AJR. Am. J. Roentgenol.*, vol. 167, no. 3, pp. 581–583, 1996.
- [103] D. Honigmann, J. Ruisz, and C. Haider, “Adaptive Design of a Global Opacity Transfer Function for Direct Volume Rendering of Ultrasound Data,” in *Proceedings of the 14th IEEE Visualization 2003 (VIS’03)*, 2003, pp. 489–496.
- [104] W. E. Lorensen and H. E. Cline, “Marching Cubes: A High Resolution 3D Surface Construction Algorithm,” in *Proceedings of the 14th Annual Conference on Computer Graphics and Interactive Techniques*, 1987, vol. 21, no. 4, pp. 163–169.
- [105] T. S. Newman and H. Yi, “A survey of the marching cubes algorithm,” *Comput. Graph.*, vol. 30, no. 5, pp. 854–879, Oct. 2006.

- [106] L. K. Wee, H. Y. Chai, E. Supriyanto, B. E. Group, and T. U. Ilmenau, "Surface rendering of three dimensional ultrasound images using VTK," *J. Sci. Ind. Res.*, vol. 70, no. 6, pp. 421–426, 2011.
- [107] G. H. Golub and C. Reinsch, "Singular value decomposition and least squares solutions," *Numer. Math.*, vol. 14, no. 5, pp. 403–420, 1970.
- [108] E. Turgay, S. Salcudean, and R. Rohling, "Identifying the mechanical properties of tissue by ultrasound strain imaging," *Ultrasound Med. Biol.*, vol. 32, no. 2, pp. 221–235, Feb. 2006.
- [109] A. Talasaz, R. V. Patel, and M. D. Naish, "Haptics-enabled teleoperation for robot-assisted tumor localization," *2010 IEEE Int. Conf. Robot. Autom.*, pp. 5340–5345, May 2010.

Appendix A: Manufactured parts

In the design phase of InterNAV3D, several parts were manufactured to help build the test bed. Different parts were designed in Solidworks and printed in a rapid prototyping machine (3D printer). This appendix provides an overview of the parts that were used in InterNAV3D.

Initial work started with a design prototype to make a holder sleeve for the laparoscopic US probe to restrict the unwanted motion at the flexible part. It was required to have an encapsulation groove to affix the electromagnetic tracking sensor. Two designs were created one which completely restricted the movement of the flexible part and the other which allowed adjustment of the flexibility. Figure A.1 shows the initial design prototypes with and without the adjustable sleeve (the adjustable sleeve allows for control of the range of flexibility).

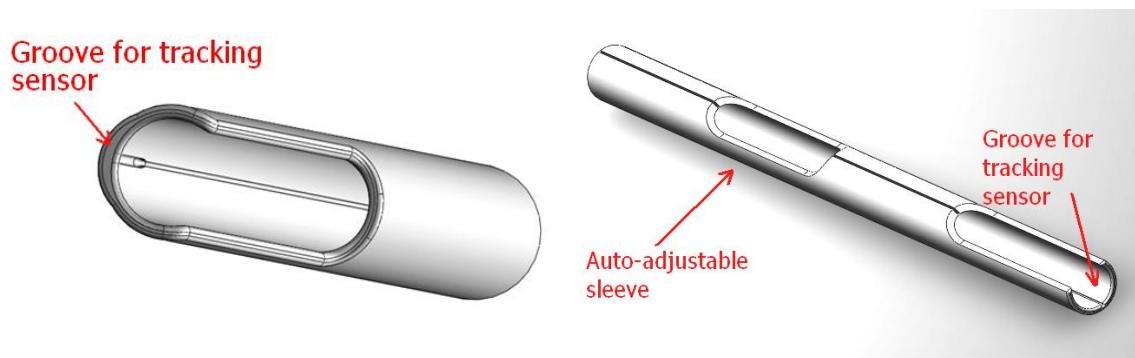


Figure A.1: US probe holder

The next step was to design a test-bed that allows conducting the necessary experiments and assists in grabbing the images using the US probe in the specified sweep format (round or flat sweep) by using the available robot arm dexterity. Figure A.2 shows the initial design of a test-bed assembly. This test-bed provides the following benefits:

- Easy access to the phantoms and tissue being imaged.
- Provides insertion points for minimally invasive interventions
- Test-bed can be moved in horizontal and vertical directions. This enables the user to change the size of the surgical workspace.

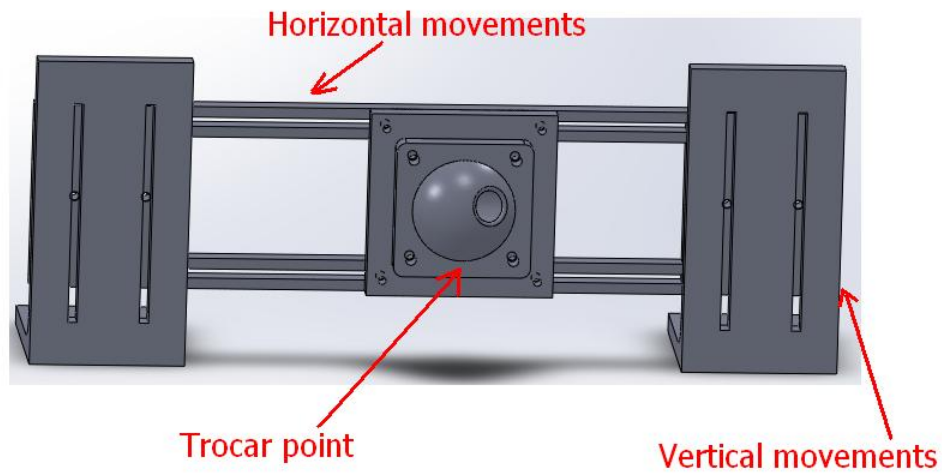


Figure A.2: Test-bed assembly

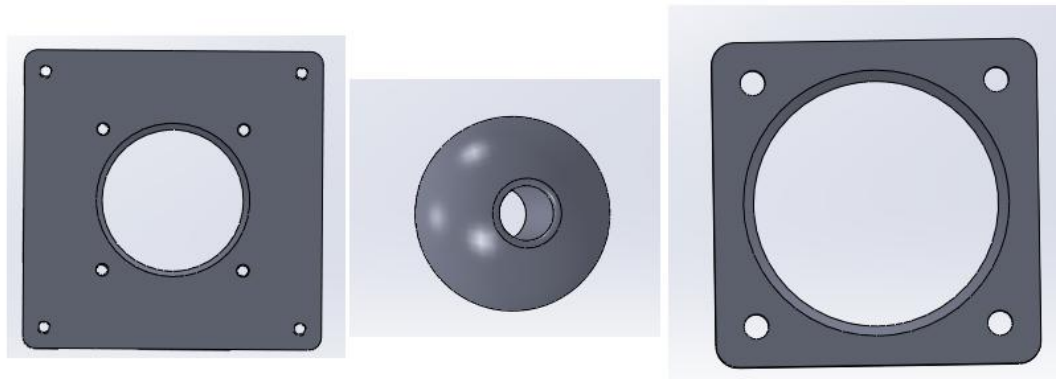


Figure A.3: Ball and socket design

The sleeves designed for the ablation probes (radiofrequency and microwave) are shown in Figure A.4. While running the experiments, it was found out that the sleeves had a disoriented axis. As the designed sleeves had a high aspect ratio of length versus width, while manufacturing the product tends to bend. Figure A.5 shows the modified design of the radiofrequency ablation probe holder where the sleeve is manufactured in two parts that are attached post production. The sleeve also has the tracking sensor groove.

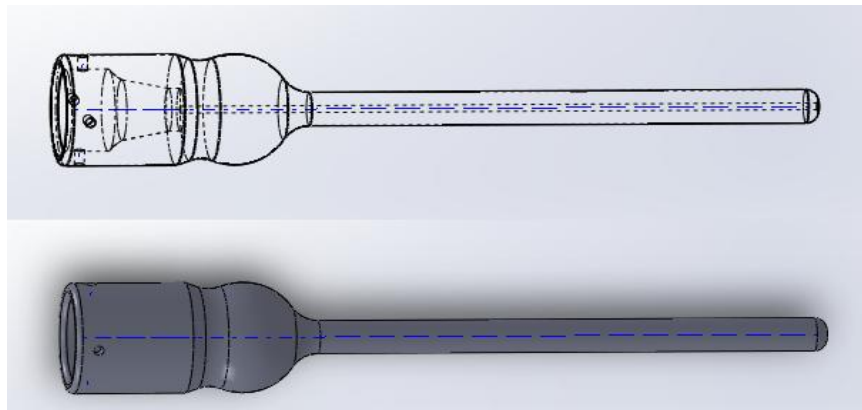


Figure A.4: Microwave ablation probe holder

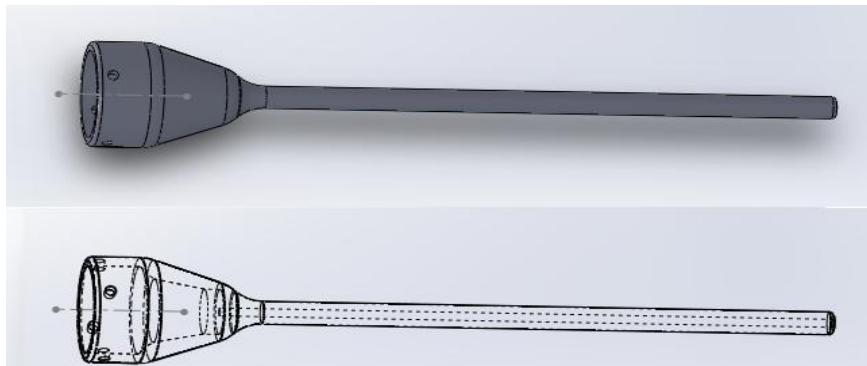


Figure A.5: Radiofrequency ablation probe holder

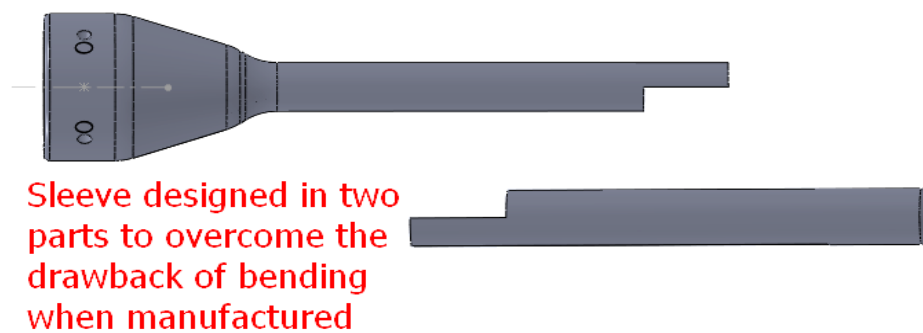


Figure A.6: Radiofrequency ablation probe holder designed in two parts

Curriculum Vitae

Name:	Srikanth Bhattad
Post-secondary Education and Degrees:	<p>The University of Western Ontario London, Ontario, Canada M.E.Sc. (Electrical and Computer Engineering) 2010-13</p> <p>The University of Pune Pune, India B.E. (Electronics and Tele-communication Engineering) 2005-09</p>
Related Work Experience	<p>Research Assistant Canadian Surgical Technologies and Advanced Robotics London, Ontario, Canada 2010-13</p> <p>Teaching Assistant The University of Western Ontario London, Ontario, Canada 2011-12</p> <p>Senior Engineer Fennec Fox Technologies Pune, India 2009</p>